UNIVERSIDAD NACIONAL DE COLOMBIA

Photoelectrocatalytic Hydrogen Production with TiO_2 Nanostructures Formed by Alternating Voltage Anodization

Pedro Jose Arias Monje

Universidad Nacional de Colombia
Facultad de Ingeniería
Departamento de Ingeniería Química y Ambiental
Bogotá, Colombia
2016

UNIVERSIDAD NACIONAL DE COLOMBIA

Producción Fotoelectrocatalítica de Hidrógeno usando Nanoestructuras de TiO_2 Formadas por Anodización con Voltaje Alternante

Pedro Jose Arias Monje

Universidad Nacional de Colombia
Facultad de Ingeniería
Departamento de Ingeniería Química y Ambiental
Bogotá, Colombia
2016

Producción Fotoelectrocatalítica de Hidrógeno usando Nanoestructuras de TiO_2 Formadas por Anodización con Voltaje Alternante

Pedro Jose Arias Monje

Tesis presentada como requisito parcial para optar al título de:

Magister en Ingeniería Química

Director:
Ph.D. Hugo Ricardo Zea Ramírez

Grupo de Investigación:
Materiales, Catálisis y Medio Ambiente

Universidad Nacional de Colombia
Facultad de Ingeniería
Departamento de Ingeniería Química y Ambiental
Bogotá, Colombia
2016

Acknowledgements

Thanks to everyone who has been part of this process: to my advisor, Hugo Zea, and to Claudia Luhrs, Sarath Menon and Jonathan Pillips, special thanks, all of you have inspired me to research and provided me of tools and ideas that I will keep using in my future professional and personal life. To Francisco, who has been by my side during this and the upcoming life path. To my parents, my brothers, my godson, my cousins and my aunt, and to the many good friends I made during my studies and the experimental part of the thesis, thank you, all of you are part of me.

Many thanks to the Universidad Nacional de Colombia and Colciencias for the financial support through the grants number 19163 of the program “Convocatoria del Programa Nacional de Proyectos para el Fortalecimiento de la Investigación, la Creación y la Innovación en Posgrados de la Universidad Nacional de Colombia 2013-2015” and 21551 of the program “Jóvenes Investigadores de Colciencias - 2013”, respectively.

Thanks to the Mechanical and Aerospace Engineering Department of the Naval Postgraduate School of the US who allowed me to use all the advance characterization equipment needed during this thesis.

Thanks to the Electromagnetic Compatibility research group and the engineers Francisco Jose Roman Campos, Carlos Andres Rivera Guerrero, Jorge Enrique Rodríguez Manrique and Carlos Fernando Hernández Prada, for their help extending the reach of this thesis.

Thank you for reading this an all the following lines, please contact me to discuss any matter you find interesting.

Pedro J. Arias-Monje
pjariasm@unal.edu.co

Resumen

Una celda fotoelectrocatalítica (PEC, por sus siglas en inglés) usa luz solar para separar el agua en hidrógeno y oxígeno. El hidrógeno es un combustible limpio, es capaz de entregar más energía que la gasolina (por unidad de masa) y durante su combustión solo se genera agua. La separación de la molécula de agua se logra en una celda PEC cuando la luz interactúa con un semiconductor fotoactivo, y se generan especies oxidativas y reductivas. Sin embargo, actualmente, las celdas PEC generan hidrógeno a un costo 3 a 5 veces mayor que el requerido para operación industrial, y demandan energía eléctrica adicional para operar a máxima eficiencia. Dos alternativas se utilizan normalmente para reducir los costos operaciones de la celda PEC, la primera consiste en incrementar la eficiencia del semiconductor fotoactivo, mientras que la segunda consiste en proveer la energía eléctrica requerida a través de fuentes de energía alternativas y de bajo costo.

En esta tesis nanotubos de TiO_2 preparados por anodización son usados como fotoanodo en una celda PEC. La morfología de los nanotubos: longitud, diámetro y número de anillos en la pared exterior del tubo, fueron estudiados para incrementar la eficiencia PEC del material. Igualmente, la celda PEC con nanotubos de morfología optimizada fue acoplada a dos sistemas diferentes de generación de energía alternativa para el suministro de la energía eléctrica necesaria para operación a máxima eficiencia. El primer sistema remueve contaminantes orgánicos de aguas residuales y usa luz para generar la energía eléctrica (es una foto celda de combustible (PFC)), y el segundo sistema usa el potencial generado naturalmente entre las nubes de la atmósfera y la superficie de la tierra (sistema de 'cosecha' del efecto corona). Cuando la celda PEC estuvo acoplada, se pudo generar hidrógeno independiente de la red de electricidad convencional.

Palabras clave: Celda Fotoelectrocatalítica (PEC cell), separación de la molécula de agua, Nanotubos de TiO_2, anodización, foto celda de combustible (PFC), corriente corona

Abstract

A photoelectrocatalytic (PEC) cell uses solar light to split the water in hydrogen and oxygen. The hydrogen is a green fuel, delivers more energy than gasoline (per unit mass) and during its combustion only water is generated. The splitting of the water molecule is achieved in a PEC cell when light interacts with a photoactive semiconductor, oxidative and reductive species are generated. Nevertheless, in its current state, the PEC technology generates hydrogen at a cost 3 to 5 times higher than the target cost for industrial operation, and demands an additional electrical power input to operate at maximum efficiency. Two strategies are commonly used to reduce the operational cost of the PEC cell, first to increase the efficiency of the photoactive semiconductor, and second to supply the demanded electrical power from alternative and cost-effective energy sources.

In this thesis TiO_2 nanotubes prepared by anodization are used as photoanode in a PEC cell. The nanotube morphology: tube length, diameter and the number of rings on the external wall, is studied in order to increase the PEC efficiency of the material. Also, the PEC cell with nanotubes of optimized morphology is coupled to two different alternative electricity generation systems in order to provide the demanded electrical power. One of those systems removes organic pollutants from wastewater and uses light to generate the electrical power (photo-fuel cell, PFC), and the second system uses the potential generated naturally between atmospheric clouds and the Earth's surface (harvesting of the corona effect). When coupled, the PEC cell was able to produce hydrogen independently from the power grid.

Keywords: Photoelectrocatalytic (PEC) cell, water splitting, TiO_2 nanotubes, anodization, photo-fuel cell (PFC), corona current

Preface

The main objective of this thesis is to determine the operational conditions of a photoelectrocatalytic (PEC) cell at which the highest amount of hydrogen could be produced, by water splitting, and using titanium dioxide nanostructures prepared by anodization. The specific objectives are: 1) to produce hydrogen in a PEC cell (including the selection and construction of the cell), 2) to determine the variables of highest importance in the functioning of a PEC cell for hydrogen production, and 3) to model the operational conditions of the PEC cell in the hydrogen production, including the morphology of the nanotubes.

The first specific objective was the most challenging of all. Before this project, no one in our research group had produced hydrogen by PEC. It took a lot of time and effort to learn and standardize the process in order to obtain reproducible results. Chapter 1 is an introduction to the concepts used in this thesis, and from that point each chapter presents detailed description of the experimental design. The purpose of this document is to serve as the basis for future researchers both in our group and worldwide

All the specific objectives were accomplished in chapters 3, 4 and 5. Chapter 2 defines the standard anodization protocol used in the thesis to produce nanotubes while varying independently tube length and diameter, and while keeping the top morphology constant. In chapter 3 the effect of the morphology of nanotubes produced by constant voltage anodization was studied. In chapter 4 nanotubes obtained by alternating voltage anodization were studied. Chapter 5 focuses in the use of the TiO_2 nanotube in a photo-fuel cell (PFC), the optimization of the operation conditions (including morphology) and the coupling of the PFC with the PEC cell. Finally, chapter 6 is and additional chapter in which the PEC cell was powered by an alternative and emerging energy source, this work was developed in collaboration with Carlos Andres Rivera Guerrero, Jorge Enrique Rodríguez Manrique and Carlos Fernando Hernández Prada of the Department of Electrical and Electronic engineering of the Universidad Nacional de Colombia.

A portion of the results obtained in chapter 3 were already disclosed during the Materials Research Society (MRS) Spring Meeting & Exhibit celebrated in California, USA, April 6-10, 2015. The information of all the other chapter will be submitted to international journals for publication.

Contents

List of Figures

Page

List of Tables

Page

Chapter 1. Introduction

Currently, our biggest source of energy are fossil fuels (78.3% of the 18.0 terawatts consumed in 2013 [1]), but their combustion produces greenhouse gases and other toxic compounds. In order to ensure environmental sustainability, humans have to implement green energy sources. Although over the past decade the amount of energy generated from renewable sources has been increasing [1], more research in new technologies is still needed, considering that the cost of many of the current green alternatives is still prohibitive, and the price of crude oil is very low.

Production of hydrogen by water splitting is a very interesting green energy alternative. The hydrogen heat power is 120MJ/kg, superior to the one of gasoline, and its combustion produces only water [2]. Also, if hydrogen is obtained from the separation of the water molecule, it can be a fuel with virtually zero carbon footprint. The work presented here focuses in an emerging technology for hydrogen production from water and solar light: photoelectrocatalytic (PEC) water splitting with photoactive TiO_2 nanotubes.

Nowadays, hydrogen is mainly obtained from fossil fuels (more than 90% of the world's hydrogen market [3]), however CO_2 is generated too as a coproduct. On the other hand, hydrogen by water electrolysis (4% of the market), which only generates oxygen as coproduct, is 3 to 10 times more expensive than the produced by fossil fuels, depending on the cost of the electricity [4]. Under this circumstances, new technologies for hydrogen generation are required, particularly those able to split the water molecule by using renewable and low cost energy sources, such as solar light.

Hydrogen can be produced in a photoelectrocatalytic (PEC) cell from only water and solar light [2]. The PEC cell uses a photoactive anode to react with the light and generate reductive and oxidative species which can split the water into hydrogen and oxygen. Nevertheless, more research is still needed, considering that the current cost of the hydrogen produced by this technology is high (6-19 USD per kg of H_2) [5]. The target cost is close to the one of hydrogen produced from fossil fuels, 2-4 USD per kg of H_2 [5]. Although the cost of the hydrogen from fossil fuels can be as low as 0.02 USD per kg.

The Photoelectrocatalytic (PEC) cell

A PEC cell consists of a photoanode and a cathode connected to each other and submerged in an electrolytic solution, as sketched in figure 1.1. Other configurations of the PEC cell are available, in which the cathode is also photoactive [6] or the anode and cathode are a single electrode [7]–[9], but the mechanism for water splitting is similar. Such mechanism is explained in the figure 1.1. When the light hits the photoactive anode (a), typically a semiconductor, the energy of the photons is transferred to the electrons (e^-) in the valence band (VB) of the material, promoting them to a higher energy level in the conduction band (CB) (b), and leaving positive carriers in the VB, or holes (h^+). Such holes are oxidative species which can interact with water or hydroxyl ions (c), depending on the pH of the solution, and produce oxygen and H^+, or oxygen and water, if acidic or alkaline, respectively. On the other side, the excited electrons in the CB move to the cathode (d), through an external circuit, and react with the electrolyte to produce molecular hydrogen (e) [2]. The reactions, valid for acid or neutral and alkali electrolytes, are presented in figure 1.1.

The cell in figure 1.1 can only generate hydrogen if three conditions are satisfied. Firstly, the difference of energy between the electrons in the CB and the holes in the VB must be greater than the redox potential of the water, 1.23eV [10]. Such difference is an intrinsic property of the semiconductor, the band gap (BG). Secondly, the CB level should be more negative than the reduction potential of the water and the VB level should be more positive than the oxidation potential of the water [11]. Finally, electrolyte near the cathode must be oxygen depleted (solution must be degassed), otherwise electrons would be consumed in reactions without hydrogen production (see equations 1.1 and 1.2) [12].

$$O_2 + 4H^+ + 4e^- \rightarrow 2H_2O \quad (1.1)$$

$$O_2 + 2H^+ + 2e^- \rightarrow H_2O_2 \quad (1.2)$$

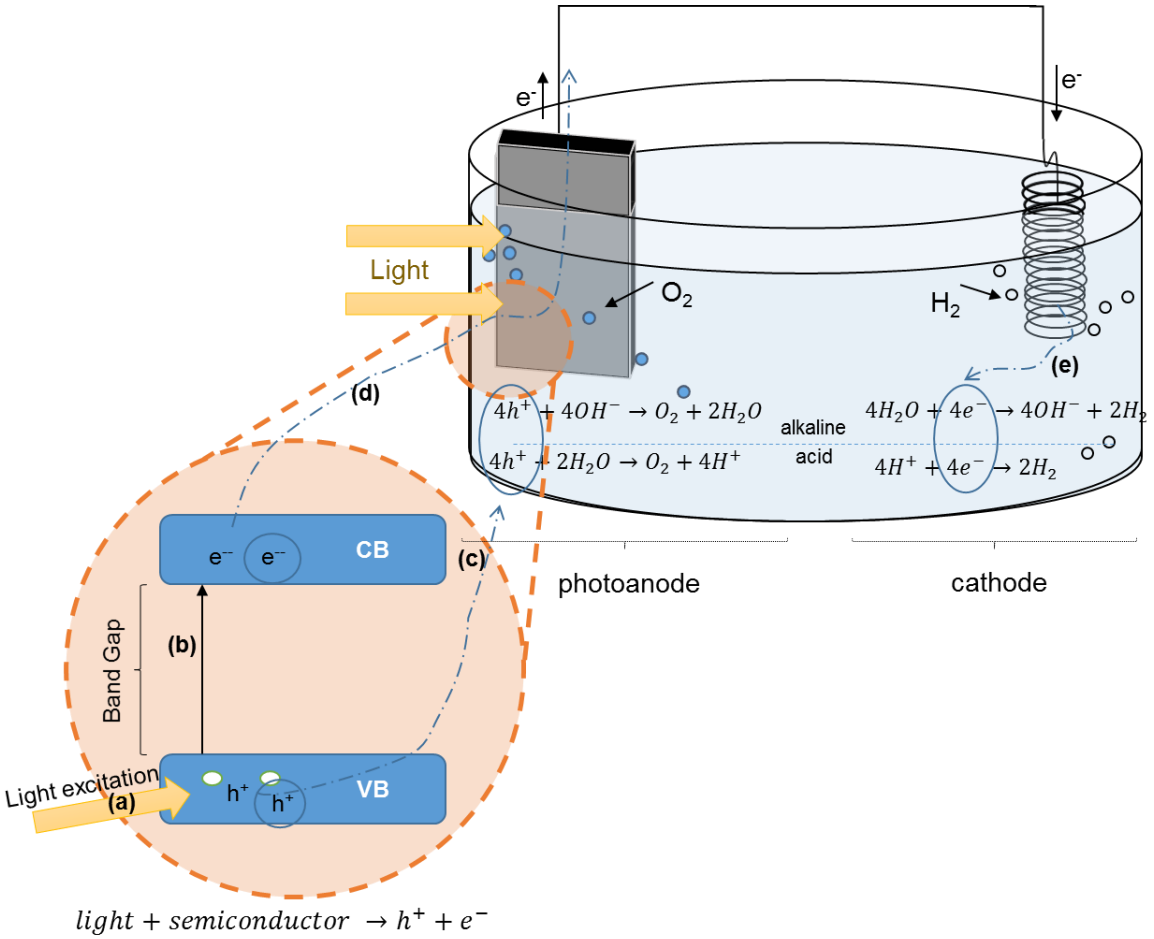

Figure 1.1: The PEC cell, reactions taken place in the photoanode and cathode in alkaline and acidic medium are shown, as well as the photoelectrocatalytic process in the energy bands of the semiconductor, (a) light excitation of electrons in the valence band (VB) to (b) the conduction band (CB), (c) oxidation reactions with the holes at the anode, (d) movement of the electrons from the anode to the cathode and (e) reduction reactions with the electrons at the cathode.

The first two conditions previously exposed are dependent of the photoactive electrode used, while the last one depends on the electrolyte conditions. Currently, the electrolyte conditions are standardized in order to facilitate the comparison of the performance of different electrodes [13]. Commonly used conditions include the use of a deionized water solution of 1 M KOH and absented of any sacrificial agent [13]. On the one hand KOH must be present to reduce the resistance of the solution (it acts as a supporting electrolyte). On the other hand, if a sacrificial agent is present, the oxidation of the substance increases the overall efficiency of the cell by delivering additional electrons to the anode [14]. The main objective of the standard conditions is to ensure that only the effect of the electrode in the PEC cell performance is studied. This is important, considering that the best way to improve

the PEC technology and bring it closer to commercial use is to increase the performance of the electrodes [5]. The electrolyte used in this thesis in the PEC cell is a degassed deionized water solution of 1M KOH.

The PEC cell performance can be calculated by directly measuring the mass or volume of the produced hydrogen, or by measuring the current that flows between the anode and the cathode [13]. The direct measuring requires the use of chromatography and sealed cells in which all the hydrogen generated can be accumulated. The measurement of the current is an indirect method to determine the PEC cell performance, by using this method the researcher also assumes that all the electrons that move from the anode to the cathode will be converted to hydrogen, which has been proven true when the cell operates with the standardized electrolyte [13]. Then, the PEC performance can be calculated with the equation 1.3 [2], where η is the PEC efficiency, *I* is the current generated by the PEC cell and normalized by the area of the anode (denominated current density), V_{redox} is the redox potential of the water 1.23V and P_{in} the input power of the cell, it is the light intensity irradiated on the photoanode (also per unit of area). The measured current density not necessarily will correlate to hydrogen produced, according to the equation (1.4), since some losses may be present too, due for example to thermal dissipation.

$$\eta = {IV_{redox}}/{P_{in}} \tag{1.3}$$

$$4H_2O + 4e^- \rightarrow 2H_2 + 4OH^- \tag{1.4}$$

Equation 1.3 is a ratio of the generated power IV_{redox} to the supplied power P_{in}. In 1.3 it is assumed too that the potential between the electrodes must be at least 1.23V in order to split water. If an additional bias or voltage V_{bias} is applied externally between the anode and the cathode, the power used IV_{bias} must be subtracted from the output power IV_{redox}.

An additional V_{bias} is applied to the PEC cell to increase its performance. It can be used if the CB level is not negative enough to reduce water, and also to reduce the recombination of the photogenerated electron/hole pair (e^-/h^+) [15]. The electrons in the CB can return to the VB by recombining with the holes and generating heat (eq. 1.5), reducing the amount of active sites available to oxidase and reduce the water.

$$h^+ + e^- \rightarrow heat \tag{1.5}$$

Indeed, the recombination rate of the electron-hole strongly determines the overall efficiency of the PEC cell, that is why much of the work in the improvement of the photoanode focuses on the reduction of the recombination and the minimization of the external voltage that must be applied to ensure high efficiency [5].

Titanium Dioxide

The photoactive semiconductor most researched for PEC applications is the TiO_2, commonly referred to as titania. TiO_2 was firstly used for water splitting by PEC in 1972 [16]. Titania accomplishes the conditions to be the photoanode in the PEC cell: it is photoactive, its bandgap is higher than 1.23eV and the energy levels of the VB and the CB are positive and negative enough to split the water molecule [17]. Also, titanium is an abundant mineral, and the oxide is nontoxic and highly photostable [17]. However, the TiO_2 can only generate e^-/h^+ pairs by action of UV light, it is, it can only use less than 7% of the solar light that reaches the surface of earth. This is due to the high band gap (BG) of the photoactive crystal structures of the oxide, 3.0 and 3.2 eV for rutile and anatase, respectively [17]. In figure 1.1 the light can only promote the electrons from the VB to the CB if the energy transferred is higher than the BG. With band gaps higher than 3.0 eV, only light with wavelength lower than 380 nm (UV light) activates the TiO_2. Research is ongoing to reduce the band gap, while keeping the photostability of the material, typically by doping the oxide, or using dye sensitizers or multimaterials with other photoactive semiconductors of lower band gap [17]–[21].

Another major obstacle to tackle to increase the efficiency of the semiconductor is the recombination rate of the electron-hole. Some tested strategies include the use of doping elements to generate trapping sites for the electrons below the CB (like fluorine), and also the use of nanostructured TiO_2 [10]. The use of titania nanoparticles or nanostructures increases the surface area of the semiconductor, and in turn increases the number of possible sites for the water adsorption and oxidation [15]. If the water oxidation rate is increased, the photogenerated holes are consumed faster, and less are available to recombine with the electrons (eq. 1.4).

TiO_2 nanotubes and anodization

TiO_2 nanotube arrays are especially attractive to be used as photoanodes in the PEC cell. If the titanium dioxide is nanostructured as tubes, as presented in figure 1.2, not only the amount of area exposed to the electrolyte increases (as compared to the same oxide

volume in a thin film), but also, a unidirectional path for electron movement is favored [22]. This 1-D path reduces the recombination rate of the electrons: while the holes are preferentially moving to the tube surface, the electrons travel in a single direction to the bottom of the tube and to the cathode. Indeed, higher efficiencies have been obtained with photoanodes composed of TiO_2 nanotubes than when the oxide is distributed in a thin film [23]. Considering this, the morphology of the nanotubes (tube length, diameter, wall thickness, roughness) defines the material performance [17], hence it is desired to have high control on the nanotube morphology.

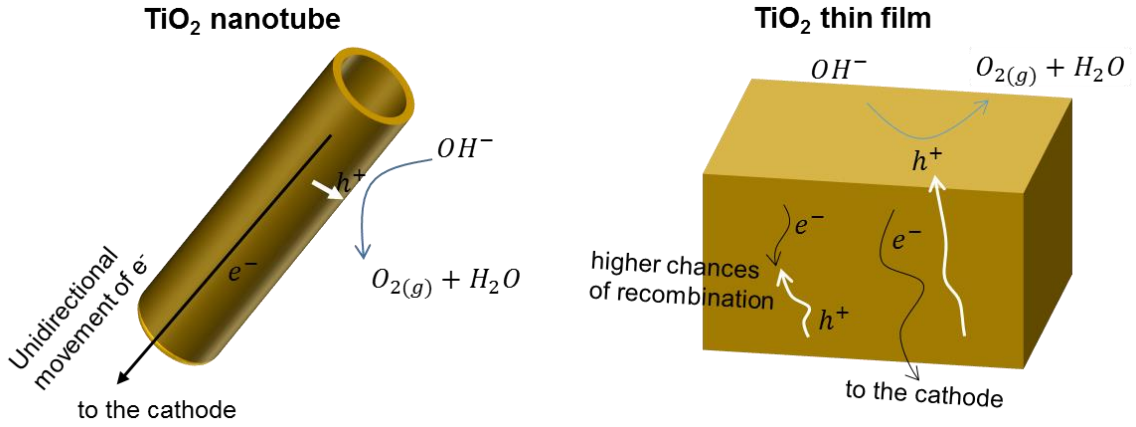

Figure 1.2: TiO_2 as nanotube and as thin film, sketch of the movement of the photogenerated holes and electrons in each case

Currently, the highest control of the TiO_2 nanotubes morphology can be obtained by preparing the material by anodization method. With anodization, tubes of up to 1 mm length have been obtained [24], and with outer diameter from 20 to 800 nm [25]. Also, the anodization is a very convenient technique, it is simple and cost-effective, it is already an industrial process used in the treatment of aluminum surfaces for other applications [26].

To produce titania nanotubes by anodization, a titanium foil is connected to a cathode, both electrodes are submerged in an electrolyte solution and a voltage is applied between the cathode and the anode by an external power supply, see figure 1.3. The composition of the electrolyte determines if nanotubes are formed or not. Such composition has evolved over time [15], [27], but nowadays the highest morphological control has been achieved in solutions of ethylene glycol, containing water and small amounts of ammonium fluoride [15].

By anodizing a titanium foil, highly organized arrays of titania nanotubes perpendicular to the foil surface are dug. When the voltage is applied an electric fields attracts oxygen (from

the water) and fluorine ions to the surface of the metal, O^{-2} oxidizes the metal, and simultaneously the fluorine dissolves that oxide, creating a porous oxide. The formed pores evolve with time and become packed nanotubes [15]. Figure 1.3 includes the reactions taking place during the anodization on the anode, needed to form the TiO_2 nanotubes, as well as images of the nanotubes produced for this thesis.. More information related the TiO_2 nanotube array formation mechanism can be found in the following selected bibliography [15], [27], [28], it is necessary to address that there is not consensus on this topic.

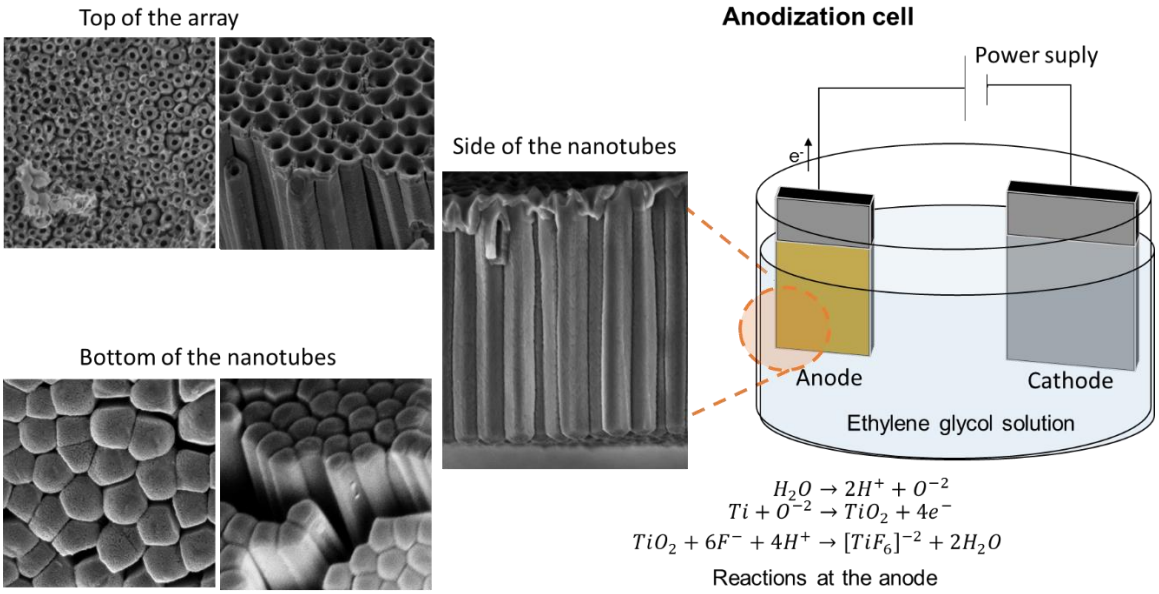

Figure 1.3: The anodization cell, reactions at the anode in a system with water and ammonium fluoride, and formation of TiO_2 nanotubes

The anodization conditions, including electrolyte composition, pH, temperature, stirring, applied voltage and voltage's time determine the morphology of the nanotubes, and usually more than one morphological feature is modified at the same time by a single anodization variable [10], [15]. For example, the magnitude of the applied voltage determines the tube diameter, tube length as well as the top morphology of the array [29]. Due to this convoluted change in more than one morphological feature, the material performance is typically related to the modified anodization condition [29]–[32], and not to the nanotube morphology. Some models [33] and experimental observations have tried to explain the role of each morphological feature in the performance of the material, but more experimental data is needed for validation, especially data with independently varied morphological features, otherwise discrepancies in the conclusions emerge [10].

The nanotubes in image 1.3 were produced by constant voltage anodization, it is, a constant voltage was provided during the whole anodization, those tubes possess smooth outside walls. If the voltage is alternated between a high and a low voltage, the process is known as alternating voltage (AV) anodization, and new morphologies are obtained, including multiple layers of nanotubes and nanotubes with bamboo-like morphology [27]. The bamboo-like nanotubes are nanotubes with periodic rings on the outside wall of each tube, which bundle all the tubes among each other (see figure 1.4). Some authors report that bamboo-like morphology nanotube have a higher surface area than tubes with smooth outside walls [34], [35], and that the PEC performance of the former ones is higher [35]–[37]. However, more research is still needed to fully explain the mechanism of such improvement. That research must make sure to not vary more than one morphological feature with the one produced by alternating voltage anodization (rings).

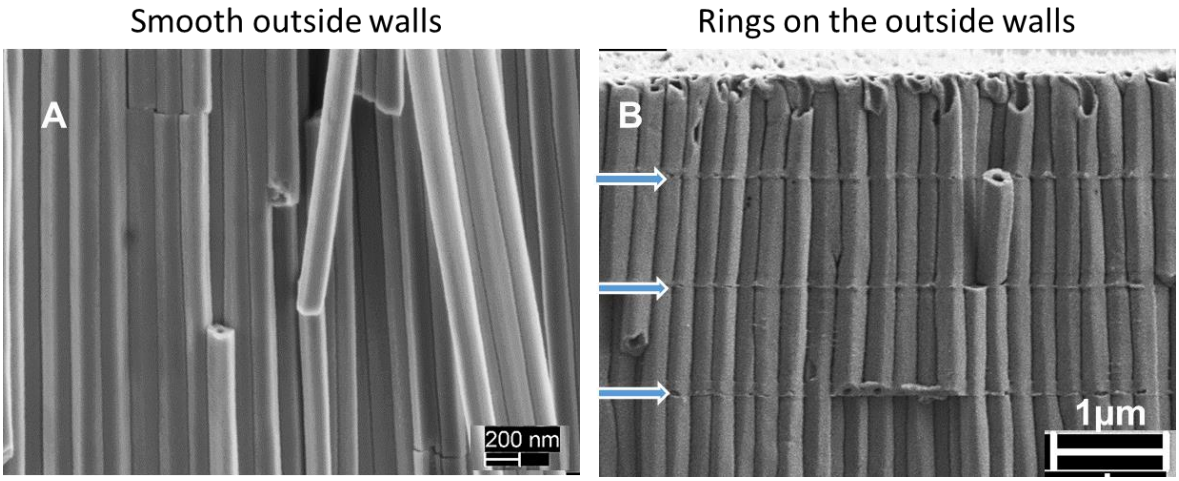

Figure 1.4: Nanotubes with smooth outside walls (A) and with rings on the outside walls (B)

The applied voltage in the PEC cell – TiO_2 nanotubes

As previously mentioned, a V_{bias} can be provided to increase the performance of the PEC cell, such is the case of the cells with TiO_2 nanotube arrays. When a voltage is applied between the anode with TiO_2 nanotubes and the cathode, the electric field enhances the unidirectional movement of the electrons in the tube (see figure 1.2) and reduces the recombination rate, increasing the overall PEC performance. The magnitude of the voltage applied strongly determines the cost of the hydrogen produced, it is related to the cost of electricity [5]. Additionally, if the electricity used is provided by the electric grid, the PEC cell will indirectly generate CO_2. In order to avoid this problem some authors have suggested

the coupling of the PEC cell with other sources of energy. Typically, green emerging technologies are preferred [38], [39], including those with low voltage output. Two of these interesting technologies are studied in this work, photo-fuel cells and power generators from the corona effect between the clouds and the Earth's surface.

The phofo-fuel cell uses a photoactive semiconductor to oxidize organic compounds, similarly to figure 1.1. Then this technology can also employ TiO_2 nanotubes [12] (with the advantages of the materials previously mentioned) and degrade an organic pollutant at the same time [40]. In other words, it is possible to treat wastewaters and produce electricity simultaneously, and that electricity can power the PEC cell. The second technology uses electrodes to harvest the corona discharge produced between the clouds and the earth and convert it to electrical power. Such corona discharge is a natural phenomenon that happens frequently from the clouds and from trees or other structures on the earth surface. More details of the PFC are provided in chapter 5, while information about the corona effect can be found in chapter 6 and in [41], [42].

In this work, the effect of nanotube morphology on the PEC efficiency was researched and a dual-cell reactor system was proposed, in order to generate hydrogen independently from the power grid. In chapter 2 the anodization process is standardized in order to obtain nanotubes with tailored morphology (tube length and diameter). Then, the effect of tube length and diameter was studied and modelled in chapter 3. In chapter 4 nanotubes of length and diameter of the highest PEC efficiency obtained in chapter 3 were produced by alternating voltage anodizing, hence were modified with rings on the outside walls. The number of rings was varied to study its influence in the PEC efficiency. In chapter 5 a photo-fuel cell using TiO_2 nanotubes was optimized and coupled to the PEC cell to produce hydrogen autonomously (independently from the power grid). Finally, chapter 6 studies the use of electricity generated by the corona effect to power the PEC cell.

Chapter 2.

In order to study the effect of nanotube morphology on the efficiency of the PEC cell, a standard two-step anodization protocol was developed. The protocol allows the independent variation of the tube length and diameter, tube morphological features studied in the next chapters. The protocol presented next also avoids the interference of the irregular porous oxide that typically remains on top of the array, varies simultaneously with other morphological features and reduces the material's performance.

Chapter 2. Two-step anodization protocol: Fabrication of TiO_2 nanotube arrays with independent diameter and length

Abstract

Tubes prepared by one step anodization typically are covered by an irregular top surface layer, which is dependent of the anodization conditions and interferes with the performance of the material. Two-step anodization was used to obtain nanotubes with uniform top surface, allowing independent manipulation of the tube length and diameter. Tube length and tube diameter were adjusted by controlling anodization time and water content in the ethylene glycol solution, respectively, in anodizations at 100 V. Results can be used to study the independent effect of tube length and diameter in the multiple applications of the material.

Introduction

Titanium dioxide nanotube arrays produced by anodization have been widely investigated since their discovery in 1999 [43] due to their broad range of applications. Photoelectrocatalytic (PEC) water splitting [44] and treatment of aqueous and atmospheric pollutants [39], electricity production by dye sensitized solar cells [45], biomaterials for implants and drug delivery systems [46], and electrical energy storage devices [47], are some of the most remarkable applications that can be listed. Particularly, PEC applications benefit highly from the material's characteristics, including its near-1D structure that allows single direction electron flow, and also its high photo stability, and non-toxicity [22].

Most of the work produced during this century has been focused on the understanding of the highly organized structure formation, correlation of anodization parameters (voltage, anodization time, and temperature and electrolyte composition) with nanotube morphology (length, diameter and wall thickness) and with the performance of the material in different applications. Examples can be found in our recent publication [28] that proposes a model to predict tube length from voltage applied, anodization time and initial water and ammonium fluoride content in the electrolyte, and in the work by Ampelli et al. [48] and Ni

et al. [25] that correlates tube diameter and length to voltage applied. However, because a single anodization condition influences more than one morphological feature, the majority of the produced research does not relate the material's performance to its morphology, but to the modified anodization parameter. For example, Sun and Yan [29] reported PEC material's response as a function of the anodization voltage, a variable that impacts simultaneous tube diameter, length and top morphology. Some models have been developed to predict isolated effect of morphology [33], based on expected effects on the amount of light absorbed, electron movement in the bulk material, and surface area among others. Experimental data is still required to validate such results. Those experiments must avoid the convoluted effect of simultaneously changing morphological features, which is considered a difficult task [10], [33].

It is proposed here a standard anodization protocol which allows independent control of two different morphological features: tube length and diameter. The independent manipulation of the tube length and diameter allows the accurate study of their effect in the material's performance. Therefore, our work in this chapter does not aim only to relate anodization conditions and morphological features, but to standardize the fabrication method then, in the following chapters, the influence of tube length and tube diameter will be directly related to material's efficiency in PEC application.

Experimental

Titania nanotube arrays were produced by a two-step constant voltage anodizing procedure. Titanium foils (0.05 mm thick, Gallium Source) were used both as anode and cathode. Electrodes were rectangles of 1 cm x 4 cm and 1.6 cm x 4 cm for anode and cathode respectively. Prior to each anodization electrodes were separately washed with ethanol and then with deionized water, and dried with pressurized air; cleaning process was repeated until a mirror like surface was achieved. Care was taken to avoid further contact of electrodes with uncleaned surfaces. Additionally, after drying, the foils to be used as anode were partially covered with Polyester tape (MightyHook) to avert foil destruction. Only the front central section of the anode facing the cathode was left uncovered. The back section as well as approx. 2 mm from each edge of the anode were covered.

Foils were submerged ca. 2 cm deep, facing each other 2 cm apart in ethylene glycol (Merck, ≥99.5%), deionized water and ammonium fluoride (Sigma-Aldrich, ≥98.0%)

solution. Used compositions are depicted in Table 1. 100 V constant voltage was applied with a programmable power supply (BK Precision XLN15010) and current data were recorded with a UNI-T UT71B Multimeter. Applied potential was held during different times. One step anodizations were always performed in fresh ethylene glycol solutions. While the second step of two step anodizations were made in the solution used during the first step. Upon the ending of the first step anodization, the anode was submerged in deionized water and put in a sonicated bath for 2 minutes, obtaining a mirror-like surface in the anodized electrode. Later the same foil was dried with pressurized air and used again in a second anodization (second step), using the same aged ethylene glycol solution. At the end of the two step anodizations anodic foils were submerged in ethanol to remove ethylene glycol solution and remaining ions, and then dried with pressurized air.

Table 2.1: Experimental conditions used, EG solution composition and anodization time for 1st and 2nd step anodization. All anodizations were performed at 100V

Set of experiments	**Initial composition in fresh EG solution (before first step)**		**Anodization time**	
	Water (%)	**NH4F (%)**	**1st step (min)**	**2nd time (min)**
1	3.8	0.15	6	1.5 - 17
2	6.9	0.20	16	3.2 - 24.2
3	10.0	0.25	84	11 - 300

Samples of each anodized foil were taken to perform morphological characterization. Scanning electron microscopy (SEM) was perform in a Zeiss Neon 40, taking images from different areas of the sample and at different magnifications, at a working distance of ca. 3 mm, a voltage of 2 kV and using an aperture of 30 µm. Serial sectioning of a sample was carried out using Focused Ion Beam (FIB) in order to evaluate the structure of the nanotube array. FIB used an energetic gallium (Ga) ion beam operating at 30 kV with a beam current of 10 pA.

Length, inner and external diameter and wall thickness were established from images collected in the SEM. Length reported was the longest measured in side view images were nanotubes were complete (when the upper and bottom sections of the arrays are present). Diameters and wall thickness were also measured from side view images of the nanotubes at high magnification, reported values are the result of statistical data analysis and definition of 95% confidence intervals of measures collected from multiple tubes.

Results and Analysis

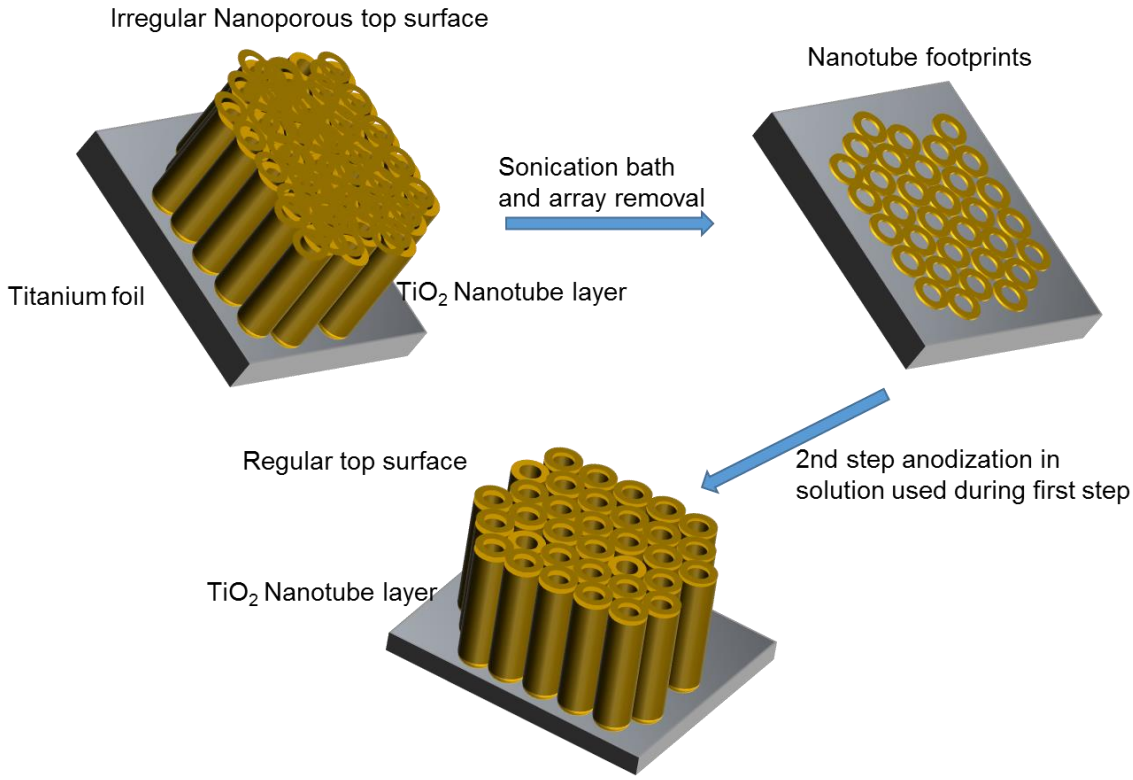

Figure 2.1: Two step anodization

Top morphology: One step anodization vs. two step anodization

Figure 2.1 depicts the changes that take place on top of a titanium foil during two step anodizations. Foremost, tubes hexagonally packed, all of them with nearly the same length and diameter, growth by consumption of the metal during a first anodization. Also, the whole array is covered by an irregular nanoporous top surface, created at the beginning of the anodization. Then, when the anodized foil is submerged in deionized water and sonicated, the nanotube array is detached, leaving an organized surface on the titanium foil composed of the nanotube footprints. Finally, by anodizing the same foil again (with only footprints), a new TiO_2 nanotube layer is created, now with a regular top surface.

Avoidance of the irregular porous top morphology is the first purpose of two step anodization, since this may affect the performance of the material. Titanium dioxide nanotubes are a promising catalyst and catalyst's support, and their porosity and surface area can be controlled by changing tube's diameter and length [49]. Nevertheless, an irregular top surface may also function as a barrier for substances moving from or to the

tube's inner pores. Additionally, top morphology changes the reflectivity of the layer [17], therefore the amount of light that can be harvested. Figure 2.2 shows SEM micrographs of a sample produced at 100 V, 10% water and 0.25% ammonium fluoride in ethylene glycol by one (A) and two (B) steps anodization. Images are at the same magnification, and the external and inner diameter of the tubes below the porous layer are ca. 300 and 100 nm respectively. The top of the tubes of the sample produced by one step anodizing (A) was covered with a layer of significantly smaller and more irregular pores than the top of the array produced by two step anodization (B).

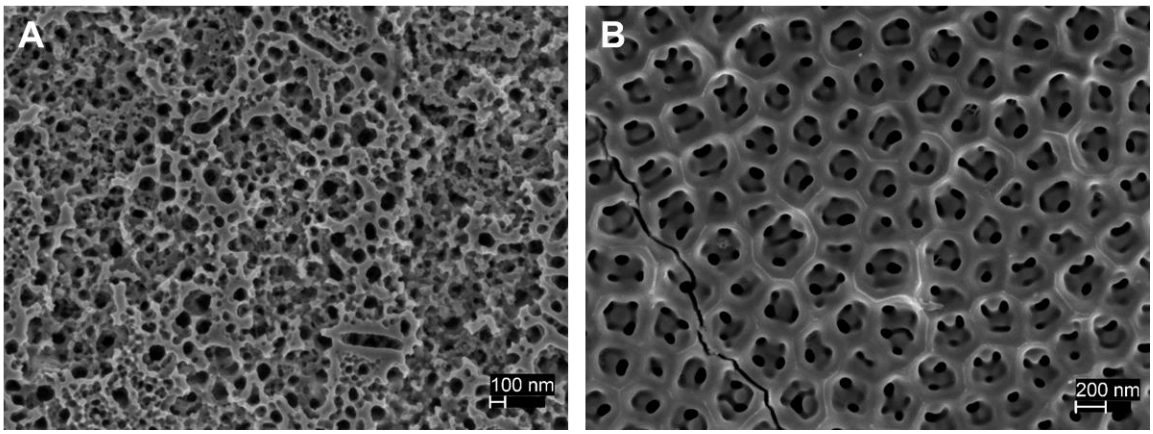

Figure 2.2: Top morphology of nanotube array produced by one (A) and two (B) step anodization

Additionally, it is also necessary to avoid this porous top layer to independently study other morphological features of the tubes. Figure 2.3 illustrates this, (A) and (B) are images of top morphologies for one step anodizations, while changing water content, which above 4% is proportional to tube diameter[50].

Tube diameter increased approximately 40% (same as wall thickness) when water concentration was raised from 6.9% to 10%, but the pores at the top of the array did not change at the same rate (figure 2.3 (A) and (B)). In fact, there is a change in the degree of organization of the topography, which implies that two variables were modified: tube's diameter (below the porous layer) and top morphology. In this case any study of material's performance in function of the tube morphology would be a result of the convoluted effect of diameter and top morphology. That is not the case when two step anodization is used. Figure 2.3 (C) and (D) shows the same water concentration change in electrolyte composition for samples produced by two step anodization, now not mayor change in level

of organization of top morphology is seen, only pore size changed in the regular top surface, and change was proportional to 40% diameter change.

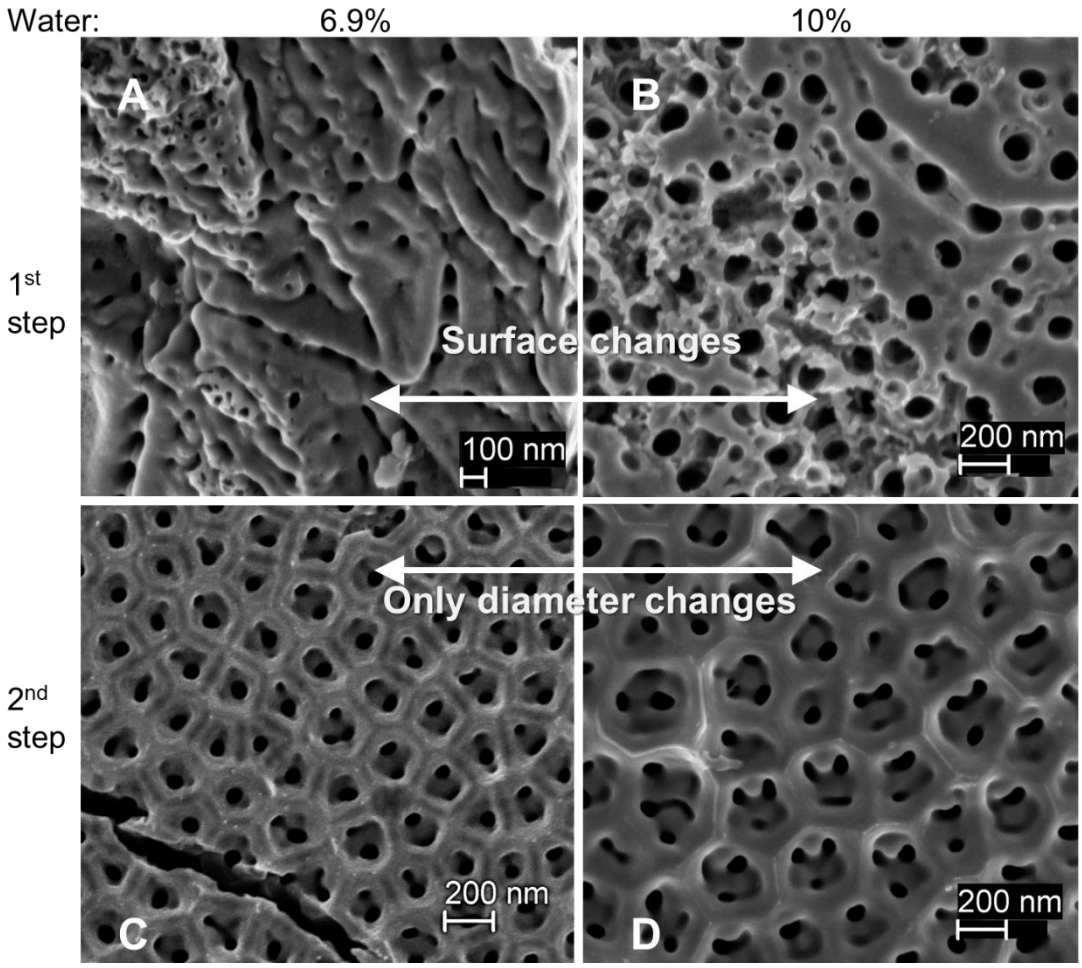

Figure 2.3: Top morphology of samples produced by one (A, B) and two (C, D) steps anodization in electrolytes with varying water concentration

Same codependence of porous top morphology with tube diameter and with tube length has been reported while changing voltage applied or anodization time. Regonini and Clemens [51] reported that change in anodizing time varied tube's length, and also the top morphology covering the array, from nanoporous (like the one observed in figure 2.3 (A)) to nanograss, which is generated when the upper part of the tubes is strongly dissolved. Under this circumstances Regonini and Clemens preferred to refer change in PEC properties to anodizing time, and not to tube length. Similar phenomenology was reported by Sun and Yan's work [29], who studied influence of anodization voltage in PEC efficiency,

since this parameter changed tube length, diameter and top morphology at the same time. More reports with similar codependence can be found in literature [30].

Other efforts have been reported to diminish the variability of the top morphology with the anodization conditions or to detach only the porous layer after anodization, such as strong electro and chemical polishing of titanium foil's surface prior anodization or sonication of the anodized foil [52]–[54]. These strategies require the use of more equipment and supplies, or may break apart -no uniformly- the formed ceramic nanotubes. Although no preliminary step is the most desirable scenario, two step anodization is a very promising option: it does not require the use of different equipment, neither a fresh ethylene glycol solution, and detached tubes may have other uses, including cheaper particulate catalyst or material for composites [55], and even membranes, if tubes are properly detached [56].

Two-step anodization

Top morphology of nanotube arrays produced by two step anodization is more regular due to the organized footprint left after sonication and removal of tubes produced during first anodization [57]. Han and collaborators call it self-templating multi-step process [58]. Formation of an irregular top morphology after a first anodization is part of the nanotube layer growth mechanism, and depends on anodization conditions. This is the initial phase of anodization: formation of pores due to simultaneous oxidation of the metal surface and dissolution of the created oxide, due to presence of oxygen and fluorine ions respectively, which in turn are attracted to surface of the foil by the applied electric field [15]. When the anodization starts from a templated surface, as happens in a second step anodization, the phase of random pores generation is minimized: tube formation starts earlier. This is due to the morphology of the footprints: hexagonally packed nanobowls, see background of figure 2.4 (A), which correspond to the closed rounded bottoms of each tube [59], see figure 2.4 (B). This morphology creates a uniform field at the surface when voltage is applied [44], and contains points of lower resistance (central of the bowl) to which ions are strongly attracted, and from which new tubes will start growing [57], [60].

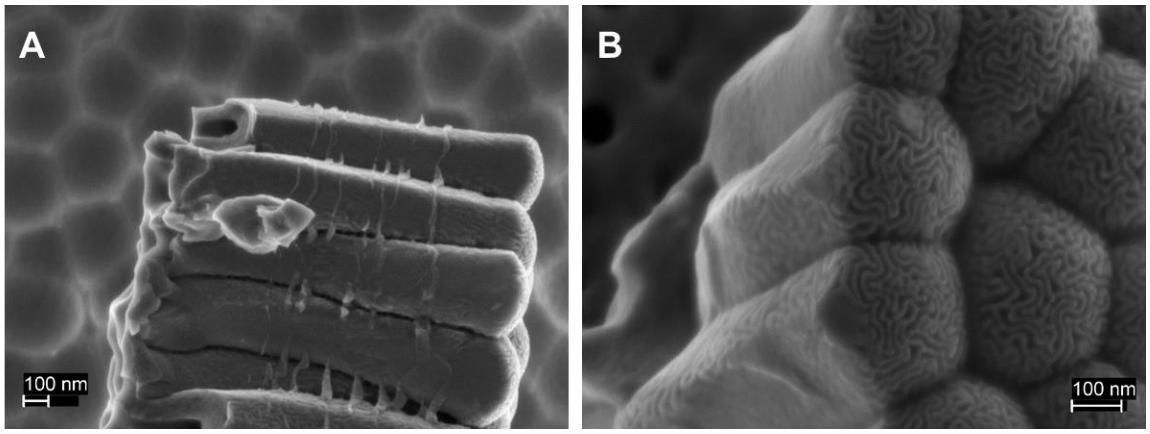

Figure 2.4: SEM micrograph showing rounded nanotubes' bottom (B) and footprints (background of A). Tubes were produced at 100V in EG solution 10.0% water and 0.25% NH_4F

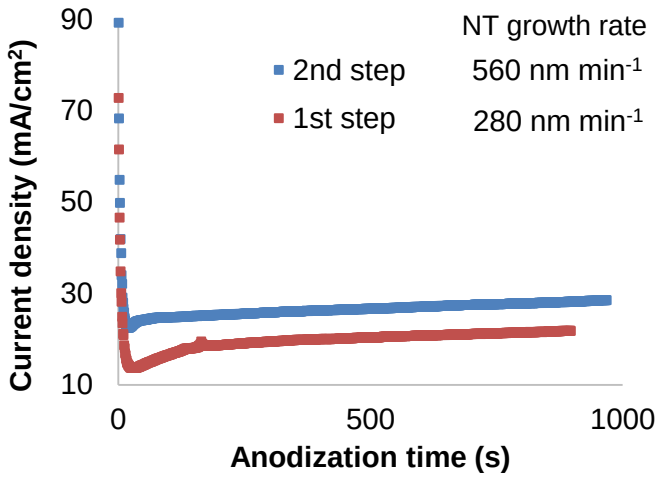

Figure 2.5: Current density during first and second step anodization at 100V in EG solution with initial water content 6.9% and ammonium fluoride 0.20%

Improvement in the growing rate of the nanotubes produced by two step anodization is evident when comparing recorded current and growth rate of the tubes, see figure 2.5. Current transients can provide information of titania nanotube formation [15]. Firstly, when voltage is applied current decreases as an oxide layer stars growing on top of the metallic anode. Then, current reaches a minimum and starts increasing, due to reduction of the oxide layer and its resistance i.e. formation of porous layer. Finally, depending on the anodization conditions, current density may increase, decrease or be almost constant during stable growing of the nanotube layer. In any case, current density can be correlated to the amount of oxide formed:

$$Ti \rightarrow Ti^{+4} + 4e^{-} \quad (2.1)$$

$$Ti^{+4} + 2O^{-2} \rightarrow Ti_2O \quad (2.2)$$

Figure 2.5 presents the current density during anodization when one and two-step protocol were used. Current density during first step anodization was lower than recorded during second step anodization, suggesting an increase in oxide formation rate (eq. 2.2) under second step anodization conditions, this was observed for all samples prepared. Similarly, nanotube layer growth rate was higher during the second step anodization, for instance, for anodizations performed at 100 V in 6.9% water and 0.20% NH_4F EG solution, growth rate during first step was calculated to be ca. 280 nm min^{-1}, and 560 nm min^{-1} during second step anodization. The oxide growth rate was calculated by relating the final measured length of the nanotubes to the anodization time.

Finally, there may be an additional benefit from two step anodization: fluorine doping, which is desirable to increase materials photocatalytic performance [61]–[63]. Figure 2.4 (B) details the front line of tube growing, the tube's bottom. It is a porous region with brain-like morphology, which is rich in fluorine ions [25]. Also, the bottom of the tubes is covered by a fluoride rich oxide layer of few nm [64]. Supposing that some of this fluoride rich oxide remains after the nanotube removal and is part of the nanotube footprints, the fluorine may remain in the top surface of the arrays produced in the second step anodization, and dope it. Consider that part of the footprints or nanobowls left after removal of the nanotubes is the organized top surface of the array produced in second step anodization (see figure 2.3 C and D).

To the best of the author's knowledge, this hypothesis has not been specifically studied, although some reports suggest that no fluorine remains after thermal treatment of the material [64], [65]. Such thermal treatment is mandatory to obtain crystalline and photoactive nanotubes, then to use the material like photo and photoelectrocatalyst. Zhang and collaborators studied material's performance in PEC water splitting on nanotubes produced by one and two step anodization [44], they found that arrays with regular top morphology had 2.5 times higher efficiency than those produced by one step anodization. In their work, tubes had the same length and diameter (independently if they were synthesized by one or two step anodizations), thus efficiency change was attributed to effect of top morphology. Although this result may also support the proposed F doping

hypothesis during two step anodization, no presence of elements beyond Ti and N was detected during EDS of the foil surface with only footprints. Other elements may be present, but not detected by EDS in FE-SEM, due to a big interaction volume during the analysis. Detailed and local composition analysis are still needed to support or disprove our hypothesis.

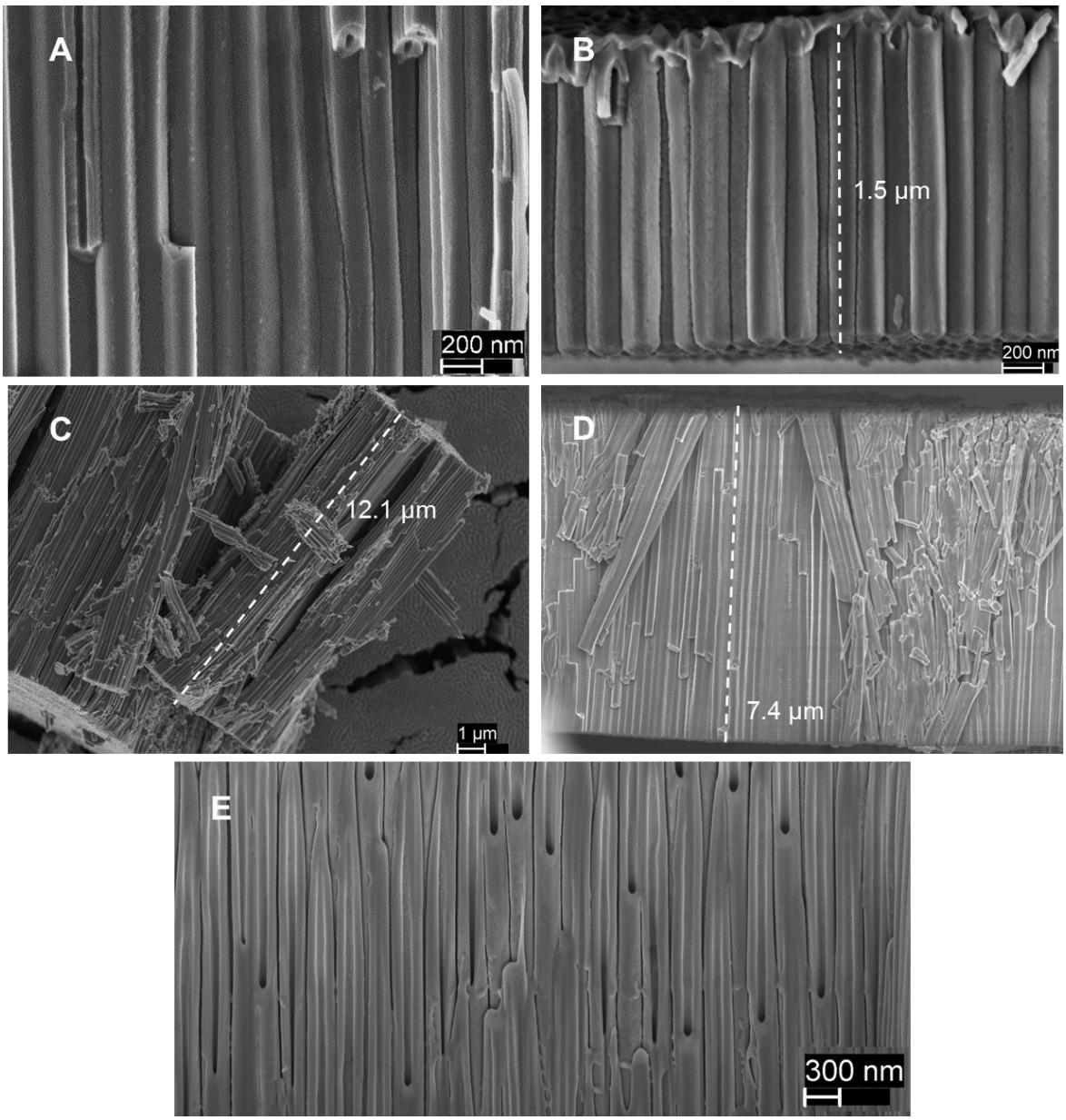

Figure 2.6: Side view morphology of TiO_2 nanotube arrays produced by two step anodization. Images (A) - (D) were taken from random points of the samples. Image (E) was acquired after cutting off a section of the array with FIB. Samples (A) and (B) were anodized with aged ethylene glycol (EG) solution (used first step) with initially 3.8% water

and 0.15% NH_4F. Sample (C) and (D) in aged EG solution with 6.9% water and 0.20% NH_4F

Morphology control: Diameter and length as independent parameters

Having obtained the desired morphological feature on the top surface of the nanotube array by the two step anodization, procedures to independently control the length and diameter of the nanotubes were investigated. Diameter was modified manipulating the electrolyte initial water concentration, and length by varying anodization time.

Figure 2.6 (A) - (D) shows typical SEM images of the prepared samples. Care was taken to examine nanotube arrays that were suitably oriented during imaging so that wall thickness, inner and outer diameter as well as tube length could be measured. All tubes presented almost the same diameter and length. Tubes had a continuous inner pore, evident in figure 2.5 (A) where a tube conveniently broke before characterization. Existence of inner pores along the tubes was also verified by cutting off sections of an array (using FIB), see figure 2.6 (E). Change in length, diameter and wall thickness for all samples is depicted in Figure 2.7. Notice that the error of the prediction model is 15% for length in all anodization conditions; the error of the diameters and wall thickness was calculated with a 95% confidence interval of multiple measurements.

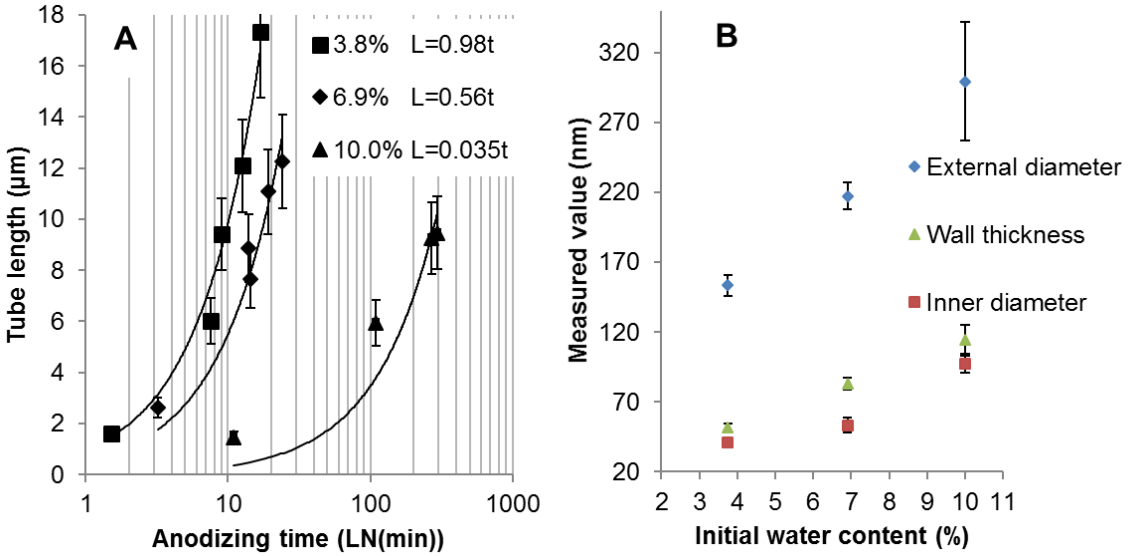

Figure 2.7: Two step anodization produced tube's length (A) and diameter (B) as a function of anodization time (A) and initial water concentration of EG solution used during first step

anodization (B). Linear growth rate equation in (A) correlates tube length [µm] and time [min]. Anodization conditions are depicted in table 2.1

Array's length changed linearly with anodization time for each concentration of water used, as shown in figure 2.7 (A). Anodization time is presented in logarithmic scale since anodizations in 10.0% water content were longer (up to 5 hours), due to a reduction in the growth rate of the nanotubes. Calculated growth rate was 980, 560 and 35 nm min^{-1} during second step anodization in used EG solutions with initial water concentration of 3.8, 6.9 and 10.0% respectively. None of the samples presented nanograss formation on top of the array (or any other morphological change at the top), which may occur when the top of the tubes is strongly dissolved. Inner and external diameter and wall thickness changed linearly with the water content of the solution, as can be seen in figure 2.7 (B). Reported water concentration is the initial amount in each fresh EG solution used during the corresponding first step anodization of every sample prepared.

The detrimental effect of water in growth rate can be explain by a reduction of the electric field and conductivity of the formed titanium dioxide. It has been reported that cell diameter (wall thickness and diameter) is directly proportional to the thickness of the rounded bottom of the tubes[50], and as reported by Yin and collaborators [50] and in this work (figure 2.7 (B)), wall thickness increases with water content. In turn, a thicker oxide at the bottom of the tubes, means a weaker electric field, and a slower oxidation and oxide dissolution rate. Also, when water content in the electrolyte increases, the created oxide is more stoichiometric, and its conductivity decreases, diminishing the ions flux through it [66].

As reported by other authors [22], [31], inner diameter and wall thickness varied along the tube. In fact, morphology of the tubes is closer to a cone, with thinner walls at the top and thicker ones at the bottom, see figure 2.8. Top of the arrays dissolves because of presence of fluorine ions in the solution, although dissolution rate is much smaller than that at the bottom of the tubes. This dissolution is the same that can create nanograss structure when walls are consumed and the structure loses stability [22]. Variation in wall thickness and inner diameter was found in all prepared samples.

Figure 2.8 shows formation of 'ribs' along the outside walls of the tubes, in contrast to the smooth surface of nanotubes' walls in figure 2.6. This ribs were only present in samples produced in aged EG solution with initial water content of 10% (figure 2.8). Ribs formation has been found before when anodizing in high water content electrolytes, and are believed

to form due to current instability [67] and oxygen bubbles evolution [68]. Some authors report that presence of ribs generated by alternating voltage anodization or by anodization in aqueous solution increases surface area and performance in dye sensitized solar cells [35] or act as efficient charge carrier trap [10], respectively. Hence, ribs' presence should be considered as a different morphological feature: outside wall roughness.

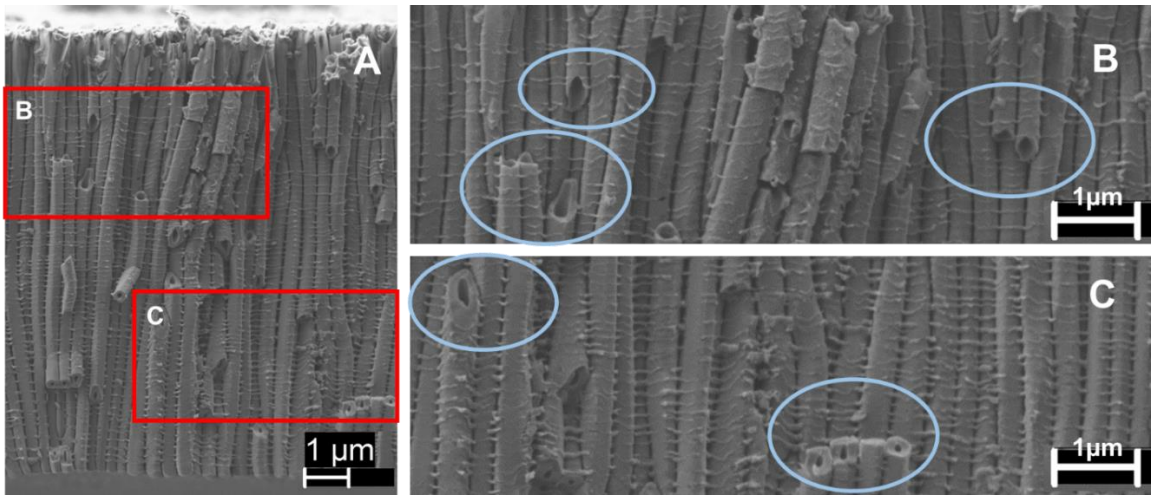

Figure 2.8: Change of wall thickness and inner diameter along the tubes (A), at upper (B) and dower (C) sections. (B) and (C) are amplified sections in (A) and are noted with a red square. Blue circles in (B) and (C) indicate broken tubes with different wall thickness. Sample was produced by two step anodization in aged EG solution 10% water and 0.25% ammonium fluoride at 100V and 5 hours

Only tube diameter and length varied when controlling initial water content up to 6.9% and anodization time. For anodization solutions with higher concentrations of water ribs appeared, changing outside wall roughness. For larger diameters than produced in anodization at 100V in 6.9% water, 220 nm, anodization voltage could be increased. In this work tube diameter was varied with water content since previous experiments [28] showed that at low water concentrations (3.8%) diameter does not vary with voltage beyond 60 V [27] and tubes of large diameter has not been studied deeply . Also, high voltage anodization was preferred in order to obtain high growth rates, previous authors have reported that growth rate increases exponentially with voltage applied [28]. According to literature, other parameters such oxide density may be changing while varying anodization conditions to obtain desired morphology, i.e. water content [69]. These changes are evident when double walled nanotubes are formed after annealing. Such double-walled structure

was not observed in the samples obtained in this chapter and characterized as prepared (no annealing).

Conclusions

A standard fabrication method to obtain nanotubes with independent morphological features: tube diameter and array length, was developed. The method consisted of a two-step anodization protocol, which provides uniformity to the top surface of the array. Length was varied by manipulating anodization time and diameter by changing initial water content in the electrolyte. Results showed that it is possible to manipulate independently length and diameter, so the effect of this variables in material's performance can be studied in the next chapter. Additionally, multiple advantages of two step anodization were presented, including a hypothetical fluoride doping of the nanotube array. This work provides a tool to relate material's performance to its morphology and not to the anodization conditions.

Chapter 3.

Following the anodization protocol and the model relating anodization conditions to nanotube morphology developed in the previous chapter, new samples were prepared in this chapter to study the independent effect of tube length and diameter on the PEC efficiency of the material. Notice that the PEC cell is operating in a standardized electrolyte, this with the purpose to study only the effect of the electrode in the PEC performance of the cell and to directly relate the current density generated to the amount of hydrogen produced.

I should mention too that the PEC cell used in all the following chapters is a single chamber glass cylinder. A PEC cell of this type and the quantification of the photoelecotrcatalytic performance by the amount of electricity produced has been used intensively by other researchers, with very good results. A reliable estimation of the hydrogen produced should consider too the Faradic efficiency of the process, it is the rate of the conversion of the measured electricity to hydrogen, according to reaction (1.4). From this point, the performance of the material will be related directly to the PEC efficiency, as per equation 3.3.

Our attempts to use a cell of two chambers were unfruitful, it was not possible to accumulate and quantify the generated hydrogen to compare the different photoanodes used, due to sealing problems and leakage of the hydrogen. Although with the accumulated hydrogen in a single experiment it was possible to qualitatively determine hydrogen presence (by using a portable H_2 detector, ToxiRAE Pro, RAE systems): the regular amount in the atmosphere was 0 ppm, and it increased to 32 ppm when the inverted burette was opened. The two chambers reactor is presented in the annex 1, and is similar to the one in [29]. New reactors should be completely sealed, similar to the one used by Ishihara et al. in [70].

Chapter 3. Effect of tube length and diameter on the hydrogen production of TiO_2 nanotube arrays

Abstract

A single chamber photoelectrocatalytic (PEC) cell was operated with titania nanotube arrays as the photoanode, the independent effect of nanotube morphology (tube diameter and length) was studied. Maximum PEC efficiency of 18.6 % was obtained with tubes 9 µm long, ~150 nm of external diameter, and ~50 nm of wall thickness. The obtained results were explained following the effect of the morphology in the crystallite size, as well as the effects in specific oxide volume and specific surface area, calculated from geometrical analysis. SEM, XRD and the PEC response of the material were used.

Introduction

Production of hydrogen by water splitting is a very promising technology. Hydrogen is a renewable fuel, able to deliver 120 MJ/kg when burned, and its combustion product is only water [2]. Then, if the energy used to split the water molecule mostly comes from solar light, the carbon footprint of this technology is virtually zero. Nevertheless, most of the current technologies that use solar light to split water into hydrogen are still prohibitively expensive, with prices in the range of 6-19 USD per kg of H_2 [5]. Hence, more research is still needed to reach the target cost of 2-4 USD per kg of H_2 to implement this technology [5], and make it competitive in the market.

Titania nanotubes arrays can be used to produce hydrogen by photoelectrocatalytic (PEC) splitting of the water molecule taking energy from the solar light. TiO_2 is nontoxic and highly photo-stable, and titanium is an abundant material. However, recombination of the photogenerated electron/hole (e^-/h^+) pair reduces its performance, and undoped TiO_2 can only use the 7% of the solar light [71]. To increase the performance of titania nanotubes two alternatives are commonly implemented. First, reduction of the recombination rate of the e^-/h^+ pair. Second, doping of the material, in order to exploit more of the solar spectrum [10].

Most of the work focusing on the reduction of the recombination rate is based on the understanding of the morphological effect of the nanotubes on their performance. Tube diameter, wall thickness and length determine the amount of light that is absorbed (the amount of catalyst) and the electronic properties of the material, i.e. how easily can the photogenerated electrons leave the material, and the holes reach the surface to react with the water. Nonetheless, the independent effects of the morphological features have not been measured experimentally, only simulated [33] or predicted from experimental observation with more than one morphological feature changing at the same time [29]–[32].

With the anodization protocol previously developed, this chapter focuses on the understanding of the effect of nanotube diameter and length on the PEC performance of the material, by manipulating independently each parameter.

Experimental

Titania nanotube arrays were produced following the protocol depicted in the previous chapter. Briefly, titanium foils were two-step anodized at 100V in an ethylene glycol (EG) solution of water and ammonium fluoride. Nanotubes produced during first step were removed to obtain a foil covered in organized footprints, which was anodized again in the same EG solution. Electrolyte composition and second step anodization time were varied to obtain nanotubes of 150, 220 and 300 nm external diameter and 3, 9 and 15 µm long, see table 3.1, according to a factorial experimental design 3^2. After anodization, anode foils were washed with ethanol and dried with air. Prepared foils were then annealed in air atmosphere to convert produced amorphous titania into its photoactive crystalline phases. Heating rate was 2°C min^{-1} until 450°C, and the temperature was held for 2 hours.

Table 3.1: Conditions used to prepare titania nanotube arrays with desired tube external diameter and length. Concentrations of water (W) and ammonium fluoride (A) correspond to measured amount in fresh EG solution (used in first step)

EG solution Water (W) and NH_4F (A) concentrations	**Tube external diameter**	**2nd step anodization time**		
		Tube length		
		3 µm	**9 µm**	**15 µm**
W: 3.8%, A: 0.15%	**150 nm**	2.9 min	8.9 min	14.9 min
W: 6.9%, A: 0.20%	**220 nm**	5.5 min	16.2 min	27.0 min
W: 10.0%, A:0.25%	**300 nm**	88 min	253 min	423 min

Predicted morphology was verified by scanning electron microscopy (SEM) in a Zeiss Neon 40, with a working distance of ca. 3 mm, a voltage of 2 kV and using an aperture of 30 µm. Crystal structure of the nanotube array was measured by x-ray diffraction (XRD) in a Rigaku Miniflex diffractometer, using Cu Kα radiation (wavelength 0.15418 Å) operating at 35 kV in a continuous 2θ scan mode from 20 to 70°, at a step size 0.02°s^{-1}. Recorded diffractograms were analyzed using the software PDXL® and data was plotted after converting it to .xy files with PowDLL [72] program.

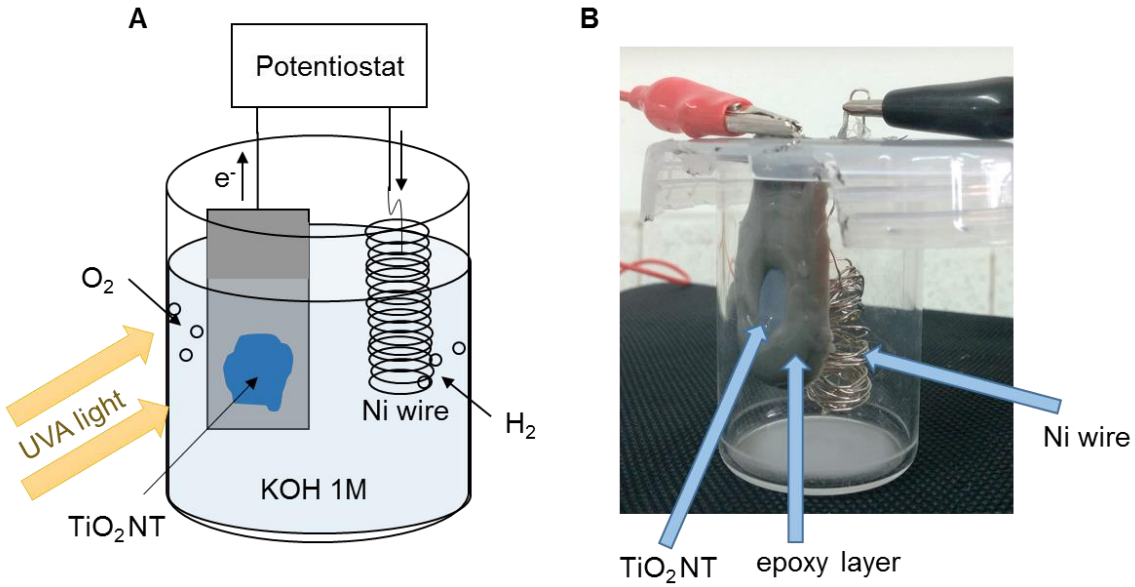

Figure 3.1: Scheme of the used photocell

Photoelectrochemical (PEC) experiments were conducted to evaluate performance of the material in hydrogen production by water splitting reaction. Experiments were carried out using a DY2300 Digi-Ivy potentiostat in a two electrode configuration, with TiO_2 nanotubes on Ti foil as the working electrode and nickel (Ni) wire as counter electrode, as depicted in figure 3.1. Area of the working electrode was controlled by covering the foil with epoxy resin (LOCTITE E40FL), curing of the epoxy layer was 48 hours at environment temperature. The whole back of the foil and borders of the face with TiO_2 nanotubes were covered (see sketch in figure 3.1). Resulting area, which varied from sample to sample, was measured with ImageJ [73] software. The anode was irradiated with UVA lamps as light source, measured irradiance was 2610 µW cm^{-2}, without considering effect of electrolyte or cell material, measurement of the irradiance was performed by placing the detector at the same position of the photoanode relative to the light source. Photocell consisted of a single chamber pyrex glass. Open circuit potential (OCP), and linear sweep voltammetry (LSV)

and current-time (i-t) measurements were performed. LSV was recorded at a scan rate of 0.02V/s. Electrodes were connected with copper wires and submerged in deionized water 1M KOH (85%, Merck) solution. Alkali solution was degassed by vacuum filtration.

Results and Analysis

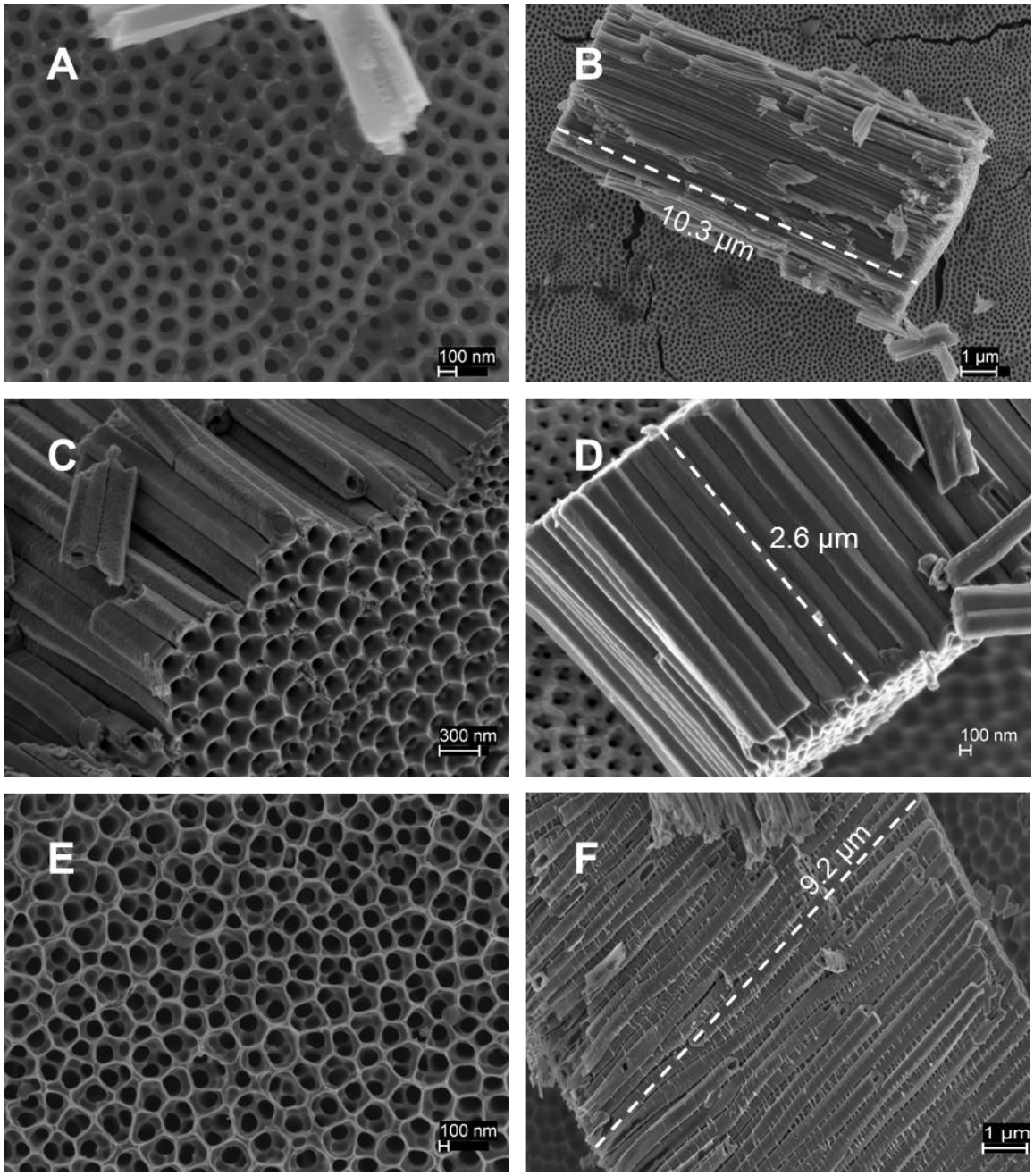

Figure 3.2: SEM characterization of prepared samples for the factorial experimental design in EG solutions of 3.8% water and 0.15% ammonium fluoride (A-B), of 6.9% and 0.20% (C-D) and of 10.0% and 0.25% (E-F)

Material morphology: tube length and diameter as independent variables

Produced nanotubes were characterized by SEM to verify the achievement of the desired morphology (tube diameter, length and top surface of the array). Top surface of the array was composed of organized open pores connected to the inner pores of the tubes (figure 3.2 (A) and (C)), and only pore diameter changed from sample to sample (no presence of random pores, neither nanograss). Average external diameters corresponded to 150, 220 and 300 nm for samples prepared in EG solutions with initial water concentration of 3.8, 6.9 and 10.0%, respectively. Deviation of diameter values was the same as reported in the previous chapter. Additionally, only samples produced in EG solution of 10.0% water presented ribs on the outside walls of the tubes (image F), which can be considered and additional morphological feature. Targeted length was also achieved, considering and error of ca. 15% for all samples (same presented in the model in chapter 2). The anodization protocol developed in chapter 2 was accurate, nanotube diameter and length independently varied while maintaining same kind of top morphology.

XRD characterization

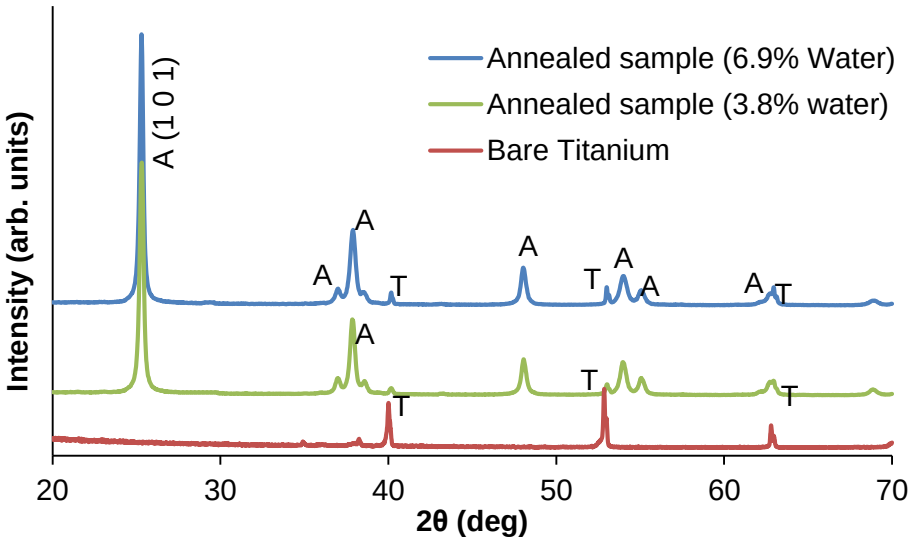

Figure 3.3: XRD patterns of bare titanium and annealed anodized foil

Figure 3.3 shows the XRD patterns of a titanium foil prior anodization and of anodized samples in EG solutions of 3.8% and 6.9% water after annealing at 450°C in air atmosphere, as previously described. Metallic foil only presented Ti peaks, which were significantly smaller in the annealed anodized foil. After annealing, TiO_2 nanotube arrays

are composed of anatase phase, as confirmed by the 25.3° (101), 38.1° (004) and 48.02° (200) characteristic peaks, among others. All samples presented the same peaks and relative peak intensities.

The average crystallite size was calculated from XRD data via the Scherrer's equation [74] (eq. 3.1) based on the line broadening effect of full width half maximum (FWHM) of the (101) peak.

$$D = \frac{k\lambda}{\beta \cos\theta} \quad (3.1)$$

Where D is the average crystallite size, k is Scherrer constant, λ is wavelength of X-ray, β is FWHM and θ is diffraction angle. Previous reports have demonstrated the same (101) crystallite size calculated by this method and measured by TEM [75]. Results are in table 3.2.

Table 3.2: Calculated average crystallite size. Samples were produced by two step anodization at 100V, in EG solution with varying water concentration (on table)

	Peak 25.3° (101)	
Sample produced in	FWHM (2θ degrees)	Crystallite size (nm)
3.8% water	0.236	36
6.9% water	0.197	43

Average crystallite size was 36 and 43 nm for annealed samples anodized in 3.8% and 6.9% initial water concentration, respectively. The increase in crystallite size can be attributed to the wall thickness, which varied, along with diameter, with the initial water concentration. Previous reports suggest that anatase crystallites' width is restricted by the wall thickness [6].

Crystallite size influences nanotubes' PEC performance [76]. In one hand, smaller crystallites may contribute to a higher recombination rate at interfacial boundaries, similarly to what is observed in polycrystalline photovoltaic materials [77]. In the other hand, bulk recombination takes place in bigger crystallites [78]. It has been reported that the increase in crystallite size in TiO_2 nanotubes decreases the specific surface area of the material. Zhang and collaborators synthesized template assisted nanotubes, and measured the adsorption of Rhodamine B in the dark, removed colorant was 10.3 and 4.4% when tubes composed of crystallites of 20 and 31 nm, respectively, were used [79].

No study of solely crystallite size effect in anodically prepared titania nanotubes' performance has been reported. In one hand, by varying anodization conditions typically various morphological features are modified at the same time. Freitas and coworkers [76] obtained nanotubes of different diameter by changing electrolyte temperature, and correlated the increase in the PEC performance of the material to the change in crystallite size from 25 to 33 nm, nevertheless they did not report tube length, and some other reports indicate that nanotubes' growth rate varied with electrolyte temperature. In the other hand, when authors study the effect of annealing conditions, crystallinity and crystallite size are modified at the same time, and rutile appears beyond 550°C. For example, Sun et al. [80] reported an increase in PEC performance of the material when annealing temperature was raised from 350 to 450 °C, that increases crystallite size from 20 to 27 nm and also relative intensity of anatase peaks. Beyond such temperature rutile was present and morphological integrity of the tubes was compromised.

The annealing conditions used in this work did not change the length neither destroy the nanotubes, although two different morphologies were obtained: double (figure 3.4 (A)-(C)) and single (fig. 3.4 (D)) walled nanotubes.

Tubes prepared at 3.8% (figure 3.4 (C)) and 6.9% (figure 3.4 (A) and (B)) had double wall structure after annealing. Walls were concentric to each other, the outer wall was a compact shell covering the tube (see figure 3.4 (A)) whereas the inner wall was composed of smaller grains (figure 3.4 (B)). When water was raised to 10.0% a compact single wall remained after annealing (figure 3.4 (D)). Xiao and collaborators found that the TEM measured size of crystallites in the outer wall of the tubes was larger than the calculated from XRD data, probably due to aggregation of smaller crystallites [81] from the inner wall.

Formation of the double wall after annealing of anodized samples in low water content can be explained by a change in oxide density. Albu and Schmuki [69] reported a reduction in the thickness of the granular inner wall while increasing water content in the electrolyte. The conditions they used ranged from 1% to 20% water. They found that increasing water content caused the granular inner wall to disappear until the whole tube wall is a single wall, as seen in figure 3.4 (D). Considering that a low amount of water generates low density oxide, the growth of crystallites during annealing creates the differentiated grains and the two walls [69]. Other studies indicate that double wall forms due to removal of impurities

during annealing process [82], and is dependent on the annealing conditions [64], such impurities are generally carbon left during the anodization in organic medium (EG). That could be the case of the different morphologies obtained here, since electrolyte concentration was varied.

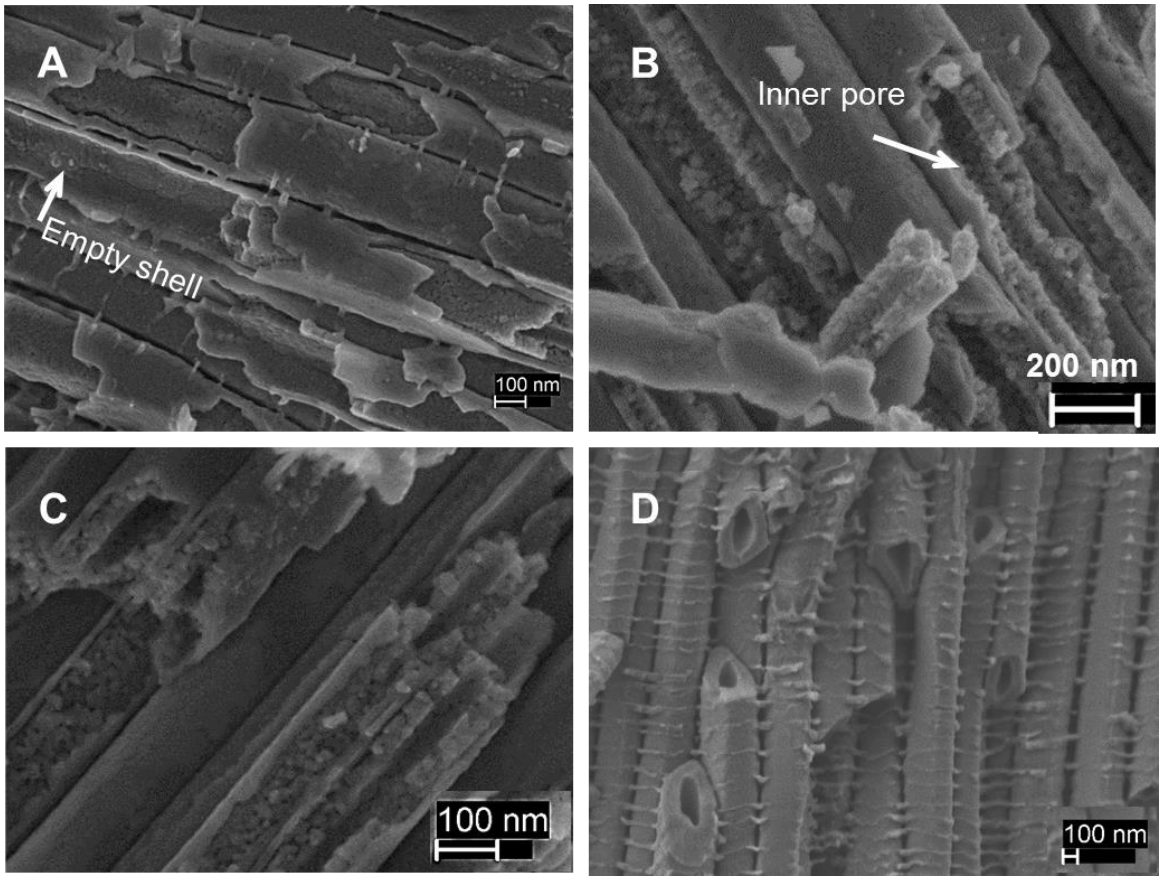

Figure 3.4: Double (A)-(C) and single (D) wall nanotubes after annealing. Samples were anodized in EG solution with initial water content of 6.9% (A) and (B), 3.8% (C) and 10.0% (D)

Double wall nanotubes have been previously studied in PEC applications, though more studies are still needed to discern if they provide an advantage against single wall tubes. Certainly dye-sensitized solar cells (DSSC) can benefit from a hypothetical higher surface area in double wall nanotubes [83], and measured electrical conductivity is higher in single wall nanotubes [82]. Nevertheless comparative studies between single and double wall nanotubes relied in samples produced in different anodization conditions, with different tube morphology [82], or did not to mention how one of the nanotubes were produced [84].

PEC experiments

Open circuit potential (OCP) during illumination was measured with no reference electrode. Typical response is depicted in figure 3.5 (A), tubes of 150 nm and 9 µm were used.

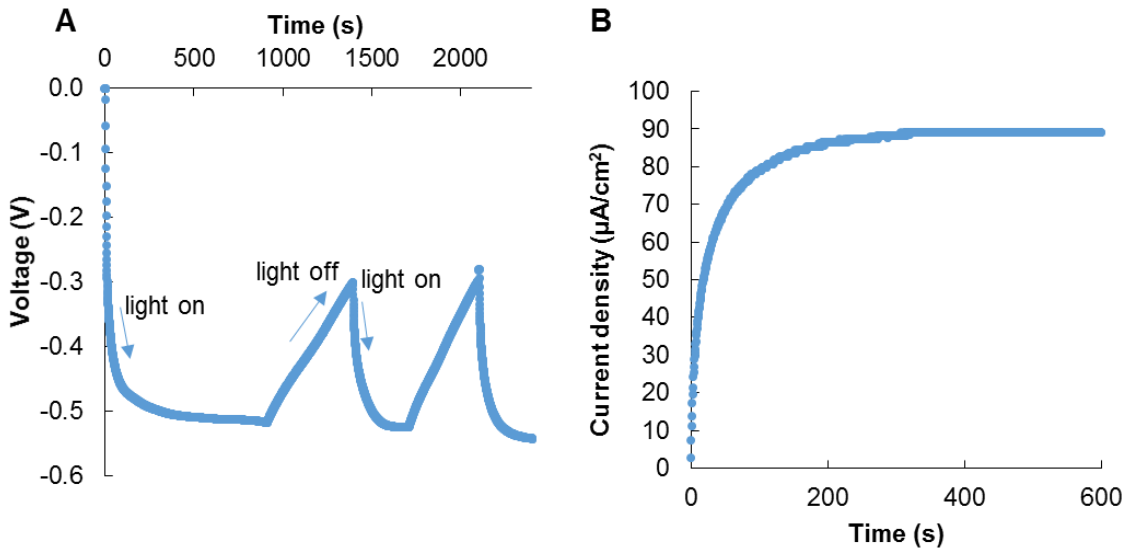

Figure 3.5: On-off illumination cycles during open circuit potential (A) and current time (i-t) profile at short circuit configuration and without voltage (B)

Potential before illumination was close to 0, when light was turned on voltage quickly dropped to more negative values, demonstrating produced nanotubes were n-type semiconductor [13]. A stable voltage was reached after a moderate time; it is the maximum potential generated between the electrodes under the studied conditions. On-off cylces of the irradiated light in figure 3.5 (A) demonstrated the photosensibility of the material. When light was turned off the potential started to disappear, when light was restored voltage decreased again until its stable value. Under UV light the voltage shift is produced when the photons generate electron-hole (e^-/h^+) pairs. Recombination of the generated pairs explains the potential decrease when light is turned off [2].

Current density transient (i-t) recorded in short circuit configuration is presented in figure 3.5 (B). Morphology of the tubes was 150 nm external diameter and 9 µm length, and no voltage was applied. When light was on, the current density increased until a stable value of 89 µA/cm^2. Current is generated when the photogenerated electrons move from the photoanode to the cathode (Ni wire), hence it is a direct measure of the material's photoelectrocatalytic performance. In one hand it will depend on the amount of light

absorbed i.e. absorbance of the material and amount of catalyst present. In the other hand, the measured current is also dependent of the recombination rate of the electrons and holes, i.e. presence of recombination sites.

The importance of the recombination in the measured photocurrent density can be seen in figure 3.6. It presents the i-t profile of the cell with tubes 3 µm long and 150 nm of external diameter, when no voltage was applied and when a potential of 0.42 V was used between the anode and cathode.

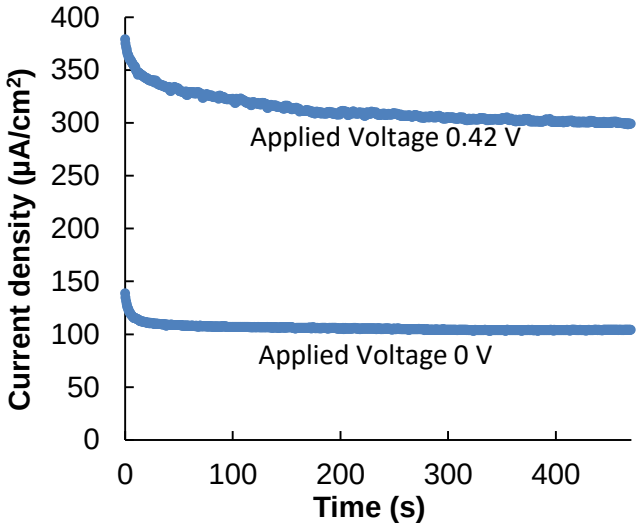

Figure 3.6: Current transients when no voltage and 0.42 V was applied. Nanotubes used were 3 µm long and 150 nm of external diameter

Current density increased from 104 to 300 µA/cm^2 when a potential of 0.42 V was applied. This is due to a reduction in the recombination rate of the pair electron hole. With the additional voltage an electric field is forcing the electrons to leave the photoanode [6]. No new electrons are generated, but less will recombine in their path through the nanotube to the cathode. This path begin in the oxide bulk (tube walls) where electrons are photogenerated [33], from there they have to move to the bottom of the tubes and leave the oxide. The more electrons leave the oxide or the lower the recombination rate, the higher the PEC performance of the material in water splitting.

Equations 3.1 and 3.2 show the reactions taking place in the anode and cathode, respectively, in alkali medium [5].

$$4OH^- + 4h^+ \leftrightarrow 2H_2O + O_2 \quad (3.1)$$

$$4H_2O + 4e^- \leftrightarrow 2H_2 + 4OH^- \quad (3.2)$$

Electrons available in the cathode (eq. 3.2) are those that were photogenerated in the anode and did not recombine. Therefore, the measure of those electrons, current density, can be correlated to the PEC efficiency of the material, by following the equation 3.3 [12].

$$\eta = {I(V_{redox} - V_{bias})}/{P_{in}} \quad (3.3)$$

Where η is PEC efficiency, I is the measured current density, V_{redox} is the redox potential for water splitting, V_{bias} is the potential externally applied and P_{in} is the illumination power or irradiance. Equation 3.3 is the rate of the power output (electrical) to the power provided (lighting). When no voltage is applied, V_{bias} is zero, and the system generates the current at the redox potential of the water i.e. 1.23 V. If a voltage is applied, the power provided (IV_{bias}) must be subtracted. The effects of the transmittance of the glass reactor and the reflectance of the body of water in front of the catalyst were not taken into account in the calculation of the PEC efficiency. Because of that, the calculated efficiency according to 3.3 may have been underestimated, since the effects of the glass reactor and the body of water reduces the amount of light that reaches the surface of the photoanode.

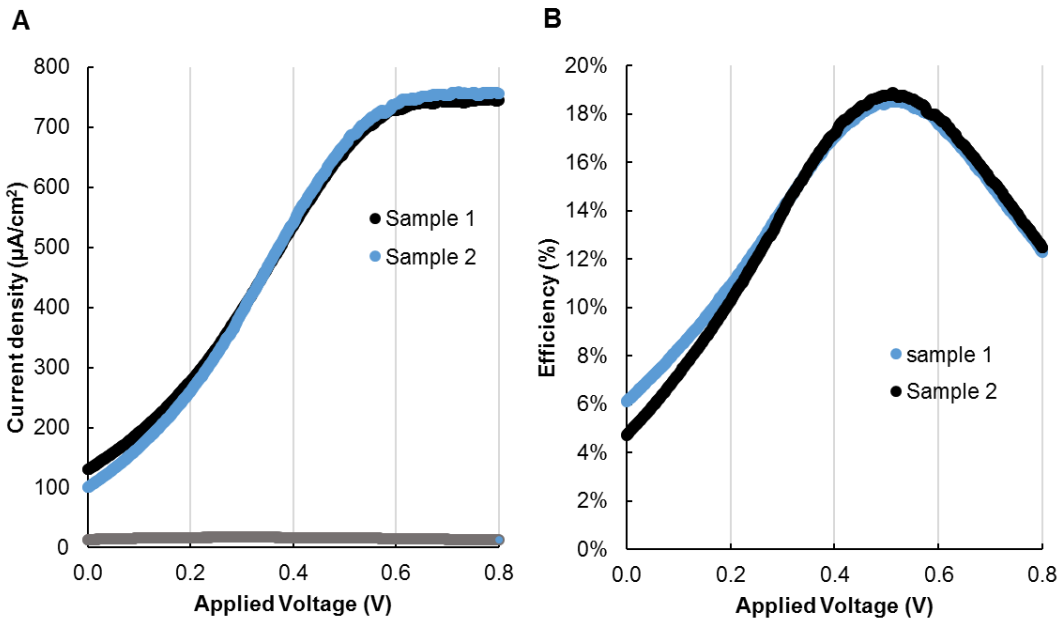

Figure 3.7: LSV recorded for two samples produced at the same anodization conditions (A), and PEC efficiency calculated from LSV data (B)

Figure 3.7 (A) shows the linear sweep voltammetry of two different samples produced at the same conditions of 100V, EG solution of 3.8% water and 0.15% NH_4F, thus with nanotubes of 150 nm of external diameter and 9 μm long. Current density was recorded

while potential was varied at a rate of 0.02V/s. Figure 3.8 (B) shows the calculated PEC efficiency, according to eq. 3.3.

Recorded LSV data was the same for both samples, it demonstrates good reproducibility of the anodization process and of the PEC experiments. In figure 3.7 (A) it is evident that current density increased when higher potentials were applied between the two electrodes, until a plateau was reached. The increase in the current density correlated to a higher PEC efficiency (figure 3.7 (B)), hence, although some electrical power was provided, the reduction in the recombination rate increased the net power output (see equation 3.3). The plateau in figure 3.7(A) is also a saturation point, regardless the potential applied no more electrons can leave the anode, because no more electron/hole pairs were generated or the recombination rate cannot be reduced further.

Comparison between different morphologies requires the identification of maximum efficiency for each sample. Calculated PEC efficiencies, from LSV data, is presented in figure 3.8 for each sample prepared.

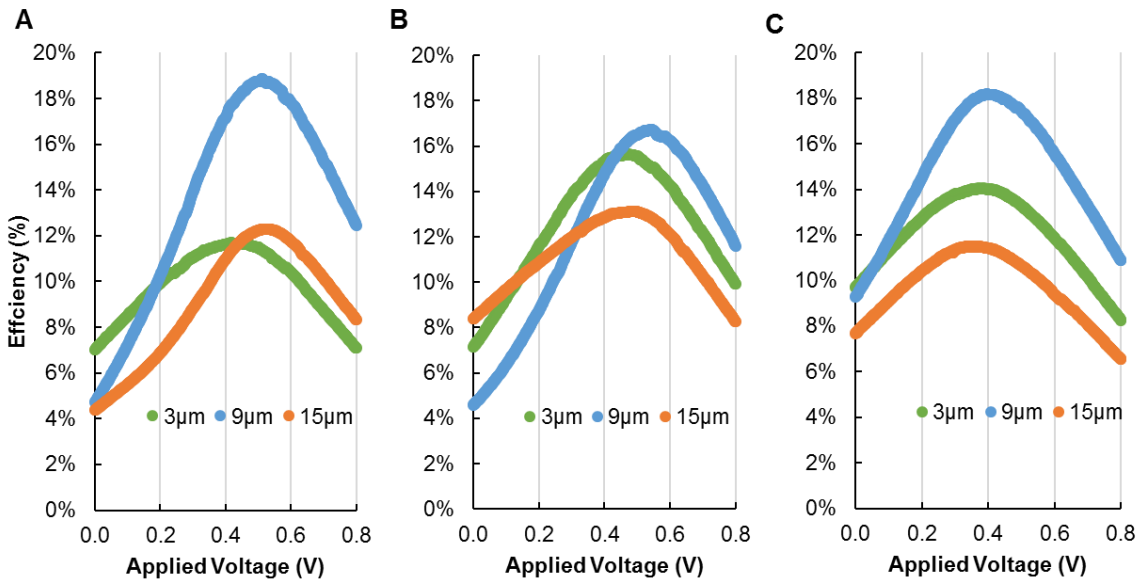

Figure 3.8: PEC efficiency of TiO_2 nanotubes of 3, 9 and 15 µm long, and 150 (A), 220 (B) and 300 nm (C) of external diameter

The highest efficiency of 18.6 % was obtained with nanotubes of 150 nm external diameter and 9 µm long (figure 3.8 (A)), the same morphology presented in figure 3.7. Maximum efficiency was obtained at different voltages for each morphology, such voltage will be referred to as optimal voltage. When the external diameter was 150 nm (figure 3.8 (A)),

longer nanotubes required the application of higher voltages to reach the maximum efficiency. In longer nanotubes, electrons need to move longer distances before reaching the tube bottom, hence there are higher chances of recombination. A similar observation was made by Adán and coworkers [85], they compared the oxidation of methanol with TiO_2 nanotubes of varied length when no voltage was applied and no cathode was used, i. e. photocatalytic (PC) degradation, and when a voltage of 1.0V was used between the photoanode and a Ni mesh cathode, i. e. photoelectrocatalytic degradation. They found that PEC degradation was higher than PC for all studied lengths, but the difference between PEC and PC degradation rates was higher for shorter nanotubes [85]. This analysis at a single applied potential provides a similar conclusion, it is more difficult to move the electrons from the tube bulk to the tube bottom in longer nanotubes than in shorter ones.

This correlation between tube length and optimal voltage was not observed in tubes of 220 and 300 nm external diameter. When tubes of 300 nm diameter were used, see figure 3.8 (C), optimal voltage did not vary with tube length, probably due to a strong effect of the wall thickness (110 nm). In tubes with thicker walls radial recombination is also an important factor [6], due to the movement of photogenerated holes. While electrons need to move to the tube bottom and from there to the metallic contact and the cathode, the holes, also photogenerated at the bulk of the tube, must move to the tube surface to react with the hydroxyl groups, see equation 3.1. Optimal voltage and tube length dependence was evident in tubes with 150 nm external diameter, since their wall thickness was 50 nm (see chapter 1) and radial recombination was not as important as axial recombination. In tubes of 300 nm external diameter and 110 nm of wall thickness radial recombination was important, and tube length did not affect optimal voltage. In the other hand, behavior of the optimal voltage while varying the length of tubes of 220 nm external diameter and 80 nm wall thickness may be a product of the two effects.

Figure 3.9 shows the surface response of maximum PEC efficiency for all morphologies used. In the studied conditions, the response was depended on tube length and not on tube diameter, as concluded from the ANOVA, see table 3.3.

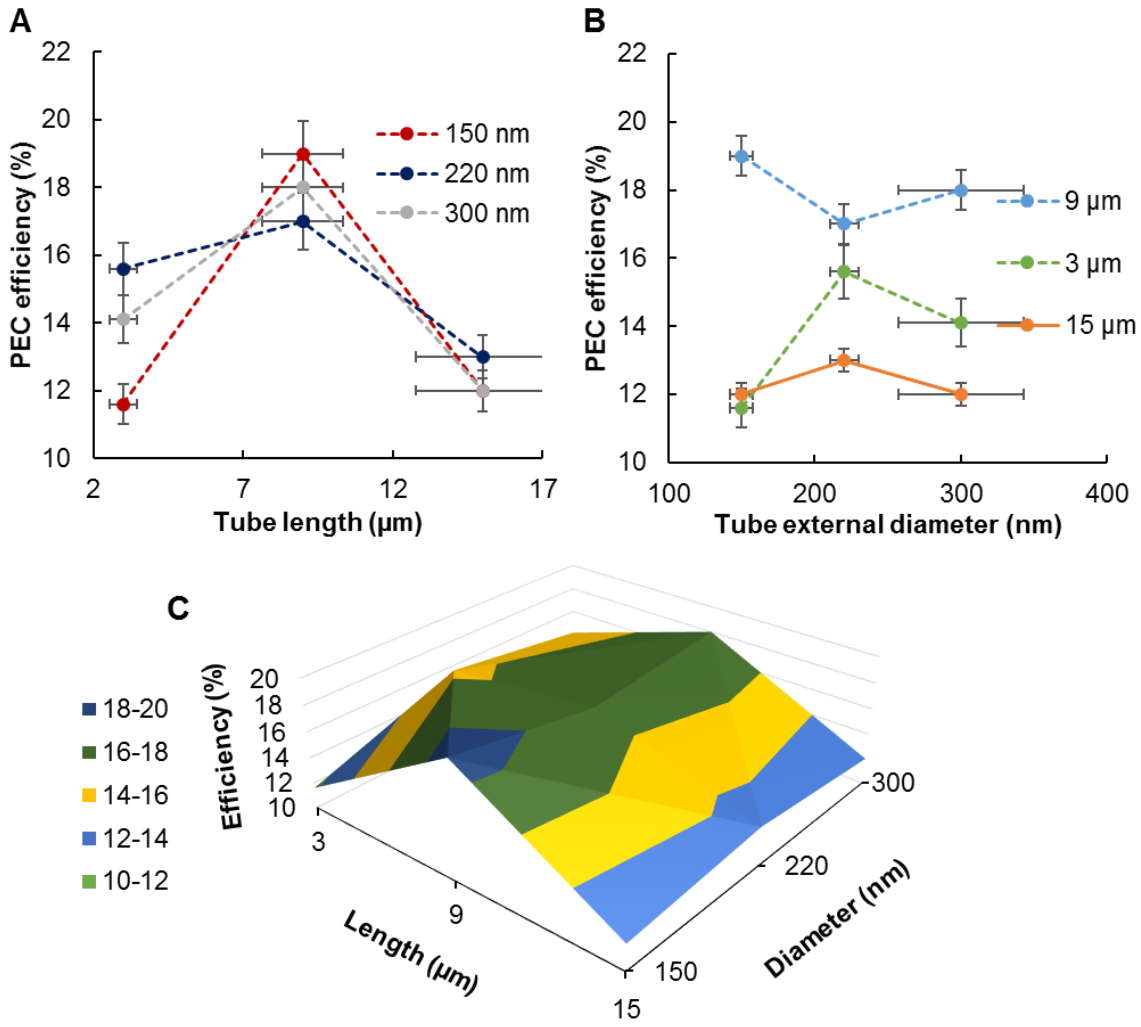

Figure 3.9: PEC efficiency while varying tube length (A), external tube diameter (B) and both variables (C). Note. Experimental points in (A) and (B) are connected by a line only to facilitate data interpretation

Table 3.3: Analysis of Variance (ANOVA) and dependence of PEC efficiency on tube diameter and length. SS denotes Sum of Squares, df degrees of freedom, MS Mean Square and F the test statistic F ratio.

Source of Variation	***SS***	***df***	***MS***	***F***	***P-value***	***F crit***	***Dependence?***
Diameter	1.50	2	0.75	0.32	0.74	6.94	NO
Length	52.28	2	26.14	11.28	0.02	6.94	YES
Error	9.27	4	2.32				
Total	63.05	8					

Material performance strongly depends on the tube length, due to its effect in the amount of light harvested and the recombination rate. The recombination rate increases with tube length, as well as the amount of light harvested [85], this two process are competitive, and

that is the reason why an optimal length was present, see figure 3.9 (A). Relation of the tube length and the recombination rate was previously explained: a longer path for the electrons to reach the metallic support increases the chances of recombination. In the other hand, tube length is also related to the amount of light harvested, due to the penetration depth of the light and the amount of catalyst present. Penetration depth of the light (PD) in the array depends on the absorbance of the material and this on the wavelength of the light, PD is higher for deep UV light than for lower light energies [17]. In our design of experiments light source was fixed, hence penetration depth was fixed. When tubes are shorter than the PD not all light is absorbed, thus efficiency is smaller. In tubes longer than PD a section of the tubes is not illuminated. Also, longer tubes increase the amount of catalyst and the surface area of the array, as predicted by the geometric model, see figure 3.10.

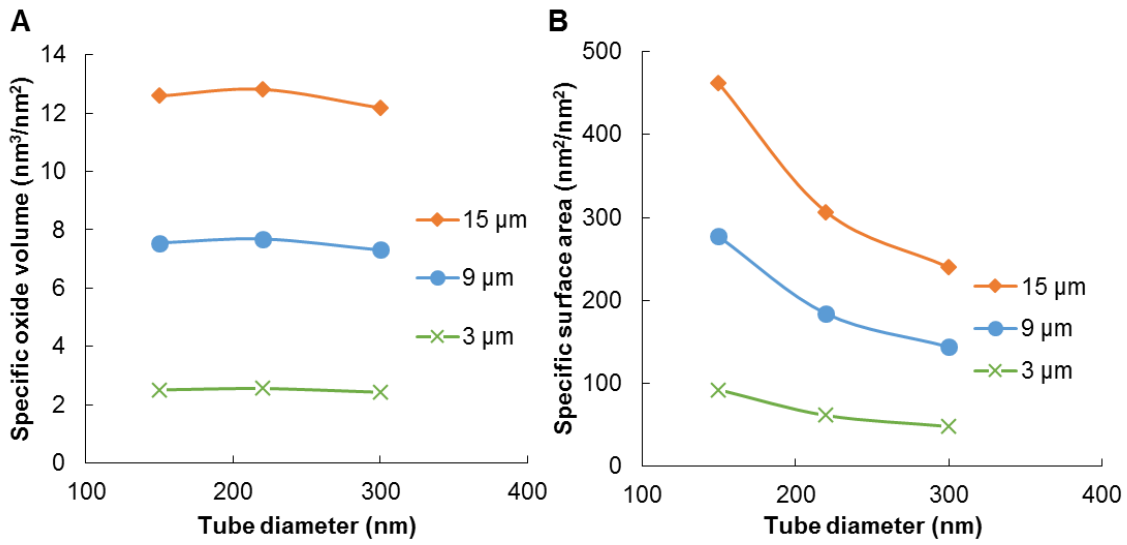

Figure 3.10: Calculated specific oxide volume (A) and specific surface area (B) of the tubes for different morphologies. Calculations were performed considering the hexagonal packing of perfect cylinders of measured diameter, wall thickness and length (see figure 2.7), and the hexagonal area occupied by such arrange or unit, see calculation in annex 2, which is similarly to [33]

The specific volume of the nanotubes determines the amount of catalyst bulk that will react with the light (for a given density), while the specific surface area relates to the amount of catalyst that can react with the reactants (OH^-, see equation 3.1). Both quantities are increased with longer nanotubes (figure 3.10 (A) and (B)).

Contrary to the strong effect of tube length, in the studied range PEC efficiency was not dependent on the external tube diameter, or the other morphological features varying simultaneously: wall thickness and inner tube diameter. In figure 3.9 (B) most of the points within each length are not statistically different. This may indicate that different effects are counteracting and that a plateau has been reached. To further explain this, additional experiments were performed, in order to obtain nanotubes of smaller diameters. Tubes of 50 and 100 nm of external diameter were obtained by two step anodizations at 20 and 40 V, respectively, composition of the EG solution varied too, all conditions are reported in table 3.4. PEC efficiencies are reported in figure 3.11.

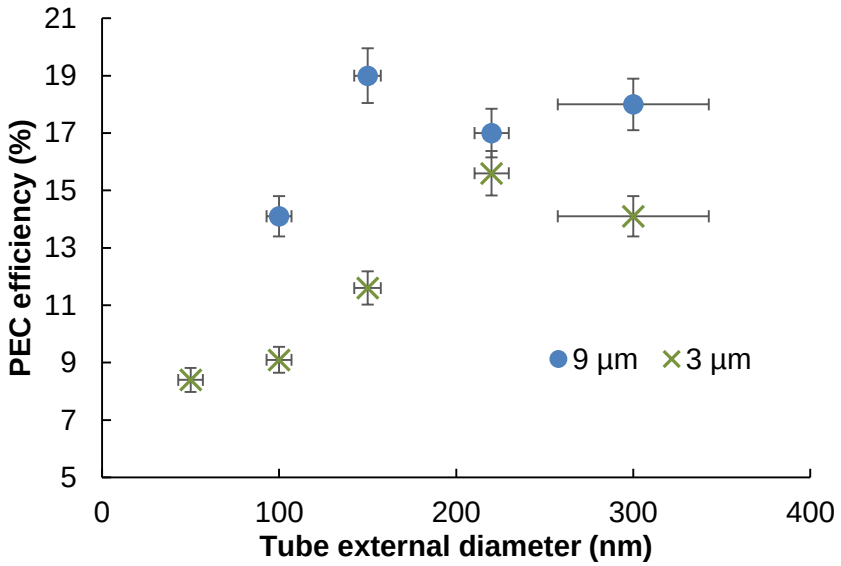

Figure 3.11: Maximum PEC efficiency while varying external tube diameter in tubes of 3 and 9 µm

Table 3.4: Conditions used to prepare nanotubes of 55 and 100 nm of external diameter. First step anodization was performed at 100 V in an EG solution of W: 3.8% A: 0.15%.

			2nd step anodization time	
			Tube length	
External diameter	**EG solution Water (W) and NH4F (A) concentrations**	**Applied potential during 2nd step**	**3 µm**	**9 µm**
100 nm	W: 2.7%, A: 0.15%	40 V	46.7 min	136.2 min
50 nm	W: 1.7%, A: 0.15%	20 V	250 min	-

Performance of nanotubes of 50 and 100 nm external diameter was lower than that of nanotubes of 150 nm, see figure 3.11. This suggests that PEC efficiency increases with tube diameter until a plateau is reached, and that the studied tubes with external diameters varying between 150 – 300 nm were within that plateau. According to the data presented here it can be seen that PEC efficiency increases with tube diameter as the crystallite size increases and the diffusion of reactants and products is facilitated, then PEC efficiency reaches a plateau due to the reduction in the surface area and higher radial recombination of the photogenerated holes.

XRD patterns showed that crystallite size increased with tube diameter and wall thickness, and as explain before the decrease in the boundary crystallite region can reduce the recombination ratio [76]. Also, a higher inner diameter facilitates the movement of reactants and products between the nanotubes' pores and the electrolyte, as predicted by the theoretical kinetic analysis of Liu et al. [33]. Liu et al. found that reactants concentration in the interior of the tube is strongly improved in tubes of bigger inner diameter, although improvement was small beyond inner diameters of 50 nm. Our nanotubes produced in EG solution of 3.8% water had 150 nm external diameter and 40 nm inner diameter, as reported in figure 2.7. In the other hand, the increase in tube diameter reduces the surface area of the array, as demonstrated in the calculated specific surface area in figure 3.10. A reduction in the surface area may be counteracting to the benefits of a larger diameter, particularly when no improvement in the reactants diffusion is evident.

According to this analysis, not a plateau but an optimal diameter may be also present, as predicted by Liu et al. with the theoretical effect of wall thickness for a given diameter [33]. Not optimal diameter (or wall thickness) was found here, even though wall thickness varied from 50 to 110 nm when the external diameter was modified from 150 to 300 nm (see figure 2.7). This may be due to the fact that diameter and wall thickness changed simultaneously, hence oxide volume did not vary (see figure 3.10), or to the fact that in tubes of 300 nm, prepared in 10% water, ribbons were present. Presence of ribbons has been reported to affect the activity of the material, since they may influence the recombination rate [10] and increase surface area. Other difference also presents in tubes prepared in solution of 10% water was the single wall structure after the annealing, in contrast of the double wall obtained in the other samples, but no conclusion can be extracted from just this fact.

Conclusions

The effects of tube diameter and length on PEC efficiency were studied. Both morphological features were varied independently according to the two-step anodization protocol develop in the previous chapter. PEC performance of the material increased with tube length until an optimal point was reached, beyond such length PEC efficiency decreased. Dependence of PEC efficiency was in direct proportion with tube diameter until a plateau region. Influence of tube length was explained by its simultaneous effect in the amount of light harvested and the recombination rate. The effect of tube diameter is due to the change in crystallite size, the diffusivity of the reactants and the surface area of the catalyst.

Chapter 4.

This chapter focuses in the production of nanotubes by alternating voltage anodization and its use in the PEC cell. The compositional and morphological characterization provided new evidence to explain how the rings on the outside walls of nanotubes with bamboo-like morphology can increase the performance of the PEC cell. Unlike the previous chapters, this chapter is divided in two sections for clarity, the first one presents the nanotubes produced by AV anodization and the morphological and compositional characterization, in the second one the effect of the number of rings is studied.

Chapter 4. TiO_2 nanotubes with bamboo-like morphology

Introduction

In the experiments described so far, anodization was carried out at constant voltage (CV) anodization, following the two step anodization protocol developed in chapter 2. In the previous chapters, the whole first and second step anodization were both performed at 100 V, or 40 V or 20 V depending on the desired morphology. Constant voltage anodization generated tubes with smooth outside walls or those with ribs, depending on the amount of water in the electrolyte. In the other hand, when an alternating voltage (AV) is used, tubes with bamboo-like morphology are generated, i.e. tubes with rings on the outside wall, with the rings connecting all the tubes among each other to form an array of bundled tubes, which may increase the mechanical stability [86].

The AV consists of a squared pulse voltage profile; it starts with a high voltage (V_{high}) held at a specific time length (t_{high}), then the voltage is suddenly dropped to a low voltage (V_{low}) and held for a different length time (t_{low}), and raised again to V_{high} to start the cycle. This cycle is repeated accordingly to the desired number of rings wanted to be formed, and the anodization is ended during a V_{high} portion of the cycle. Under the appropriate conditions [27] the tubes will growth during high voltage and the rings will form during low voltage, hence the number of low voltage periods determines the number of rings, and the number of high voltage periods determines the number of sections between rings. Additionally, the t_{high} determines the length of the sections between rings and the total length of the nanotubes.

As an example, micrographs from sample produced by AV are shown in figure 4.1, where 9 cycles of V_{high}/V_{low} were completed, and the anodization ended in a V_{high} period. The nanotubes formed have 9 rings and 10 sections between them. Figure 4.2 shows the current density transients recorded during the anodization of the sample in figure 4.1, it shows each V_{high} and V_{low} period, note that periods of V_{high}, correspond to a higher oxide production (see eq. 2.1 and 2.2).

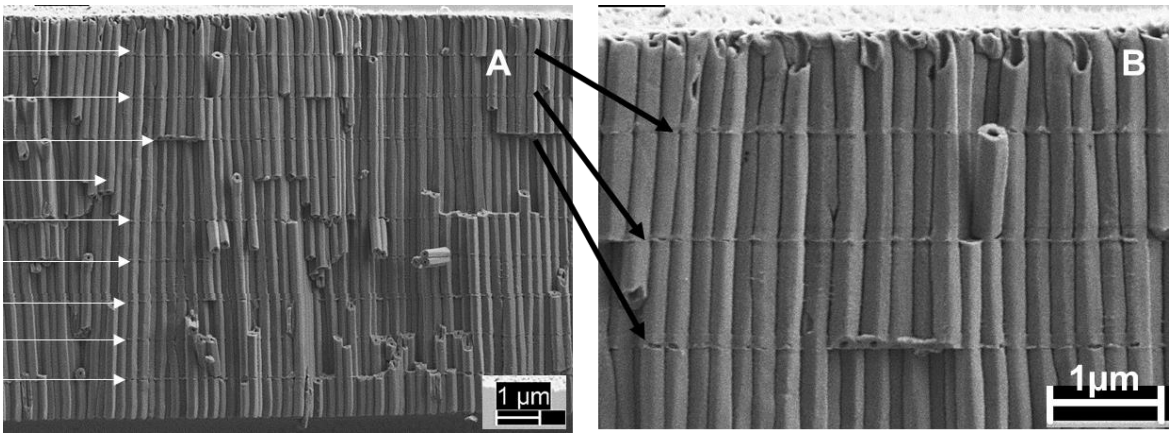

Figure 4.1: Sample produced by AV anodization. White arrows in (A) indicate the positions of the 9 rings formed, black arrows show the first three rings, magnified in figure (B). This sample was prepared following the two step anodization protocol. First step was performed at constant voltage anodization of 100 V in EG solution of 6.9% water and 0.20% ammonium fluoride. Second step was performed in the same aged EG solution and voltage was changed between 100 V and 20 V. Each t_{high} was 86 s and each t_{low} was 600 s

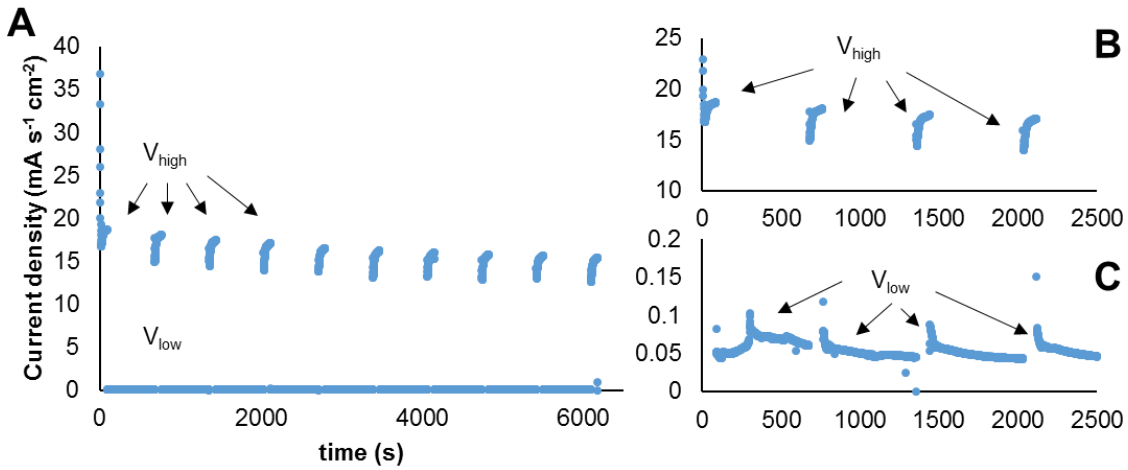

Figure 4.2: Current density transients recorded during AV anodization of sample in figure 4.1. (A) shows all the 9 cycles plus the last V_{high} period. (B) details the current during the V_{high} periods of the first 4 cycles, and (C) of the V_{los} periods. This sample was prepared following the two step anodization protocol. First step was performed at constant voltage anodization of 100 V in EG solution of 6.9% water and 0.20% ammonium fluoride. Second step was performed in the same aged EG solution and voltage was changed between 100 V and 20 V. Each t_{high} was 86 s and each t_{low} was 600 s

Previous authors have reported an increase in the photoelectrocatalytic (PEC) hydrogen generation and energy storage when tubes with bamboo-like morphology are used [37] and in the performance in dye-sensitized solar cell (DSSC) [35], [36]. Such improvement is always attributed to the increase in the surface area, although in some cases more than

one morphologic feature was simultaneously modified [34]. An increase in the performance of the material may reduce the cost of hydrogen production [5] and make the technology more competitive for industrial application. In this chapter the effect of the number of rings on the outside wall of tubes 9 µm long and 150nm of external diameter (morphology with the highest PEC performance found in the previous chapter) on PEC was determine. The results did not show an improvement in the PEC efficiency of the material, but more remarkably it was found that rings generated during AV anodization possessed more Fluorine than the rest of the nanotube, which may explain the higher PEC performance found by other authors. This chapter is divided in two parts, in the first part it is show how the nanotube rings are doped during AV, and then, in the second part the effect of the number of rings in the PEC performance of the material will be discussed.

4.1 Fluorine doping in the rings of TiO_2 nanotubes produced by alternating voltage anodization

Abstract

Nanotubes with bamboo-like morphology were produced by AV anodization at different potential profiles and electrolyte compositions. SEM images and the current transients recorded during anodization were used to explain the formation of the rings. TEM-EDS data showed that nanotubes were F doped, and that F composition on the rings was higher than in the section between rings. Finally, FIB characterization was used to demonstrate that rings connect all the tubes among each other.

Experimental

Anodization was performed following the two step anodization protocol previously developed. In the first step the titanium foil was anodized during 15 min at 100 V in EG solution of 6.9% water and 0.20% ammonium fluoride. After anodization the formed nanotube array with irregular top surface was removed by sonication in deionized water. The same foil was then anodized again with an AV profile. Voltage was alternated between

a V_{high} of 100 V and a V_{low} of 20 V, t_{high} was 45 s and t_{low} was 600 s. In total 18 cycles were completed, hence total anodization time at V_{high} was 14.2 min and the overall anodization time was 3.23 hours. After anodization the samples were washed with ethanol, dried with air and later annealed during 2 hours at 450°C in air atmosphere, used heating rate was $2°C min^{-1}$.

Scanning electron microscopy (SEM) analysis was performed under the same conditions detailed in the previous chapter. Transmission electron microscopy (TEM) and Energy-dispersive X-ray spectroscopy (EDX) were made in a FEI Tecnai Osiris TEM, equipped with Super-X detector EDX, in STEM mode and at 200 kV. Collection times for EDX data were 15 min during mapping and 100 s on point measurements. Analysis of the collected images was done with ImageJ [73] software. A different sample was cut with Focus Ion beam (Ga ion beam operating at 30 kV with a beam current of 10 pA) to analyze the morphology of the nanotube array produced by alternating voltage anodization.

Results and Analysis

SEM characterization

Prepared titania nanotube array was 5.2 µm long, with tubes of ca. 220 nm of external diameter and with 18 rings in the outside wall. Top of the array was very flat (figure 4.3 (A)) and completely composed of uniform pores, as expected from the two-step anodization protocol used. Distance between rings was ca. 270 nm (figure 4.3 (B) and (C)) and the number of rings corresponded to the number of low voltage periods during the alternating voltage anodization. Also, nanotubes presented double walled structured, see figure 4.3 (B) and (C), evident in tubes with the outside wall broken and the inner wall exposed.

Previous authors [37] have reported that nanotubes produced by AV voltage anodization have the same length as tubes prepared by constant voltage (CV) when the high voltage and anodization time at the such voltage is the same than in CV anodization. Thus tubes prepared by the above described conditions in AV should have the same length as those prepared at 100 V after 14.2 min of CV (see chapter 2). That was not the case for the sample prepared here, in fact, considering the linear correlation found in chapter 2, after 14.2 min at 100 V in aged EG solution of 6.9 % water and 0.20% NH_4F, tube length is expected to be ca. 7.9 ± 1.1 µm. Obtained tubes here by AV were 35% shorter, probably due to a combined effect of the number cycles and the water concentration in the

electrolyte. On the one hand, previous experiments demonstrated that tubes produced after 9 cycles of AV anodization in EG solution of 6.9% water and 0.20% NH_4F had the length predicted by the linear model found for constant voltage anodization. Those tubes are the ones in figure 4.1, total length was ca. 8.5 µm and the predicted one 8.1 µm, the same value considering the 15% error given to the model. On the other hand, tubes produced by 18 cycles of AV anodization (V_{high}: 100V, V_{low}: 20V) in EG solution of 3.8% water and 0.15% NH_4F, i.e. same number of cycles and lower amount of water than the studied in this chapter, had a total length of 8.4 µm, length close to the 9 µm predicted for constant voltage anodization at 100 V (images are shown in figure 4.10). To further explain the effect of the water content and the number of cycles consider figure 4.4, it compares the current transient recorded during AV anodization and CV anodization.

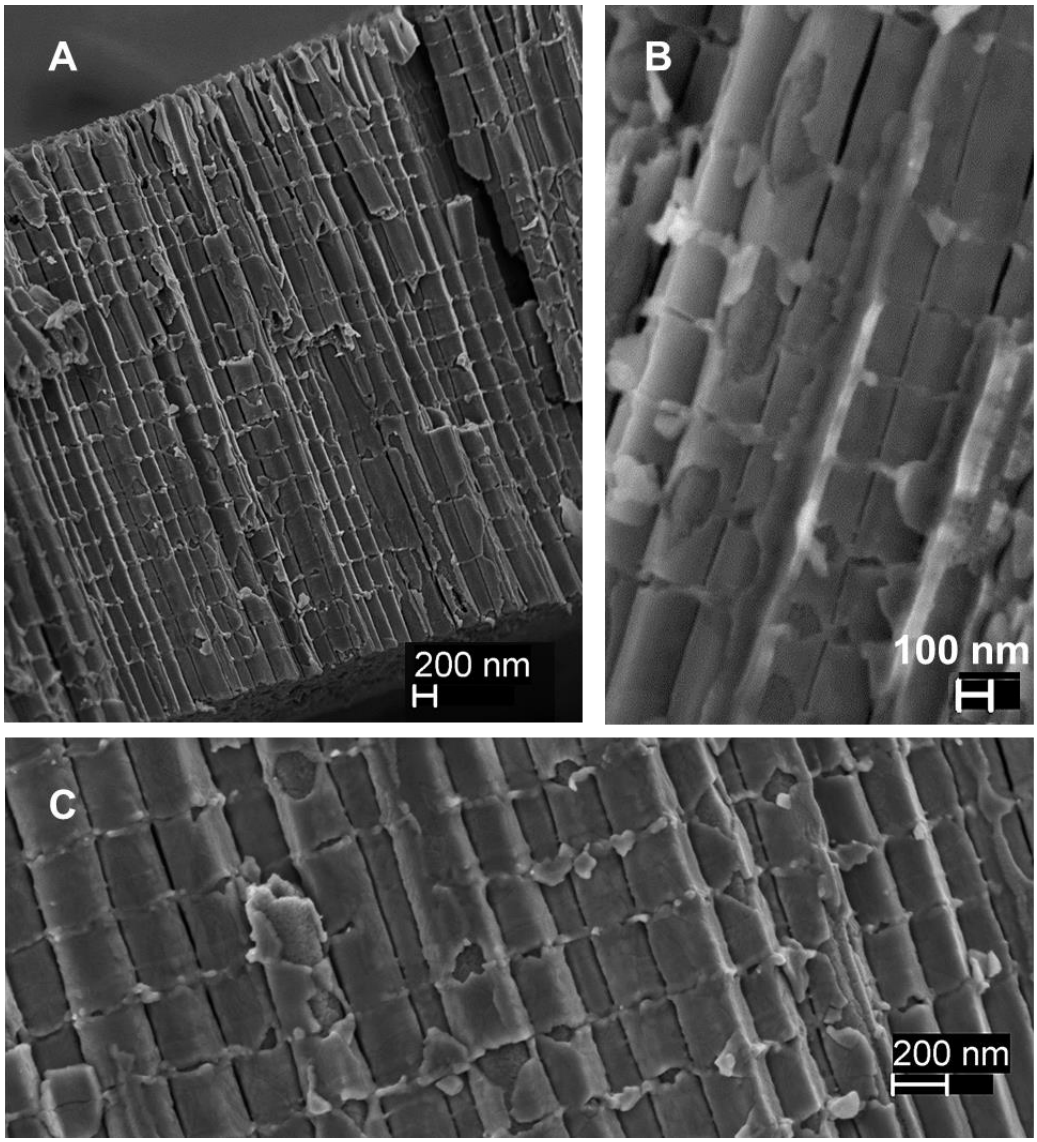

Figure 4.3: Appearance of a sample produced with 18 rings, total array (A), and close up of tubes with evident double wall structure and their outside wall rings (B) and (C)

Current measured during the anodization can be correlated to the amount of formed oxide (see equations 2.1 and 2.2 and discussion in chapter 2). Figure 4.4 shows the current density during high voltage periods in AV anodizations (electrolyte conditions: EG solutions of 6.9% water and 0.20% NH_4F) and during constant voltage anodizations at the same electrolyte conditions. When only 9 cycles were completed, the total measured charge during AV anodization was 15% lower than during CV anodization (as can be observed in figure 4.4 (A) corresponding to the tubes presented in figure 4.1), i.e. transferred charge or amount of oxide generated was very similar. In contrast during the AV anodization with 18

cycles (figure 4.4 (B), tubes in figure 4.3) total measured charge was 33% lower than the accumulated during CV anodization, thus the amount of generated oxide was very different.

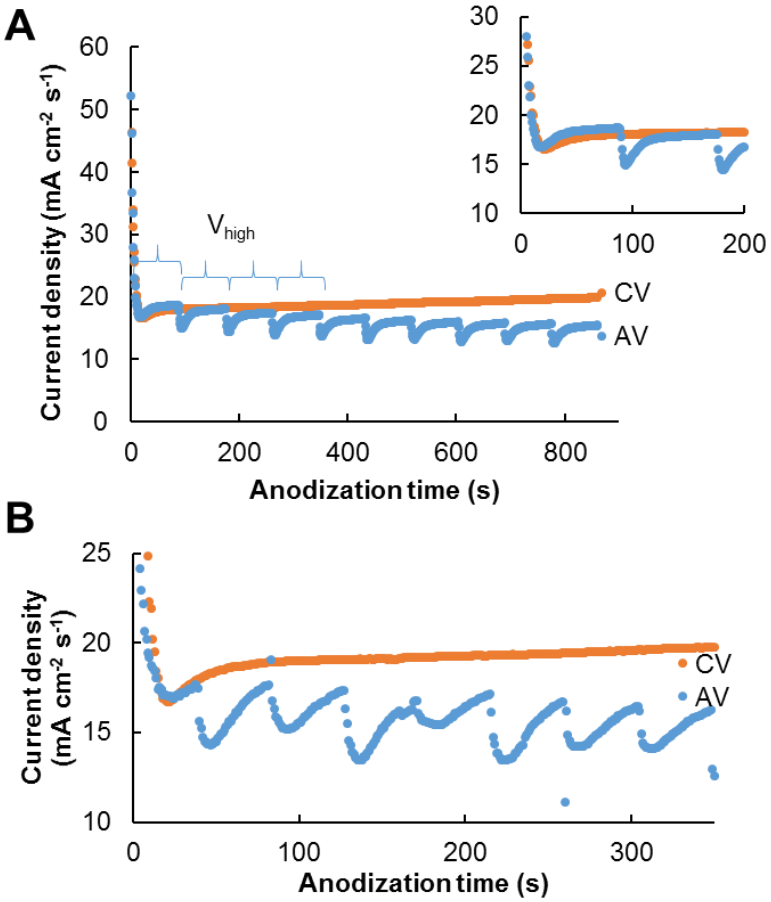

Figure 4.4: Current density transient during anodization at CV and AV when 9 (A) and 18 (B) cycles were completed. For AV only current during high voltage periods is shown. (B) only shows the first 8 cycles. In both cases fresh EG solution was 6.9% water and 0.20% NH_4F

This results support the evidence found during the morphological characterization, and the shape of the current transient provides a suitable explanation: the tube growth has to start over again with every V_{high} period. At the beginning of the CV and the AV anodization the current transients had the same behavior: exponential decay first, then a minimum current is reached and finally the current started to increase again. In the case of the AV produced nanotubes the current transient differs from the one of CV anodization when the high voltage is interrupted. Then, when the V_{high} was restored again, the anodization started one more time: exponential decay, minimum current and finally the current increase, and this

was observed during every V_{high} period. The fact that the anodization had to start again during every V_{high} period explained the lower oxide growth rate during the AV anodization. During those initial seconds of the anodization the nanotube growth rate is smaller than when a stable current is reached, as suggested by the amount of electrons generated. Additionally, there may be no growing in absolute before the minimum, which is a period typically associated to compact oxide growth [67].

Furthermore, considering that growth rate diminished with the increase in water content (see chapter 2), in electrolytes with higher water concentration the anodization process should take longer to reach a stable growth rate. Indeed, if estimated from the CV current transients, it took at least 47 s to reach the stable growth rate when water content was 6.9% (figure 4.4 (B)) and ca. 15 s in EG solutions with 3.7% water. Such time was estimated as the point after which current increase slowed down. When nanotubes of 18 rings were produced in EG solution of 6.9% water t_{high} was 45 s, while it was 86 s to produce tubes of 9 rings (figure 4.1), such values were calculated from dividing the estimated total anodization time at high voltage by the total number of high voltage periods.

Explanation for the restarting of the tube growth rate with every voltage change has been previously provided by other authors. Consider first that the voltage determines the diameter of the tube (as shown in chapter 3). If the difference between the diameters at V_{high} and V_{low} is high enough, every time the voltage changes to the low voltage period the anodization process will start again in order to generate tubes of smaller diameter. During V_{low} new oxide will start forming again, first between the tubes external wall (intertube spacing) and then at the bottom of them, in fact if t_{low} is long enough such oxide will become porous and a new layer of nanotubes will form [27]. The presence of such oxide may be the reason why when V_{high} is restored the growth of the nanotubes restarts as well. Also, during t_{low} the reactants concentration profile at the interior of the tube and the porous bottom may have change, particularly at the oxide-metal interface, thus it will take some time after the start of V_{high} to restore the concentrations needed for a stable growth rate.

TEM characterization

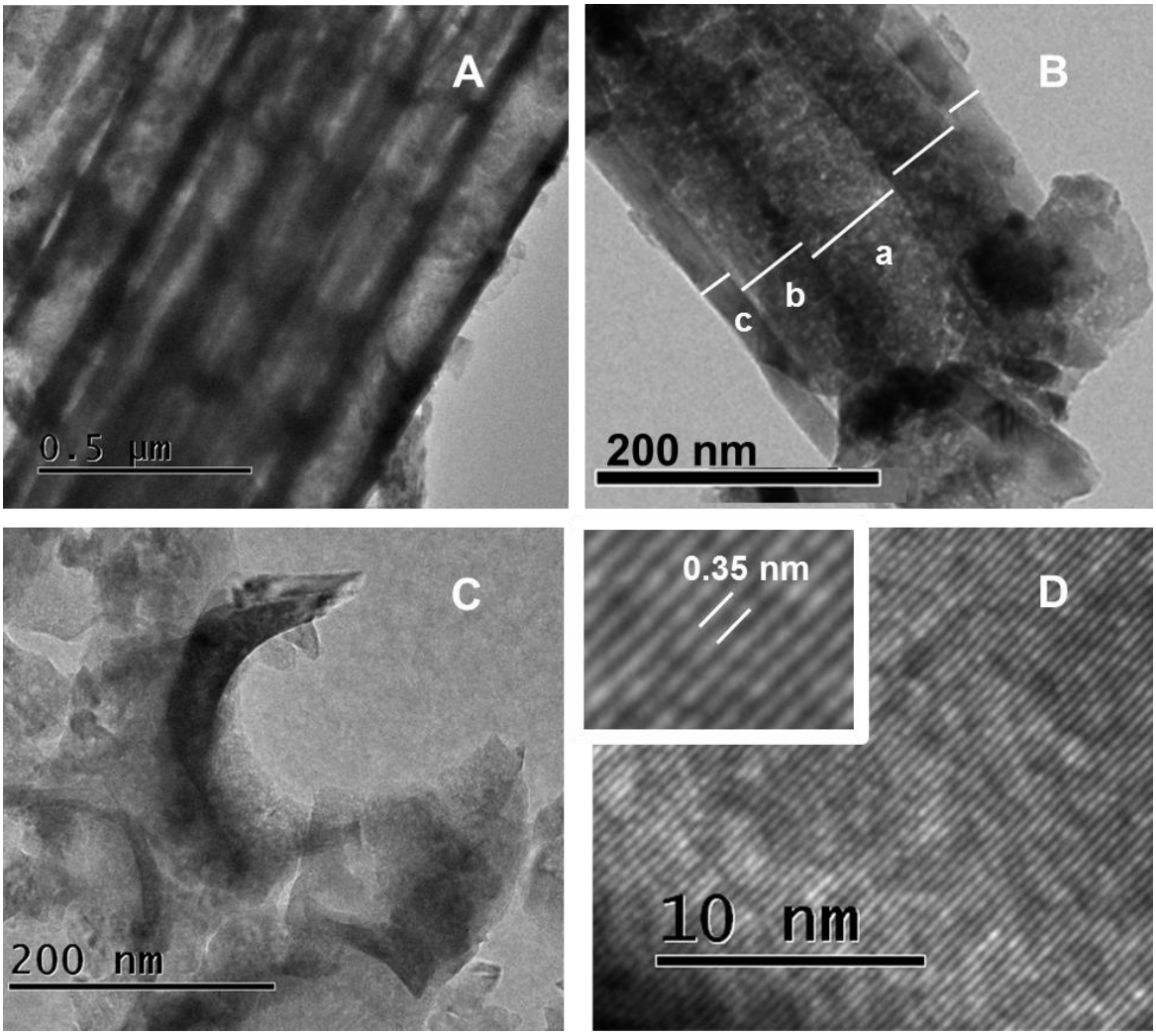

Figure 4.5: TEM images of sample prepared with 18 rings in EG solution of 6.9% water and 0.20% NH_4F. At least four rings are evident in (A), (B) shows double wall structure and inner pore, (C) unattached ring and (D) spacing of (101) lattice plane of the anatase TiO_2

TEM characterization provided morphological and compositional information of the nanotubes. Sample was prepared for TEM analysis by sonicating the annealed anodized foil in ethanol, then a drop of the solution with suspended nanotubes was placed on a holey carbon copper grid. Sonication process broke apart the tubes from the metallic support, some tubes conveniently broke in the axial direction and some rings were completely detached from the outer tube wall. Images of those views are provided in figure 4.5.

Figure 4.5 (A) is an image of the nanotubes with equidistant rings, noted for darker regions of thicker oxide. In (B) a nanotube broke in the axial direction exposes its inner pore tube and its double-wall. The inner pore diameter, inner tube wall thickness and the outer tube wall thickness are denoted by a, b, and c respectively in this bright field image. As explained in chapter 2 inner diameter and wall thickness vary along the tube length due to dissolution, nevertheless inner diameter (a) in figure 4.5 (B) was ca. 72 nm, inner wall (b) ca. 54 nm and outer wall (c) ca. 26 nm. Image (C) corresponds to a detached and broke ring. Finally figure 4.5 (D) shows a lattice image from a nanotube and the typical spacing of the (101) lattice plane of anatase TiO_2 as indicated in the inset, which was the strongest peak found during XRD characterization of CV anodized foil (chapter 3).

Compositional data are presented in figure 4.6. Compositional mapping revealed that nanotubes are uniformly composed of Titanium (figure 4.6 (B)) and Oxygen. Fluorine was also detected, see figure 4.6 (C), brighter areas indicate a higher amount of fluorine, located in the same positions of the rings (figure (A)). From these maps, it appears that there is a F enrichment at the rings compared to the matrix, this was studied in detail by EDS analysis at discrete points. Such points are indicated in figure 4.6 (A) and (E). The EDS spectra for point 1 in figure (A) is presented in (D), typical peaks for oxygen, fluorine and titanium were present, at kα positions of 0.52, 0.68 and 4.51 keV respectively. In average, normalized atomic composition of fluorine was 3.7% on the rings and 2.6% on the sections between rings, i.e. amount of fluorine increased ca. 40%.

Fluorine doping

Fluorine presence in CV anodized nanotubes has been previously reported. Authors agree that as-anodized nanotubes (without annealing) retain some fluorine due to encapsulation of the electrolyte in the amorphous structure, and that the thermal treatment causes some of the retained F to be loss due to formation of volatile F species [32], [65]. For example, Mor and coworkers[32] found by XPS analysis that CV anodized nanotubes in organic medium had 15% atomic concentration of fluorine (value normalized with titanium and oxygen concentrations) before annealing, after annealing at 550°C during 6 h the fluorine concentration was reduced to 1.7%. Reports of even lower amounts of fluorine (<1 %) can be found in two publications of Prof. Schmuki group's[64], [65], when annealing was 500°C/10s or 450°C/3h, and in the work of Yang et al.[87], who obtained nanotubes with fluorine content <1% after 3 h of annealing at different temperatures (200-800°C).

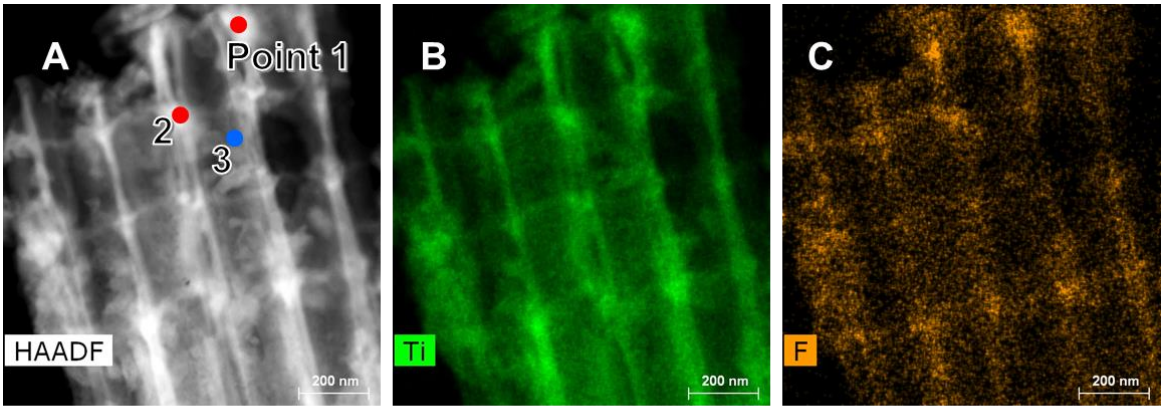

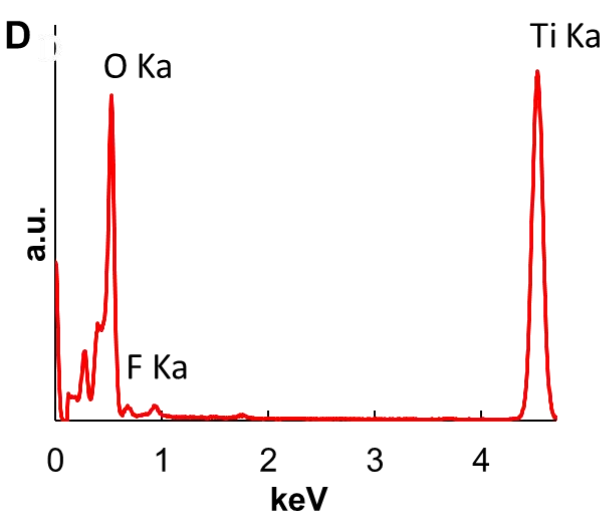

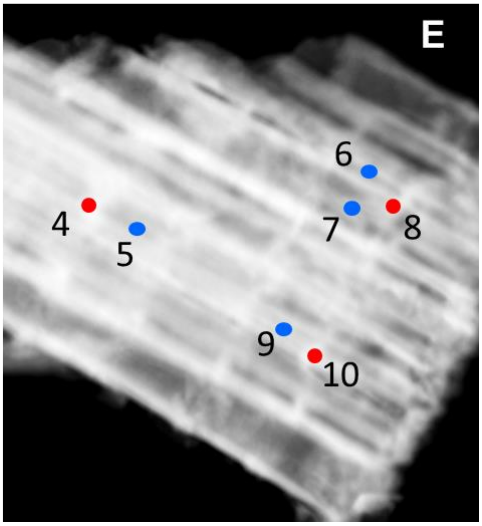

F

	on rings					between rings				
	1	2	4	8	10	3	5	6	7	9
F (nom. at. %)	3.9	3.6	3.4	3.7	3.6	2.8	2.5	2.4	2.7	2.5

Average F (nom. at. %) on rings: 3.7%
Average F (nom. at. %) between rings: 2.6%

Figure 4.6: EDS data for nanotubes produced by AV anodization (18 rings). (A) TEM-STEM mode image of the nanotubes, (B) compositional mapping for Titanium, (C) for Fluorine. (D) EDS spectrum for spot 1 in (A). (E) TEM image of a different set of nanotubes, with other locations at which point composition was measured. Normalized at. % of fluorine is provided in (F). Red points correspond to ring locations and blue points to locations between rings

A comparison between our results and those found in the literature is not possible, since our sample was prepared by AV anodization, and the voltage and electrolyte composition were different, as well as the annealing conditions. Then, it is better to compare only the amount of F identify during this thesis on the rings and on the section between rings: F

composition was higher on the rings than on the sections between them, in the annealed sample. After the annealing the nanotubes had on the sections between rings 2.6% of F and 3.7% on the rings. This should be due to a higher trapping of the F species in the rings than in the walls. There may be two mechanisms causing a higher F trapping in the rings, each will be explained next. The first explanation considers that the difference is created during the growing of the rings on the external walls of the tubes, and the second considers that the difference in F content is a process generated during the nanotubes growing.

1. With each period at low voltage the anodization process restarts again, a new oxide layer grows at the inter-tube spacing (outside wall of the tubes) and at the bottom of the array [27]. During this oxide growth, and similarly as happens with CV anodization, at the bottom of the oxide a fluoride-rich layer forms (see chapter 2), due to a higher migration of fluoride species than oxygen ions [88]. Considering that rings are in fact the oxide formed in the intertube spacing during V_{low} [27], and that such oxide may be a porous fluoride rich layer, the concentration of F in the rings after the annealing would be higher than that of the sections between rings.
2. During the stable growth of the nanotubes, there is ion movement from the bulk electrolyte to the bottom of the tubes in the inter-tube spacing. Such movement is generated by the electric field direction. Considering that in nanotubes with bamboo-like morphology the inter-tube channels are blocked by porous barriers or rings, these porous barriers can act as dams that accumulate F ions. Fluoride concentration in the rings would be higher than in the walls since in the walls only the ions moving in radial direction are trapped, and due to the electric field ion movement is preferentially axial.

Fluorine doping plays a pivotal role in the PEC performance of the titania nanotube arrays. Thermodynamic studies suggest that F replaces the O atom and yields a Ti-F-Ti bond, affecting the carrier diffusion in the material [62]. Presence of F generates surface oxygen vacancies, a higher amount of Ti^{3+} ions (not only Ti^{4+}) [89], [90]. In turn, the Ti^{3+} generates an energy level below the conduction band of the TiO_2, this energy level can trap electrons and reduce the recombination rate [91]. Consider the representation of the energy bands of the TiO_2 in figure 4.7. In the undoped anatase the electron-hole pair are generated in the valence band (VB) and conduction band (CB), respectively, when the band gap of 3.2 eV is surpassed (a). The presence of an energy level below the CB allows that some electrons,

instead of going back to the VB (b), remain trapped (c) and available to react or move to the cathode.

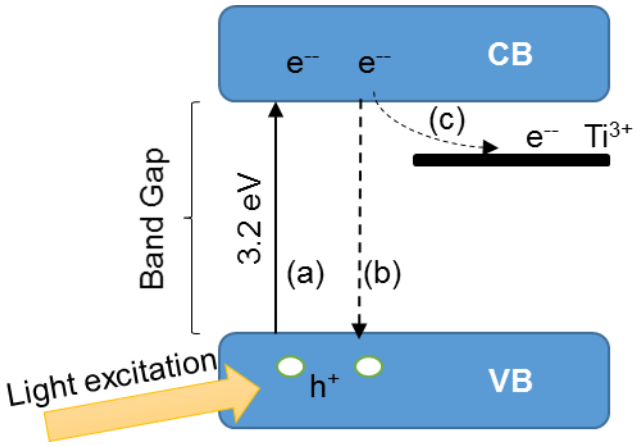

Figure 4.7: Energy bands of F-doped TiO_2. Upon light excitation electrons and holes are generated (a) in the conduction band (CB) and valence band (VB), recombination (b) is reduced for the trapping of electrons (c) in the energy level of Ti^{3+}

Many studies found an increase in the photocatalytic activity of F-doped TiO_2 nanoparticles due to the above mentioned reasons [61], [63], [90], [91], and in some cases activity under visible light has been found [63][20]. Presence of the Ti^{3+} energy level will not modify the band gap of the bulk semiconductor, hence the activity under visible light is attributed to direct excitation of the absorption bands of the oxygen vacancies.

Rings in nanotubes with bamboo-like morphology

FIB characterization was performed to investigate the 3D structure of the nanotube array. Sample characterized by FIB was produced by AV anodization in EG solution of 6.9% water, 0.20% NH_4F and with 9 rings, it is sample presented in figure 4.1.

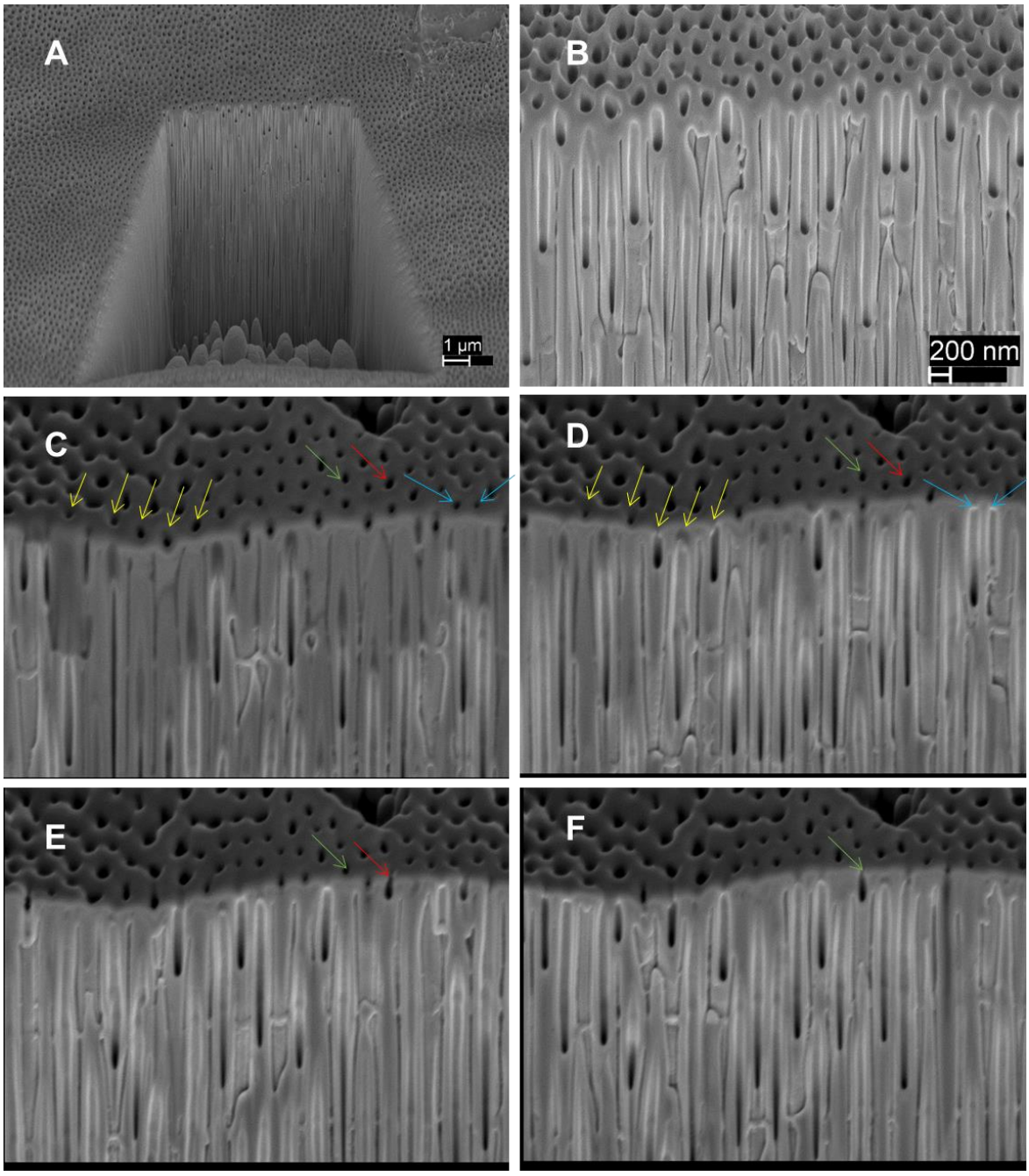

Figure 4.8: FIB results. (A) trench cut for FIB analysis, (B) close up of the trench's wall before serial milling, (C)-(F) sequential imaging after several cuts

To do the FIB characterization a section of the sample with unbroken nanotubes and flat surface was selected, i.e. where only open pores were evident. A trench was cut with a 10pA ion beam in order to exposed the nanotubes (figure 4.8 (A)). Image (B) is a SEM image of the wall of the trench. Then a serial sectioning was carried out using ion milling, and sequential SEM imaging was performed. Image (C) shows with arrows top pores of

the nanotubes that were removed during the ion milling. Images (C)-(F) show the nanotube structure at various depths in the array, it is evident the presence of open inner pores in each tube and of rings in all the tubes at the same high. Notice that only first and second ring were focused. From the sequential imaging a 3D analysis of the nanotube array structure was performed using ImageJ software. Result are in figure 4.9.

During the FIB axial sectioning of the sample was performed, and with it, it was evident that all the tubes possessed rings on the outside wall at the same high. On the other hand, the reconstruction 3D allowed radial sectioning of the sample, and demonstrated that the rings connect all the tubes among each other. Figure 4.9 (A) shows an axial cut of the array at a section between rings, at that position, the tubes are differentiated and the inter-tube spacing is void. Contrary, when the axial cut is observed at a ring position (figure 4.9 (B)) the inter-tube spacing is filled with oxide. Considering this, it can be presumed that by alternating voltage anodization arrays with bundled tubes are formed, those are the titania nanotubes with bamboo-like morphology, and that the F rich oxide connecting the tubes (the rings) is distributed across all the array.

More research is needed to identify other elements that may doped the bamboo-like nanotubes, and to control the amount of dopant inserted. Alternating voltage anodization may be a new technique to dope TiO_2 nanotubes on located positions, new functionalized nanomaterials could be created.

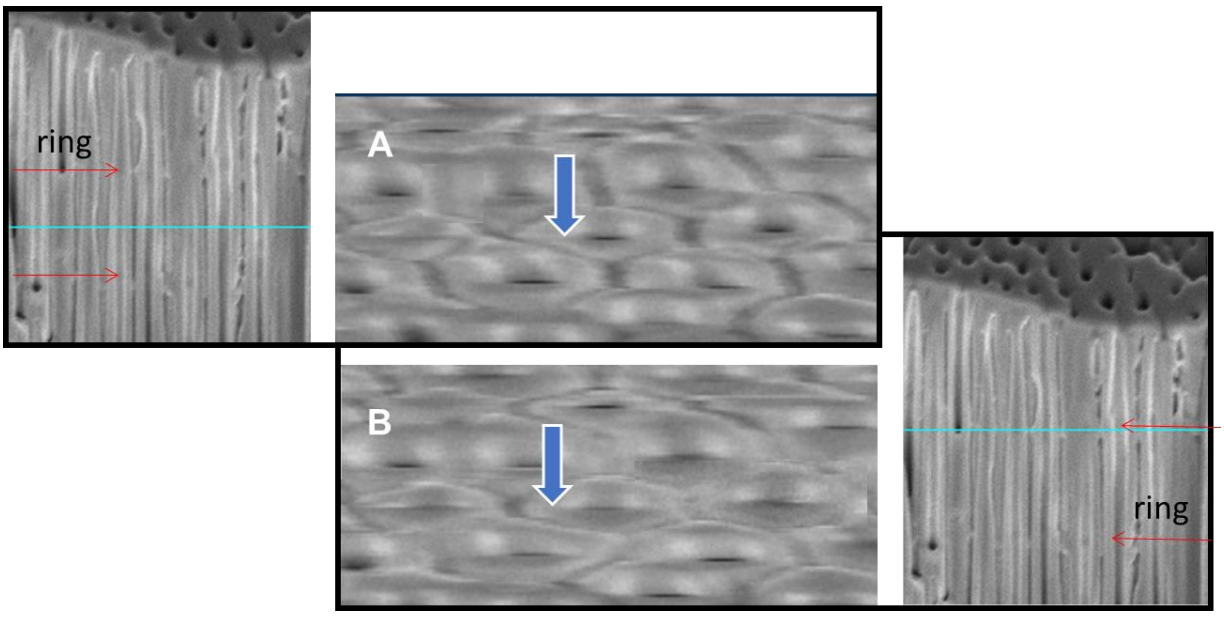

Figure 4.9: 3D model of the nanotubes from collected data during FIB. (A) shows radial section at a position between rings and (B) at ring location. Blue arrows are pointing the same nanotube to facilitate comparison

Conclusions

Alternating voltage anodization generates titania nanotubes with bamboo-like morphology. The rings on the outside wall of the nanotubes connect all the tubes among each other and fill the voids. Such rings possess a higher amount of fluorine than the oxide between rings, then the whole array of nanotube has sections of oxide bundling all the tubes and with higher amount of F. A higher F doping on the rings may be due to the formation of fluorine rich oxide during the low voltage period in AV anodization, or to a higher trapping of the electrolyte in the pores of the rings during the nanotube growth caused by ion movement in the axial direction.

4.2 Photoelectrocatalytic performance of titania nanotube arrays produced by alternating voltage anodization

Abstract

The previous section showed how titania nanotubes with bamboo-like morphology are produced during alternating voltage anodization, and that the produced nanotubes are F doped, particularly in the rings. This section focuses in the effect of such morphology in the photoelectrocatalytic (PEC) performance of the material. To study this, the optimal morphology found in chapter 3 was modified by adding 9, 18 and 27 rings in the outside walls, while keeping the tube length and diameter. Results showed that the PEC response of the material increased with the number of rings, as well as the potential needed to reach the maximum efficiency. This convoluted effects caused a lower overall PEC efficiency with the increase in the number of rings.

Experimental

All samples were formed by two-step anodization protocol. First step of each anodization was performed at 100V during 6 min in fresh EG solution of 3.8% water and 0.15% NH_4F. Then the anodized foil was sonicated to remove the nanotube layer with irregular top morphology. Foil with only footprints was anodized again in the EG solution aged during the first step. Second anodization was performed applying a square pulse voltage, voltage was alternated between 100 and 20 V. Number of pulses was varied in order to obtain nanotubes with 9, 18 and 27 rings on the outside wall. Pulses at 20 V were always 10 minutes long, while the duration of pulses at 100 V was modified according to the number of rings. Desired length was 9 µm, hence total anodization time at V_{high} was 8.9 min (see model for CV in chapter 2). t_{high} was calculated dividing the total time at V_{high} in the number of sections between rings, i.e. 10, 19 and 28.

After the anodization all samples were rinsed with ethanol and dried in air stream. Annealing was performed in air atmosphere to obtain photoactive titanium dioxide nanotubes. Heating rate was 2 °C min^{-1} until 450 °C, and the temperature was hold during 2 hours. Scanning electron microscopy (SEM) and X-ray diffraction (XRD) analysis were performed under the conditions previously described. Only sample with 18 rings was subject of morphological and crystallographic characterization.

Photoelectrocatalityc (PEC) experiments were conducted to evaluate the performance of the material in hydrogen production by water splitting reaction. Conditions were exactly the same as reported in chapter 3. The epoxy covered photoanode was connected with a Ni wire as counter electrode in a two electrode configuration, and the electrolyte was a 1 M KOH (85%, Merck) solution. Alkali solution was degassed by vacuum filtration. Irradiated UVA light was 2610 µW cm^{-2}. Open circuit potential (OCP) and linear sweep voltammetry (LSV) were measured using a DY2300 Digi-Ivy potentiostat.

Results and Analysis

Morphology and Crystallography

SEM images for the sample with 18 rings are provided in figure 4.10. Top of the array was composed of highly organized pores as a result of the two-step anodization protocol (A).

Total length of the array was 8.4 µm, within the 15% error of the used model to predict the length of tubes anodized at CV of 100 V. Number of rings was 18 (figure 4.10 (B)) and the distance between rings was constant along the tubes and ca. 440 nm (C). Tube external diameter was close to 150 nm, the predicted one for anodization in EG solutions of 3.8% water and 0.15% ammonium fluoride. XRD patterns are provided in image (D), typical peaks for anatase phase were observed.

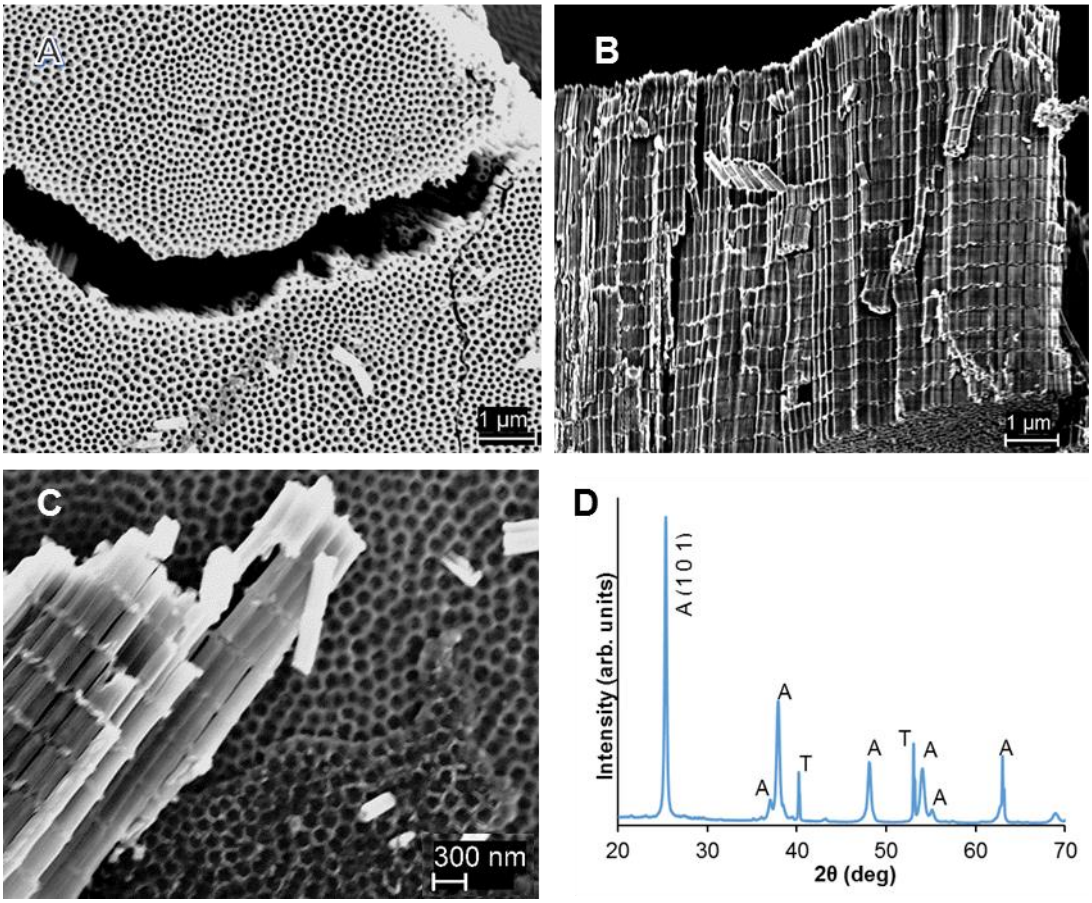

Figure 4.10 Morphological characterization of the sample prepared with 18 rings. (A) organized top morphology, (B) total array with 18 rings and 19 sections between rings, (C) close up of the tubes. (D) XRD analysis showing anatase (A) and titanium (T) peaks

It is possible to assume that the tubes with 9 and 27 rings also had a total length within the error of the prediction model used, considering an analysis of the current transients similar to the developed in the previous section. In one hand the difference between the charge generated during the AV anodization of tubes with 9 and 27 rings and the constant voltage anodization at similar conditions was 15 and 20%, very similar to the difference of 17% for tubes with 18 rings. The length of the tubes with 18 rings was only 0.6 µm lower than the

targeted of 9 µm, then a similar difference in the lengths of tubes with 9 and 27 rings can be expected. In the other hand the time needed to reach the stable growth rate of the nanotubes was 10 s during the CV anodization, time lower than the t_{high} during each AV anodization performed here (see discussion for figure 4.4 of the previous section).

With these results it is possible to presumed that the changes in the PEC performance of the materials prepared by AV with 9, 18 and 27 voltage changes were due to the effect of the number of rings, and not to the change of other morphologic features as tube length or diameter.

PEC performance

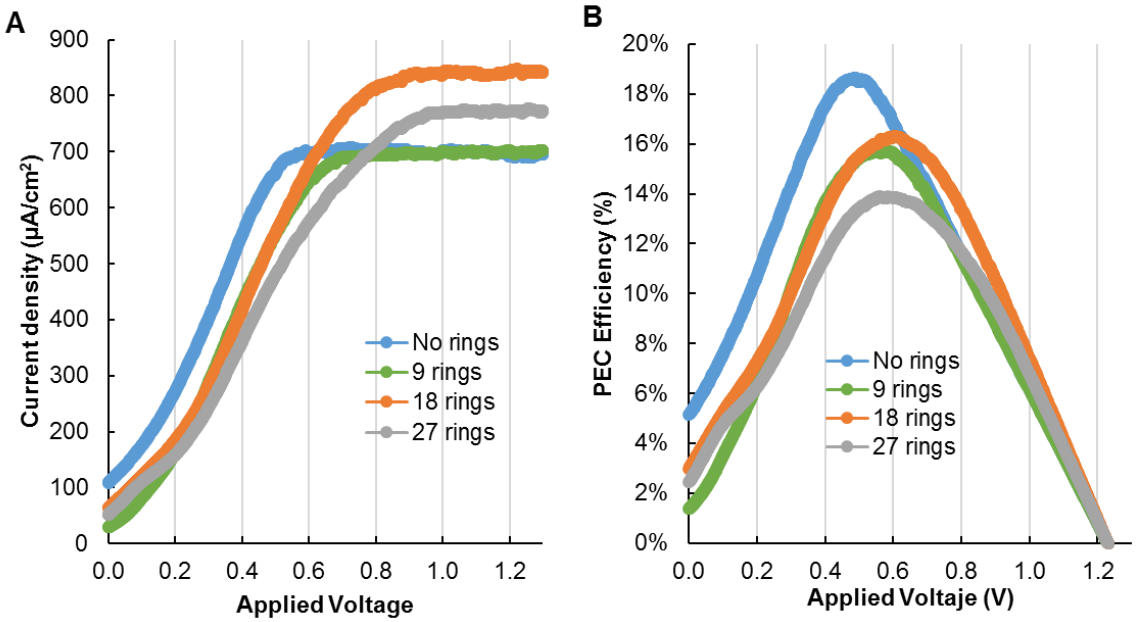

Figure 4.11: PEC performance of nanotubes produced by AV anodization while varying the number of rings, (A) shows the current density recorded during LSV analysis and (B) the calculated PEC efficiency

PEC response of the nanotubes with 9, 18 and 27 rings and without rings is presented in figure 4.11. Maximum current density first increased and then diminished with the number of rings (image (A)), it was ca. 707 µAcm^{-2} when tubes with no rings were used, and ca 700, 840 and 770 with tubes of 9, 18 and 27 rings, respectively. However, the potential needed to reach the maximum current (optimal potential) increased with the number of rings, meaning that more energy was needed to extract the additional electrons generated during the PEC process, this energy can be estimated as the term IV_{bias} in equation 3.3.

Calculated PEC efficiency, according to equation 3.3, is shown in figure 4.11 (B). PEC efficiency was higher when tubes with no rings were used, and diminished down by 25% with tubes with 27 rings.

The maximum current density of the nanotubes increased with the number of rings and then diminished. The initial increase is probably due to a higher presence of fluoride in the array or the increase in surface area. In one hand the rings can increase the surface area of the material and the oxide volume, hence facilitate the amount of holes that can interact directly with the water molecules (equation 3.1) and increase the amount of photons that can be absorbed (see discussion in chapter 3). The increase in surface area has been previously validated by measuring the amount of dye that can be loaded in nanotubes with and without rings for DSSC[35], but the direct measurement can be a difficult task, considering the needed amount of sample for BET analysis. In the other hand, a higher presence of fluoride in the samples with more rings can also explain the increase in the maximum current density achieved. As showed in the previous section, fluorine reduces the chances of recombination of electrons, by trapping some of those in an energy level below the conduction band of the semiconductor. The decrease in the maximum current density in tubes with 27 rings may be due to loss of integrity of the nanostructure.

The negative effect of the number of rings, i.e. the increase in the voltage that needs to be applied to reach the maximum current density, can be explained by an increase in the number of defects in the 1D structure. TiO_2 nanotubes are preferred among other nanostructures due to the facilitated transport of the electrons from the bulk of the oxide to the bottom of the nanotubes and the counter electrode. This is due to the 1D transport of the electrons: they only need to move in one direction, along the tube wall, and this transport is enhanced by the electric field, which is also in axial direction. The presence of rings in the outside walls may interfere with the axial movement of the electrons, by introducing ‘bridges’ between tubes and areas for radial movement. If so, the recombination rate of the electrons would increase with the number of rings, and more energy would be required to compensate such phenomena, as was observed in figure 4.11 (A).

Chen, Hou and Lu[37] found a different result, in their experiments the PEC efficiency increased almost 3 times when tubes with 10 rings were used, compared with tubes with smooth outside walls. High voltage and total anodization time at the high voltage during AV anodization was the same as during CV anodization (no change in tube diameter or length),

hence they attributed the increase in PEC efficiency to the number of rings. Nevertheless, there was an important difference between their experiments and those conducted in this thesis, the annealing atmosphere. During their studies they annealed the samples in hydrogen atmosphere, which increases the number of oxygen vacancies and the conductivity of the nanotubes [37], [92], and has been used to dope the nanotubes with carbon [93], [94], by reduction of the organic electrolyte trapped in the pores of the oxide.

Such important effects of the hydrogen atmosphere may be the key to exploit the advantages of nanotubes produced by AV anodization against those produced by CV. An increase in the tube conductivity can diminish the detrimental effect of the radial recombination within the rings, also, in a reductive atmosphere other elements can dope the nanotubes with increase surface area and oxide volume.

Conclusions

The presence of rings in the outside wall of nanotubes produced by AV anodization increases the maximum current density obtained under UVA light and in conditions for water splitting, probably due to the preferential F doping of the rings and an increase in the surface area and the oxide volume. However, with the number of rings the potential required to separate the produced charges also increases, leading to an overall diminish of the calculated PEC efficiency.

Chapter 5.

In this chapter another application of the TiO_2 nanotubes is studied, which also exploits it photoelectrocatalytic performance: simultaneous electricity production and wastewater treatment in a photo-fuel cell (PFC). Operational conditions of the PFC were studied and finally the PFC with the highest power output was coupled to the PEC cell. With this coupling the PEC cell developed in the previous chapter is able to operated disconnected from the power grid, since the potential required to work at maximum efficiency is supplied by the PFC cell.

Chapter 5. An autonomous dual-cell reactor for hydrogen production by water splitting with TiO_2 nanotubes

A photoelectrocatalytic cell (PEC cell) and a photo-fuel cell (PFC)

Introduction

As found in the previous chapter, titania with bamboo-like morphology demanded higher potentials to function at maximum efficiency during PEC water splitting than the demanded by nanotubes prepared by constant voltage anodization. Such increase in the bias, or the electrical energy input, reduced the overall PEC efficiency. Under such circumstances the use of nanotubes with bamboo-like morphology did not reduce the cost of hydrogen production, in fact, the cost was probably higher. Krol & Grätzel [5] showed how the bias requirement can significantly impact the hydrogen production cost. Considering the price of such electricity, or its generation cost with photovoltaic devices, they concluded that the improvement of the PEC technology requires materials able to generate higher photocurrents, and demand lower bias [5]. Many efforts have been focusing in the reduction of the bias needed in the PEC cell, or the elimination of it by using multijunction photocatalysts or tandem cells [2], [5], [8], [9].

Some authors focus in the implementation of more cost effective and environmentally friendly electrical energy. The use of different energy sources does not reduce the bias requirement of the PEC, but allows the use of other emerging energy sources with low voltage output. Authors have coupled the TiO_2 nanotubes PEC cell with microbial fuel cells (MFC) [38] for hydrogen production, and with photofuel cells (PFC) [39] for wastewater treatment. A PFC uses an organic compound as ‘fuel’ and generates electricity by the oxidation of the fuel [12]. The oxidation is caused by the generation of electron/hole pairs in a photoresponsive electrode [12]. The photoactive electrode can be made of TiO_2 nanotubes, and the organic compound can be a pollutant [40]. The presence of the organic compound is required, since the oxidation of organic substances is more efficient than that of water (water splitting) [95]. The research on PFC with TiO_2 nanotube arrays typically

focuses in the optimization of the cell conditions: pollutant and supporting electrolyte concentration and pH of the solution [39], [40], [96], nanotube morphology has been studied, while changing simultaneously more than one morphological feature [40].

This chapter focuses on the coupling of the PEC cell for hydrogen production developed in the previous chapters with a PFC cell fueled with the actual organic wastes produced during the anodization, i.e. ethylene glycol solutions. The chapter is divided in two sections, the first one focuses in the optimization of the PFC, including the independent effect of tube length and diameter in the photoactive electrode. In the second section the PEC cell is coupled with the PFC, demonstrating that the last one can act as an adequate energy source for the water splitting in the PEC cell.

5.1 The Photo-Fuel Cell (PFC) – Optimization and morphology effect

Abstract

A suitable PFC to power the PEC cell was developed. Pollutant concentration, pH solution, supporting electrolyte and nanotube morphology were studied. Maximum efficiency of the PFC with the best performance was 1.9 ± 0.2% under UVA light, and output potential was ca. 0.46 V, a voltage close to the one demanded by the PEC cell of chapter 3 with highest performance (0.50 V). The reasons for the effect of each operational conditions were discussed.

Experimental

All samples were prepared following the two-step protocol developed in chapter two. The study of the composition of the solution in the PFC was performed with foils produced in EG solutions of 3.8% water and 0.15% ammonium fluoride (composition is that of the fresh electrolyte in the first anodization). First anodization was performed at 100V during 6 min, second anodization at 100V during 8.9 min, hence tubes were assumed to be 9 μm long and 150 nm of external diameter, which were those with the highest efficiency in chapter 3. The used EG solution of each anodization was collected and storage to be used as the

organic pollutant in the PFC. After anodization each sample was rinsed and dried, and then annealed, following the same procedures previously explained. Samples used to study the effect of nanotube morphology were the same used in the DoE 3^2 of chapter 3, previous washing with water and drying with pressurized air.

PFC experiments were conducted in a two electrode configuration, with the anodized foils as photoanode and Ni wire as cathode. The area of the electrodes with TiO_2 nanotubes was controlled by covering it with epoxy resin (see chapter 3). Solution composition and pH was varied in different ranges by using di-water (20 and 80 %), Na_2SO_4 (0.0025 – 0.1 M), H_2SO_4 and NaOH (pH range 1.09 – 13.8), during those experiments irradiated light was 2100 µW cm^{-2}. The study of the tube morphology was conducted in aqueous solution of 20% EG wastes and 0.2 M NaOH (pH 12.4), irradiated light was increased to 3050 µW cm^{-2}. The electrodes were always connected with a copper wire and a home-made circuit with variable resistors, along a voltammeter, as sketched in figure 5.1. The electricity generation capability of the cell was measured by following the potential between the electrodes in open circuit condition (OPC) and when different resistors were closing the circuit, from 99 Ω to 98 kΩ.

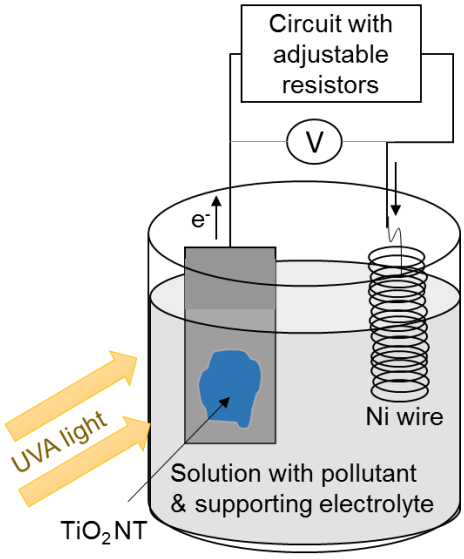

Figure 5.1: Scheme of the used photofuel cell

Results and Analysis

Effect of the pollutant amount and nature

For this study actual organic wastes were employed: the ethylene glycol solutions used in the anodization of the samples with morphology of 9 µm and 150 nm of length and external diameter. Compositional analysis of the wastes was not performed, hence the exact concentration of substances or the total organic carbon (TOC) was unknown. The wastes were mainly composed of ethylene glycol, which was >95.5% of the fresh anodization solution; water, ammonium fluoride and $[TiF_6]^{-2}$ along with other ions may be present too in the wastes. Water composition is surely different to that of the fresh solution since water was continuously split during the anodization. Also, part of the initial F ions was consumed to create soluble complex $[TiF_6]^{-2}$ by dissolving the titania.

Nature of the pollutant plays a major role in the electricity generation capability of the PFC. Liu et al.[40] described in their work the use of different substances, including actual wastewater (pharmaceutical wastes, chemical plant and dying wastes, and natural urine solution). They found that the highest power output was reached with acetic acid solutions (model compound), but no study of EG solutions was performed. The higher energy generation with acetic acid was due to the small redox potential of the substance (to CO_2), -0.4eV, i.e. acetic acid was easily decomposed. Typically, decomposition of the substances is produced by direct interaction with the photogenerated holes at the surface of the semiconductor (equation 5.1), or with *OH radicals (eq. 5.3) produced according to eq. 5.2.

$$R + nh^+ \rightarrow R' + nH^+ + e^- \quad (5.1)$$

$$OH^- + h^+ \rightarrow {}^*OH \quad (5.2)$$

$$R + {}^*OH \rightarrow R' + H_2O + e^- \quad (5.3)$$

In reactions 5.1 and 5.3 the organic compound simultaneously acts as a hole scavenger and as a sacrificial agent. In the one hand, it reduces the recombination rate of the electron/hole by consuming the available holes at the surface of the semiconductor or the hydroxyl radicals, and in the other, during the oxidation an electron is released [14]. Ethylene glycol can act as fuel for the PFC, it has been already used in direct fuel cells (no photo-fuel cells) [97] and can be degraded by *OH radicals, EG/CO_2 redox potential is

1.22eV [97] and the redox potential of *OH radicals is 2.81eV [98]. Possible reaction route of the oxidation of the EG has been proposed by other authors and can be found in: considering the direct reaction of the EG with the holes (reaction 5.1) [99], or the reaction of the EG with the hydroxyl radical (reaction 5.3) [100], [101]

Concentration of the pollutant can also strongly affect the PFC performance. Figure 5.2 (A) shows the current-voltage profiles obtained in PFCs with EG solutions at different concentration as the fuel. Image (B) shows the output power (*V* x *I*) at each potential. Amount of EG wastes (EG-w) was varied between 0, 20 and 80%. NaOH 0.2 M was used as supporting electrolyte and photoanode was composed of nanotubes 9 µm long and with 150 nm of external diameter (according to the model developed in chapter 2). Results showed that the maximum output power was ca. 15 µW cm^{-2} at ca. 0.35 V when no pollutant was added, and it increases ca. 2.4 times when a solution of 20% of EG-w was used as fuel. In the PFC with 20% EG-w the maximum power was also obtained at a higher output voltage, ca. 0.46 V. Such potential is close to the required bias to power the PEC cell in chapter 3 with nanotubes 9 µm long and with 150 nm of external diameter (with which the highest PEC efficiency was reached).

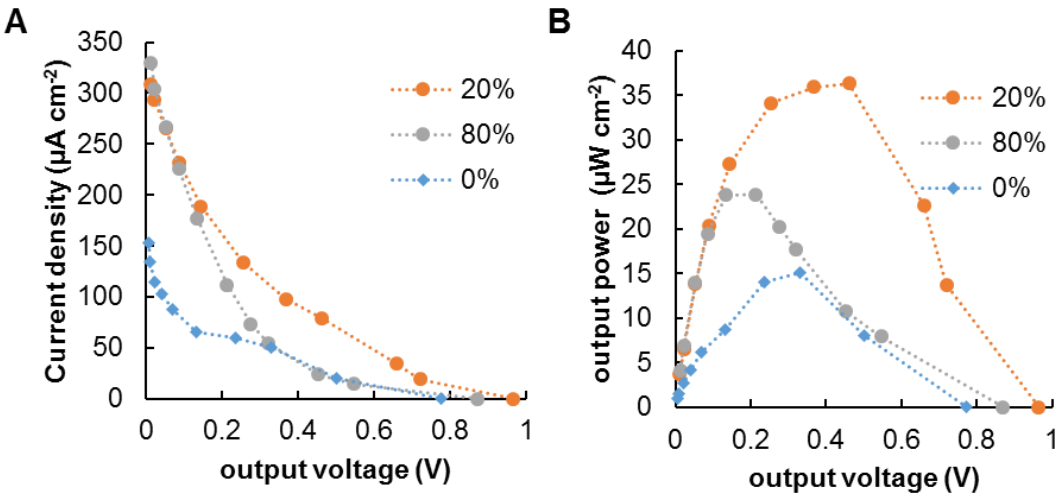

Figure 5.2: PFC when amount of pollutant was varied, (A) shows the current voltage profiles and (B) the output power at each potential. Experimental points are united with lines only to facilitate data interpretation

When the amount of EG-w was raised to 80% the maximum power was ca. 24µW cm^{-2} at 0.21 V. The PFC efficiency was higher when the pollutant was used than when the concentration of EG-w was 0 %, but high concentration of the EG-w reduced the PFC

performance. This is due to the reduction in the amount of water, which in turn increases the electrolyte resistance and reduces the amount of hydroxyl radicals that can be generated, as less hydroxyl groups will be adsorbed on the surface [102]. Solutions mainly composed of EG are preferred in the anodization precisely because they have a higher viscosity and lower ionic conductivity. High concentration of alcoholic pollutants can also induce formation of bigger organic compounds (aldol condensation) [103], reducing the PFC efficiency [104]. PFC efficiency was 0.7%, 1.8% and 1.1% when EG-w concentration was 0, 20 and 80%, respectively. PFC efficiency was calculated considering only the light irradiated (P_{in}) and the maximum output power (VI_{max}), according to equation 5.4. It should be noted that if the cell is operated at a different output potential the output power will change, as well as the PEC efficiency, hence PFC efficiency calculated by eq. 5.4 is the maximum efficiency.

$$PEC\ eff = \left({VI_{max}}/{P_{in}}\right) x\ 100 \qquad (5.4)$$

The shifting in the potential of maximum output power is due to a variation of the anode potential. In the presence of sacrificial agent the holes consumption is higher, then the relative amount of electrons increases in the semiconductor and the anode potential becomes more electronegative [12].

Effect of pH and supporting electrolyte

The pH of the solution of 20% EG-w was varied between 1.09 and 13.8 units of pH, results are presented in table 5.1. The highest output power was obtained at pH solution of 12.4 (NaOH composition 0.2 M), and was ca. 37.2µW cm^{-2} at 0.46 V. The strong dependence of EG oxidation with pH solution was previously observed in direct fuel cells [97]. In the case of a PFC the effect of pH can be understood according to equations 5.1 and 5.2. In acidic solutions the direct oxidation of the EG with the photogenerated holes is preferred, hence EG must be adsorbed in the surface of the oxide. In alkali medium holes are mainly consumed by hydroxyl groups which are adsorbed more easily than EG since they are smaller. This explains the higher PFC efficiency in alkali mediums.

Table 5.1: Effect of pH in the PFC efficiency, solution was 20% EG-w, irradiated light 2100 µW cm^{-2}

pH	IV_{max} (µW cm^{-2})	V at IV_{max} (V)	PFC eff (%)
1.09	11.1	0.11	0.5

2.72	16.3	0.13	0.8
4.37	28.5	0.27	1.4
5.48	28.4	0.27	1.4
9.62	32.2	0.44	1.5
12.4	37.2	0.46	1.8
13.8	22.3	0.36	1.1

The NaOH also acts as a supporting electrolyte, by reducing the solution resistance, similarly as done in the PEC cell [13]. Other substances have also been used with this purpose, including Na_2SO_4 [40]. Sodium sulfate at varying levels of concentrations were used to study the effect of supporting electrolyte (see results in table 5.2). Results are in agreement with those found by Liu et al. [40], performance of the cell first increased with the sulfate concentration and then diminished.

Table 5.2. Effect of Na_2SO_4 concentration in the PFC efficiency, solation was 20% EG-w, no NaOH was added, irradiated light 2100 µW cm^{-2}

Na_2SO_4 (M)	**IV_{max} (µW cm^{-2})**	**V at IV_{max} (V)**	**PFC eff (%)**
0	6.9	0.26	0.33
0.0025	9.1	0.29	0.43
0.01	7.8	0.22	0.37
0.025	7.5	0.27	0.36
0.1	6.8	0.25	0.32

Although a weak trend was observed while varying sulfate concentration, further experiments did not include this supporting electrolyte in the PFC solution because the effect of sodium sulfate is not significant. All the PFC efficiencies in table 5.2 are statically the same. The deviation of PFC efficiency is 0.2%. Such deviation was calculated by measuring PFC performance of 4 different anodes at the same conditions.

Effect of the nanotube morphology

Effect of the nanotube morphology in the PFC efficiency may be different than the effect in the PEC cell since during electricity production no external bias is applied. In a PFC the recombination rate of the electron/hole pairs depends only on the hole consumption by the electrolyte and the facility of electron transport to the bottom of the tubes, without any external field (no external bias). Under this circumstances a strong effect of the nanotube morphology is expected, as observed from the results in figure 5.3. Table 5.3 summarizes the data presented in figure 5.3.

The tube length strongly affected the PFC performance in tubes of 150 and 220 nm of external diameter, as observed in figure 5.3 (A), (B) and (E). The output power and the PFC efficiency first increased with tube length and then diminished. As explained in chapter 3, longer tubes allow the absorption of more photons, until no more light can penetrate the array and the extra length becomes only an extra and unnecessary path for the electrons, increasing the recombination rate.

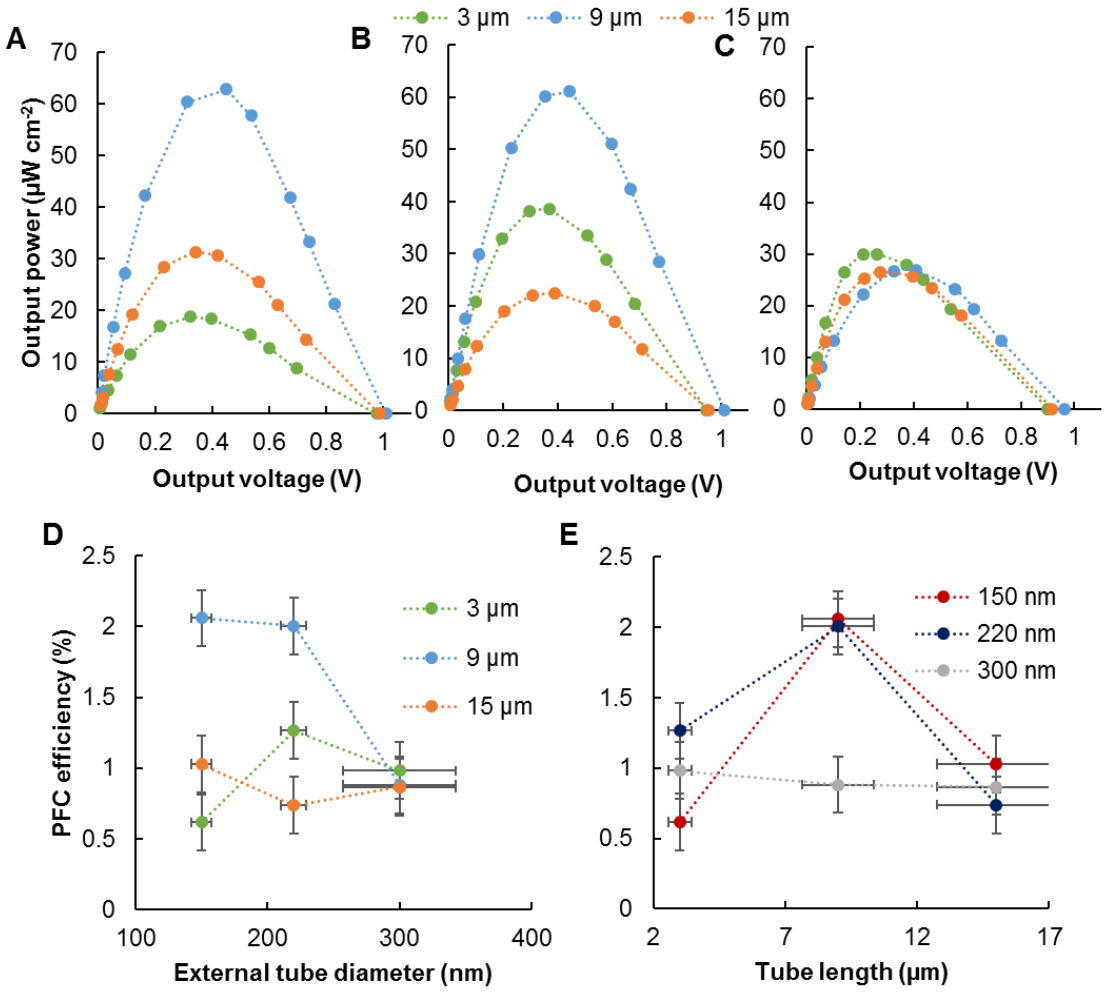

Figure 5.3: Tube morphology effect on the PFC performance. (A), (B) and (C) show the output power as a function of output voltage for each studied morphology: tubes of 3, 9 and 15 µm length and outside diameter of 150 (A), 220 (B) and 300 nm (C). (D) the maximum PFC efficiency while varying external tube diameter and (E) when tube length was modified. Fuel was composed of 20% EG-w, supporting electrolyte was NaOH 0.2 M (pH 12.4) and irradiated light was 3050 µW cm^{-2}. Experimental points are connected to facilitate data interpretation

In the other hand, there was no variation in the PFC performance of tubes of 300 nm of external diameter and different lengths (figure 3.5 (C) and (E)). This can be explained considering the wall thickness of the nanotubes. In tubes with 300 nm of external diameter the wall thickness of 110 nm increased the radial recombination rate. The holes photogenerated in the oxide bulk must move to the oxide surface, and a longer distance (wall thickness) rises the recombination rate. This dependence with the wall thickness in the PFC is stronger than in the PEC cell since no voltage was applied, and electrons can easily recombine, not only in the axial direction but also in the radial one. Hence the external diameter and the wall thickness influenced the PFC performance.

Figure 3.5 (D) shows that in tubes of 3 µm the PFC efficiency first increased with tube diameter and then decreased. The explanation for this behavior is similar to the provided in chapter 3, initially, thicker walls increase crystallites size, reducing the recombination rate of the electrons. Also, bigger internal diameters facilitate the movement of reactants and products between the inner pore of the nanotubes and the electrolyte. The efficiency decreased with a further increase in the diameter due to the high radial recombination rate into the wall thickness. In tubes of 9 µm the dependence of the PFC efficiency with external tube diameter only showed the final diminish, a plateau behavior was obtained between 150 and 220 nm of external diameter. In tubes of 15 µm the external diameter did not influence the PFC performance, due to the strong and negative effect of long tubes in the axial recombination rate (see figure 3.5 (D).

Table 5.3: Tube morphology effect on the PFC performance

Tube morphology		**IV_{max} (µW cm^{-2})**	**V at IV_{max} (V)**	**PFC eff (%)**
Diameter (nm)	**Length (µm)**			
150	3	18.8	0.32	0.6
220	3	38.6	0.37	1.3
300	3	30.0	0.26	1.0
150	9	62.8	0.45	2.0
220	9	61.2	0.44	2.0
300	9	26.9	0.41	0.9
150	15	31.4	0.34	1.0
220	15	22.5	0.39	0.7
310	15	26.4	0.27	0.9

The highest PFC efficiency of 2.0% was obtained with two different nanotube arrays: with tubes of 9 µm long and 150 nm of external diameter, and with tubes of the same length and

220 nm of external diameter. Both morphologies produced similar output power at nearly the same potential ca. 0.45 V, which is close to the demanded potential (ca. 0.5 V) in the PEC with higher hydrogen production found in chapter 3.

Conclusions

PFC efficiency was strongly affected by the pollutant concentration in the used fuel, the pH of the solution and the morphology of the nanotubes. Pollutant concentration improved the performance by acting as a hole scavenger and a sacrificial agent, but too much of the alcoholic pollutant reduces the PFC efficiency. The higher output power was obtained with solution of pH 12.4, the sodium hydroxide acted as a supporting electrolyte and the OH^- presence facilitated hydroxyl radicals generation. Morphology effect was explained by following the effect of tube diameter and length in radial and axial recombination, respectively, as well as other effects described in chapter 3, as the crystallite size and the amount of photons absorbed. A suitable PFC to power the PEC cell was identified: with nanotubes of 9 µm and 150 nm of length and external diameter, and fueled with solution of 20% EG-w at a pH of 12.4 (NaOH 0.2 M).

5.2 An autonomous dual-cell reactor for hydrogen production: PEC cell and PFC

Abstract

The PEC cell was operated independently of the power grid, by connecting it to a PFC which also functioned with TiO_2 nanotubes and decomposed a pollutant, the same ethylene glycol wastes produced during the preparation of the TiO_2 nanotubes. The performance of the PEC cell was the same when the bias was provided by the power grid or by the PFC.

Experimental

Both the photo-fuel cell (PFC) and the photoelectrocatalytic cell (PEC cell) worked with titania nanotubes of 9 µm long and 150 nm of external diameter. Nanotubes were produced by the two-step anodization protocol developed in chapter 2. Foils were anodized first in a

fresh EG solution of 3.8% water and 0.15% NH_4F at 100 V for 6 min, then the nanotube were removed by sonication of the sample in di-water and the foil was anodized again. Second anodization was performed in the used EG solution by each first step at 100 V during 8.9 min. After anodization all samples were rinsed and dried, and finally annealed in air atmosphere at 450 °C for 2 hours. In order to control the exposed area of each electrode with nanotubes foils were covered with epoxy resin, according to chapter 3.

The PFC functioned using as fuel an aqueous solution of actual wastewaters, 20% of the wastes generated during the anodization of the samples, and at pH 12.4 (0.2 M NaOH). Irradiated light in the PFC cell was 3050 µW cm^{-2}. The PEC cell worked as in chapter 3, in an aqueous and degassed solution of KOH 1 M, irradiated light was 665 µW cm^{-2}. The two cells were connected to each other as depicted in figure 5.4 (A). The electrode with nanotubes of the PFC was connected to the cathode of the PEC, while the photoanode of the PEC cell was connected to an ampere meter and to the cathode of the PFC. The output voltage of the PFC was controlled with a voltammeter. Figure 5.4 (B) is a photograph of the actual two-cell configuration during operation. Efficiency of the PFC was calculated according to the equation 5.4, while the efficiency of the PEC cell was determined following equation 3.3.

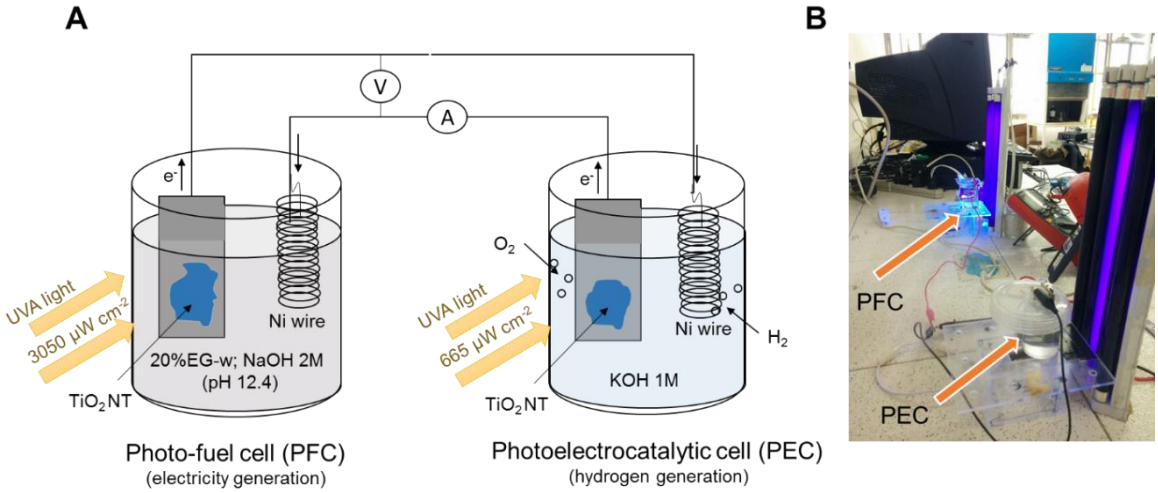

Figure 5.4: Two cells connected to produce hydrogen independently of the external power grid, the PFC generates the electricity demanded by the PEC for hydrogen splitting (A), (B) is an actual photograph of the experimental setup during operation

Results and Analysis

The proper functioning of the coupled two cells was verified. Results are presented in figure 5.5. When light was turned on the voltage and current density of the system increased and a small period of time was needed before stabilization. Then the output power of the PFC was ca. 0.53 V during all the experiment, and the current density of the PEC cell was ca. 170 µA cm^{-2}. Values remained constant even after a perturbation of the system, when the photoanode of the PEC cell was slightly taken out of the solution to shake off accumulated bubbles in the epoxy resin. The efficiency of the PEC cell was 18.3%, same as the one found in chapter 3 for nanotubes with the same morphology and at the same electrolyte composition. The calculated efficiency of the PFC in the coupled system was 2.4%.

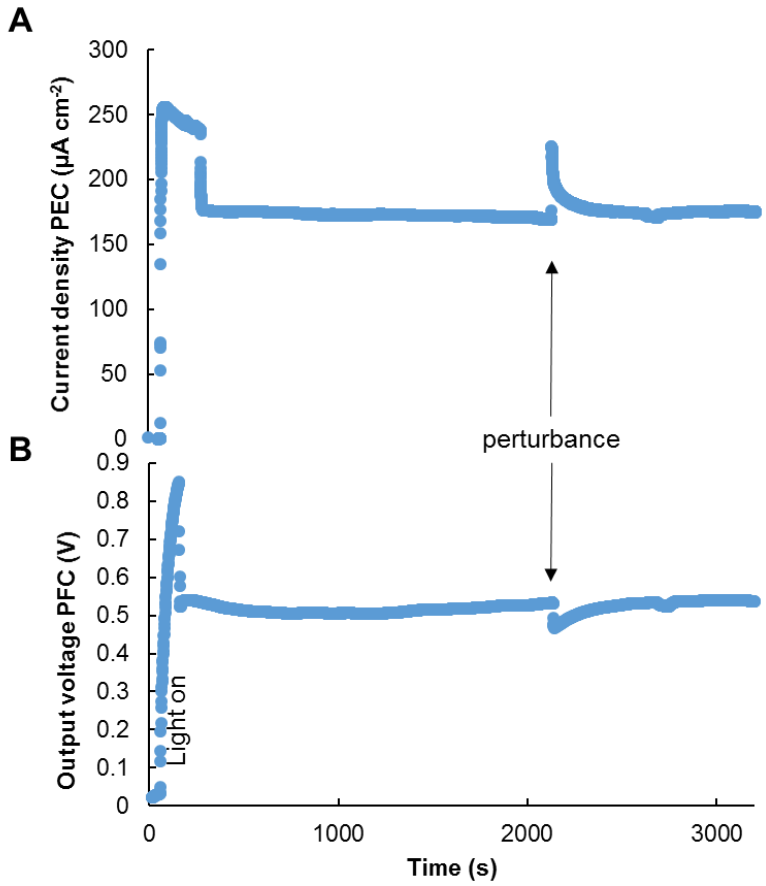

Figure 5.5: Experimental data when the PFC was coupled to the PEC cell, (A) is the current density of the coupled PEC cell, and (B) the output voltage of the coupled PFC

The efficiency of the PFC coupled to the PEC cell was higher than the determined in the stand alone PFC probably due to the potential of each electrode in the PEC cell. In the stand alone PFC the maximum efficiency was 2.0%, and no external bias was applied to

reduce the recombination rate of the electron/hole pair. When the PFC was coupled to the PEC cell, the reactions taking place in the photoanode and the cathode of the PEC cell acted as a small external bias for the PFC. Consider that although the redox potential of the water is 1.23V the PEC cell can split water, this means that the PEC cell generates its own potential.

The performance of the PEC cell, operated at exactly the same conditions, was equal when the required bias (0.53 V) was provided by the PFC and when the voltage was provided by the power grid (potentiostat). When the PEC cell in figure 5.4, with the same nanotube foil and irradiated light, was connected to a potentiostat and 0.53 V of bias was provided, the current density was 170 μA cm^{-2}, same as in figure 5.5. when the PFC was used instead.

Equivalence between the performance of the PEC cell when connected to the PFC or the potentiostat was also tested when the applied bias was 0.31 V (a voltage lower than the required to operate at the maximum efficiency of the PEC cell). Under such circumstances the current density of the PEC cell was 88.3 and 84.7 μA cm^{-2} when the potentiostat (power grid) and when the PFC were used, respectively.

The net efficiency of the dual-cell reactor (coupled PEC cell and PFC) was 4.9 %. Efficiency was calculated according to equation 5.5 which considers only the power output (Net current x 1.23 V) and the power input (light irradiated on PEC cell and on PFC). This efficiency is remarkable high, considering that the dual-reactor functioned independently from the power grid, produced hydrogen and treated a pollutant at the same time. Further improvement of the material response will increase the efficiency of the dual-cell reactor.

$$dual-cell\ efficciency = \frac{Net\ current\ x\ 1.23\ V}{Light\ on\ PEC\ cell + light\ on\ PFC} \times 100 \qquad (5.5)$$

In conclusion, the two-cell reactor was able to generate hydrogen at the same rate that the PEC cell did while connected to the power grid. Although the PFC demands also the use of photoactive electrodes and more surface area for light trapping, which in practice may increase the capital costs of a plant [5], the two cell reactor is a very convenient system. With the PFC-PEC cell hydrogen is produced, pollutants can be decomposed and no energy from the power grid is required. The independence of the power grid reduces the operational costs, as well as the negative impact of the technology associated to power consumption of the power grid, which is usually produced with CO_2 producing technologies. The PFC also generates CO_2, but it is a coproduct of the treatment of organic pollutants.

Chapter 6.

This is an additional chapter that surpasses the original objectives of this thesis. In this chapter, an emerging technology for electricity generation is used to power the PEC cell. This technology uses the corona effect to create usable electric power from the spontaneous potential created between the atmospheric clouds and the surface of the Earth. The technology is yet in its initial stages of development, but the results found here are promising. The experiments were conducted using the corona-effect-harvesting system developed by the electromagnetic compatibility research group of the Universidad Nacional de Colombia and with the engineers Carlos Andres Rivera Guerrero, Jorge Enrique Rodríguez Manrique, Carlos Fernando Hernández Prada and Francisco Javier Quintero Cortés.

Chapter 6. Use of the power harvested from atmospheric corona effect on a PEC cell for hydrogen production

Abstract

A PEC cell was operated while coupled to a corona-effect-harvesting system. The PEC cell demands an additional electrical power to function at maximum efficiency, and such power was provided here by the formerly mentioned harvesting system. Such system uses the natural potential created between the clouds and floating electrodes on earth to generate electrical power. The results presented here show that the corona effect can be used as power supply, and that such power can be converted to chemical energy.

Introduction

The corona effect is a phenomenon that happens around of high voltage systems. It is generated when the electric field is strong enough to ionize the air and a chain reaction begins: when the atoms are ionized, positive ions and free electrons are generated, such electrons can be energetic enough to strike other atoms, ionize them, and produce more free electrons, and so on, this process is called an electron avalanche [41]. This corona effect occurs in high tension lines (surrounding the conductors), and in nature: a corona current or point discharge can be produced from vegetation at the ground or from hydrometeors in clouds [41], by accumulation of charges and the creation of an electric potential, just as lightning is created [105].

The corona current happening in nature between the clouds and the surface of the earth can be harvested, generating usable electrical power. This has been done by the Electromagnetic Compatibility research group of the Universidad Nacional de Colombia by using floating electrodes [42]. While research has been conducted to relate the behavior of the corona current to the atmospheric conditions [106], [107], more work is still needed to evaluate its use. The electric storage of the obtained power from the corona effect was originally proposed in [42], but its transformation to chemical energy (fuels), is also an

interesting alternative, just as has been proposed for other non continuous energy sources, as solar or wind energy.

This chapter focuses on the use of the electrical power generated from the corona effect in the photoelectrocatalytic water splitting. The hypothesis studied is that a PEC cell coupled to the corona-effect-harvesting system behaves the same as when the PEC cell is connected to a regular power supply (potentiostat) that uses energy from the power grid.

Experimental

The photoelectrocatalytic (PEC) cell use in this chapter was a single chamber two electrodes cell. The photoanode was composed of titania nanotubes of 9 μm long and 150 nm of external diameter, which was the morphology with the highest PEC performance found in chapter 3. The cathode was a Ni wire. The TiO_2 nanotubes were prepared following the two-step anodization protocol previously explained, and as before the anodized foil was annealed in air atmosphere and covered with epoxy resin after the anodization. Both electrodes were submerged in a degassed deionized water solution of 1 M KOH, and the incident irradiance on the surface of the photoanode was ca. 2600 μW cm^{-2}.

The harvesting system of the corona current is explained in [42] and in [106]. It used five (5) floating electrodes installed on top of a building and at 21 m from the ground, and a diode bridge. During the experiment the electric power is not only generated from the corona effect between the clouds and the electrodes, but also from the broadcasting of the radioelectric spectrum in the atmosphere (including radio station's signals). When the harvesting system was connected to the PEC cell, the atmospheric conditions reported by the nearby weather station were temperature of 19.4 °C, wind speed of 3.5 km/h and humidity of 53% [108]. After the experiment, the obtained potential with the harvesting system of the corona effect was provided by a potentiostat (DY2300 Digi-Ivy) and the PEC performance was measured again. Current was recorded with a Uni-Trend 71b multimeter.

Results and analysis

An initial experiment demonstrated the applicability of the power provided for the corona effect in the functioning of the PEC cell. The experiment, although short, demonstrated that during the coupling of the PEC cell and the corona-effect-harvesting system a current

density was generated only when the light was on. In figure 6.1 it can be observed that a current density of approximately 710 µW cm^{-2} was generated when the light was turned on, the current decreased sharply until zero when the light was turned off and raised again to the stable value when the light was restored. During this experiment the atmospheric conditions were 25.4°C of temperature, 1.1 km/h of wind speed and the humidity was 43 %. The potential measured between the anode and the cathode was ca. 0.58 V

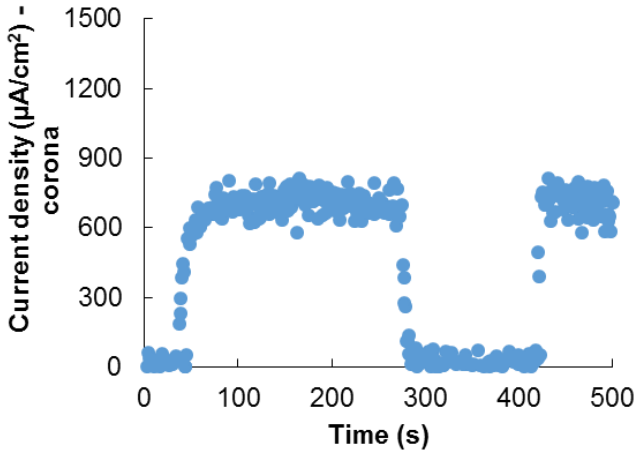

Figure 6.1: On-Off cycles during coupling of the PEC cell and the corona-effect harvesting system

Comparative results between the data obtained using the power obtained from the corona effect and the potentiostat is presented in figure 6.2. The voltage of the corona system before connection (open circuit voltage) was ca. 1.5 V. When the PEC cell was connected and the light was turned on the potential decreased down to a value which fluctuated over the time, 1.37 V was the most usual value (see figure 6.2 (A)). Image (B) presents the recorded current density, the value strongly fluctuated over time, at difference of the experiment performed previously and shown in figure 6.1. Nevertheless, the average current density was very similar, 720 µW cm^{-2}. The same PEC cell was tested then connected to a potentiostat and applying a voltage of 1.37 V between the photoanode and the cathode. The current density transient is presented in figure 6.2 (C), the average value was ca. 820 µW cm^{-2}, 10 % higher than the obtained when the same voltage was provided by the corona effect (image (B)).

From this experiments it can be concluded that the power harvested from the corona effect can effectively provide the additional power demanded by the PEC cell for maximum

performance. The current density obtained when the PEC cell was coupled to the potentiostat was very similar to the measured when the system was coupled to the corona harvesting system. The difference of 10 % can be attributed to losses in the circuit used to transform the corona discharge in usable power. The high fluctuation of the voltage delivered by the corona system (figure 6.2. (A)) is the reason of the high variation of the current density of the PEC cell (figure 6.2 (B)). A mild variation of the current density was observed too in the experiment resumed in figure 6.1, the difference in the intensity of the variation is probably due to the atmospheric conditions of each day. For example, previous experiments in simulated conditions and conducted by the electromagnetic compatibility research group demonstrated the strong effect of the wind in the corona discharge [109]. When the experiment of figure 6.1 was conducted, the wind speed was ca. 1.1 km/h, while it was 3.5 km/h during the experiments of figure 6.2. Probably the higher wind speed produced a higher power from the current discharge [109], which in turn was more unstable. The higher power during the experiments of figure 6.2 is supported by the voltages values obtained that day 1.37 V, while that voltage was 0.56 V during experiments presented in figure 6.1.

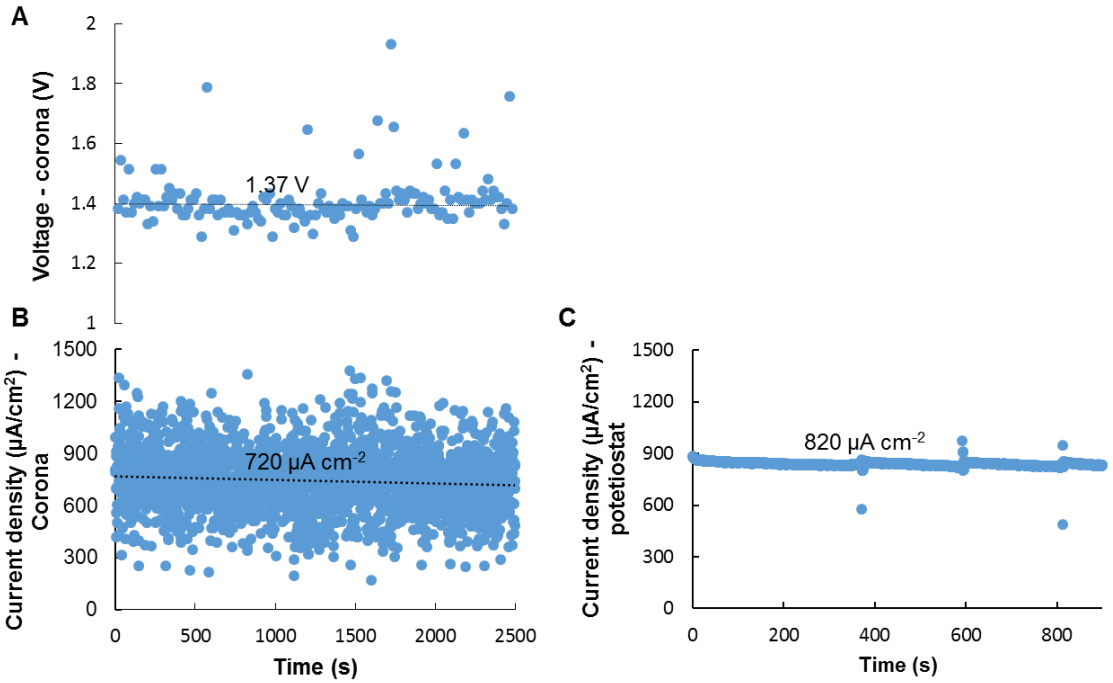

Figure 6.2: Comparative result when the power from corona effect was used and when the potentiostat was employed. (A) and (B) show the voltage and the current density obtained during coupling of the PEC cell with the corona harvesting system, (C) shows the current

density transient when a potential of 1.37 V was applied with the potentiostat. Current density was recorded every second, while the sample time of the voltage was 10 s

More studies are needed to improve the corona-effect-harvesting system, in order to make output power more stable, although the results obtained demonstrated that the system can be used as it is now for water splitting in a PEC cell. That is precisely an advantage of converting the electric power harvested in chemical power, the last one can be generated although the quality of the electrical power is not optimal.

Conclusions

The power harvested from the atmospheric corona discharge can effectively be used to operate the PEC cell. While coupled to the harvesting system, the PEC cell behaved similarly as when a conventional power supply connected to the power grid was used.

Conclusions and recommendations

Conclusions

The proposed objectives of this thesis were satisfied. To wit, the initial compromises were: 1) to produce hydrogen in a photoelectrocatalytic (PEC) cell, 2) to determine the variables of highest importance on the functioning of the cell and 3) to model the operational conditions of the cell for the hydrogen production. It was found that, effectively, the employed PEC cell was able to split water using the TiO_2 nanotubes produced for this thesis, and that the morphology of the nanotubes strongly affected the performance of the cell, consequently, reasonable explanations were provided for the effect of each morphological feature, including a qualitative analysis of how and why the PEC performance varied while increasing or diminishing tube diameter, length and the number of rings on the outside wall of the tubes.

Furthermore, in the development of this thesis a two-step anodization protocol was proposed. This protocol allows the independent variation of tube length and diameter, as well as the number of rings on the outside wall, by manipulating anodization time, water concentration in the electrolyte and the number of pulses during alternating voltage anodization, respectively. With this protocol, it is avoided too the presence of the irregular porous oxide typically found on top of the array of TiO_2 nanotubes and produced during conventional one step anodization.

In chapter 3 the effect of the tube morphology and tube diameter was studied, and the PEC performance was related directly to such morphological features, and not to the modified anodization parameter. On the one hand, the PEC efficiency increased with tube length, until an optimal length, beyond such length the performance of the material was lower. On the other hand, with tube diameter the PEC efficiency increases until a plateau is reached. The tube length effect is consequence of the amount of catalyst and its effect in the recombination rate. The effect of the tube diameter is a consequence of the variation of crystallite size, as well as the surface area of the material. The maximum PEC efficiency (18.6 %) was obtained with tubes of 9 µm of length and 150 nm of external diameter.

In chapter 4 nanotubes produced by alternating voltage anodization were studied. From the compositional analysis it was possible to conclude that the rings of the nanotubes possess

higher amount of fluorine (40% higher) than the sections between rings. The preferential doping can be explained by a higher accumulation of the F ions during the anodization, due to the nature of the oxide of the rings (enriched with F) or to constant accumulation of the F species in the porous oxide of the rings. The tubes produced by alternating voltage anodization are bundled among each other, and the inter-tube spacing is filled at each ring position, meaning that the whole array is enriched with F at selected positions, and probably uniformly.

Concerning the PEC performance of the nanotubes with bamboo-like morphology, the calculated PEC efficiency decreases with the increase in the number of rings on the outside walls of the nanotubes, probably due to an increase in the recombination rate of the electrons and holes in the ring positions, although the fluorine that is doping the array and the oxide volume increase simultaneously with the number of rings. This results challenge those found by other researchers, who found that tubes with bamboo-like morphology have a higher PEC efficiency than tubes with smooth outside walls. The discrepant results may be due to differences in the annealing conditions.

Two strategies to operate the PEC cell independently from the power grid are proposed in this document. The first strategy consists of a dual-cell reactor, one cell is the PEC cell and the second one is a photo-fuel cell (PFC) that generates electricity by oxidizing organic pollutants. The electrolyte composition of the PFC cell was optimized to ensure maximum power output, as well as tube morphology of the photoanode. The tube morphology affects more strongly the performance of the PFC than the performance of the PEC cell, since in the former one no potential is used and radial recombination of the photogenerated electrons is important. In the second strategy the PEC cell is powered by a system that harvest the corona effect that naturally forms between the clouds and the surface of the Earth. Both of the proposed strategies can effectively be used to operate the PEC cell at maximum efficiency.

The maximum PEC efficiency found in this thesis for hydrogen production by water splitting was 18.6%, and was achieved with tubes produced by two-step constant voltage anodization. The cell was operated under UVA light with wavelength measured in the range of 350-390 nm (maximum peak at 365 nm). The photoanode with the highest PEC

performance was composed of nanotubes 9 µm long and with 150 nm of external diameter. Optimal tube length and diameter may be slightly different, and a finer study is necessary.

Table C-1 presents the highest efficiency reached here in contrast to recent literature reports. As observed by Augustynski et al. [110] the comparison is difficult due to the use of very different operational conditions, although typically the discrepancies in the reported optimal tube morphology are attributed to the difficulty in varying independently the morphological features of the tube (and the presence and simultaneous variation of the porous oxide at the top of the array) [10]. Regarding the discrepancies in the experimental conditions, for example, some authors use xenon lamps which emit light in a broad range, including wavelengths lower than UVA and inside the visible spectrum. Also, some authors use organic compounds in the electrolyte to reduce the recombination rate of the holes [111], but the efficiency can also increase due to the same oxidation of the compound [14]. The PEC cell operated by Regonini & Clemens [51] was run at experimental conditions very similar to those in this thesis. Their tubes of 1 µm long, external diameter < 100 nm (predicted value considering the anodization conditions used [27]) had an efficiency very similar to the one reported here: 18%. Nevertheless, their experiment was conducted with light of 340 nm (using a monochromator), a more energetic light than the one used in this thesis.

Table C-1: Comparison of the maximum efficiency found in this thesis and reported by other authors

PEC efficiency (%)	**TiO_2 nanotube morphology**		**Electrolyte composition**	**Type of light used**	**Cathode employed**	**Annealing conditions**	**Ref.**
	Length (µm)	**Diameter (nm)**					
5.3 %	12	80	1 M KOH	Xenon lamp	Pt coil	480°C in air 3 h	[34]
16.2 %	45	120	1 M KOH	UV light	Not reported	550°C in dry O_2	[112]
18 %	1.1	Not reported	1 M KOH	UV light	Pt plate	450°C in air 1h	[51]*
18.6 %	9	150	1 M KOH	UV light	Ni wire	450°C in air 2 h	This work
25.5 %	1	110	1 M KOH; 10 % EG	Xenon lamp	Pt foil	480°C in air 9 h	[111]

* the authors reported incident photon to current (IPCE) efficiency with voltage application and under UV light 340 nm

The experiments conducted in this thesis avoid the interference of the top morphology, also tube length and diameter were varied independently, and all the anodes were evaluated at exactly the same conditions, then it is possible to assume that the optimal tube morphology is near 9 µm of length and 150 nm of external diameter.

Recommendations and new research questions

Further research and characterization can be performed to enrich the analysis presented in this thesis. It would be useful to evaluate the material under the irradiance of standardized simulated solar light, and with a monochromator to calculate IPCE at each wavelength. The band gap of the material must be determined too, preferably by determining the response to light at different wavelengths (determination by absorbance, transmittance, reflectance is complicated since the nanotubes are supported on an opaque substrate).

In chapter 2 a hypothesis was proposed suggesting F doping on the top of the nanotubes prepared by two-step anodization (which can be extended too to multiple step anodization). EDS analysis in TEM is needed to prove or disprove the hypothesis. If found to be true it may give more reasons to the increase in the PEC performance of nanotubes prepared by multiple step anodization.

Our analysis of the effect of tube diameter included its effect in the crystallite size, the surface area and the diffusivity of the reactants. It can be interesting to investigate independently the crystallite size. Enachi et al. [113] reported that by manipulating the temperature of the anodization bath it is possible to vary the wall thickness independently of the tube external diameter. It is possible to use their observation to obtain nanotubes with different wall thicknesses and the same inner diameter, hence with different crystallite size but the same parameter affecting diffusivity of the reactants.

As presented in chapter 4, by annealing the nanotubes with bamboo-like morphology in H_2 atmosphere, it is possible to avoid the increase in the recombination rate due to the presence of the rings, and obtain higher PEC efficiencies. This hypothesis will be studied

for sure in future work. Furthermore, no report of preferential doping on the rings was reported prior to this work, more compositional analysis is necessary to identify if more elements such as C and N are preferentially doped on the rings, and if other elements can be included. Such compositional analysis probably should be performed by x-ray photoelectron spectroscopy (XPS) or electron energy loss spectroscopy (EELS). It may be possible to dope TiO_2 nanotubes in-situ during alternating voltage anodization!

Each proposed strategy to operate the PEC cell independently of the power grid needs to be study further, particularly the one using the power harvested from the corona effect. The PFC must be studied using other organic compounds, preferably wastes. Also, TOC is required to determine the decomposition rate of the pollutant.

Finally, having an optimized nanotube morphology it is possible to study in detail strategies to dope the TiO_2 nanotubes, or decorate them with other nanoparticles [17], in order to increase the response of the material to the visible light. It is mandatory to reduce the bandgap to use the nanomaterial in real-life applications [5]. The tubes produced in this thesis of 9 µm length and 150 nm of external diameter had a PEC efficiency of 1.1 % when white light was irradiated. Wavelength of white light was measured to be in the range of 410-630 nm.

More research is needed in order to use PEC cells with TiO_2 nanotubes to produce hydrogen by water splitting at industrial scale, and there are researchers all over the work working on it. We must, here, in Colombia, contribute to such research and improve the technology, we already have the most important of the resources: the human one.

References

[1] REN21, *Renewables 2015 Global Status Report*. Parias: REN21 Secretariat, 2015.

[2] C. A. Grimes, O. K. Varghese, S. Ranjan, T. S. Generation, and W. Photoelectrolysis, *Light , Water , Hydrogen*, 1st ed. Springer US, 2008.

[3] B. Kruse, S. Grinna, and C. Buch, *Hydrogen: Status og Muligheter*, no. 6. The Bellona Foundation, 2002.

[4] A. T-Raissi and D. L. Block, “Hydrogen: Automotive fuel of the future,” *IEEE Power Energy Mag.*, vol. 2, no. 6, pp. 40–45, 2004.

[5] R. Van De Krol and M. Grätzel, *Photoelectro - chemical Hydrogen Production*. 2012.

[6] C. a. Grimes and G. K. Mor, “Chapter 4: Application to Photoelectrochemical Water Splitting,” in *TiO2 Nanotube Arrays*, Boston, MA: Springer US, 2009, pp. 149–216.

[7] L. J. Minggu, W. R. Wan Daud, and M. B. Kassim, “An overview of photocells and photoreactors for photoelectrochemical water splitting,” *Int. J. Hydrogen Energy*, vol. 35, pp. 5233–5244, 2010.

[8] J. Rongé and J. A. Martens, “A Two-Compartment Photoelectrochemical Cell for Solar Hydrogen Production,” *Comm. Appl. Biol. Sci.*, vol. 78, no. 1, pp. 179–183, 2013.

[9] E. Selli, G. L. Chiarello, E. Quartarone, P. Mustarelli, I. Rossetti, and L. Forni, “A photocatalytic water splitting device for separate hydrogen and oxygen evolution,” *Chem. Commun. (Camb).*, pp. 5022–5024, 2007.

[10] I. Paramasivam, H. Jha, N. Liu, and P. Schmuki, “A Review of Photocatalysis using Self-organized TiO2 Nanotubes and Other Ordered Oxide Nanostructures,” *Small*, vol. 8, no. 20, pp. 3073–103, Oct. 2012.

[11] M. Ni, M. K. H. Leung, D. Y. C. Leung, and K. Sumathy, “A review and recent developments in photocatalytic water-splitting using TiO2 for hydrogen production,” *Renew. Sustain. Energy Rev.*, vol. 11, no. 3, pp. 401–425, Apr. 2007.

[12] P. Lianos, “Production of electricity and hydrogen by photocatalytic degradation of organic wastes in a photoelectrochemical cell The concept of the Photofuelcell: a review of a re-emerging research field,” *J. Hazard. Mater.*, vol. 185, no. 2–3, pp. 575–90, Jan. 2011.

[13] Z. Chen, H. N. Dinh, and E. Miller, *Photoelectrochemical Water Splitting. Standards, Experimental Methods, and Protocols*. Springer, 2013.

[14] E. Kalamaras and P. Lianos, “Current Doubling effect revisited: Current multiplication in a PhotoFuelCell,” *J. Electroanal. Chem.*, vol. 751, pp. 37–42, 2015.

[15] P. Roy, S. Berger, and P. Schmuki, “TiO2 nanotubes: synthesis and applications,” *Angew. Chem. Int. Ed. Engl.*, vol. 50, no. 13, pp. 2904–39, Mar. 2011.

[16] A. Fujishima and K. Honda, “Electrochemical photolysis of water at a semiconductor electrode,” *Nature*, vol. 238, no. 5358, pp. 37–38, 1972.

[17] I. Paramasivam, “Self-Organized TiO2 Nanotubular Arrays and their Modifications for Photocatalytic Applications,” Universität Erlangen-Nürnberg, 2012.

[18] R. P. Antony, T. Mathews, P. K. Ajikumar, D. N. Krishna, S. Dash, and a. K. Tyagi, “Electrochemically synthesized visible light absorbing vertically aligned N-doped TiO2 nanotube array films,” *Mater. Res. Bull.*, vol. 47, no. 12, pp. 4491–4497, Dec. 2012.

[19] Y. Muramatsu, Q. Jin, M. Fujishima, and H. Tada, “Visible-light-activation of TiO2 nanotube array by the molecular iron oxide surface modification,” *Appl. Catal. B Environ.*, vol. 119–120, pp. 74–80, May 2012.

[20] D. Li, H. Haneda, N. K. Labhsetwar, S. Hishita, and N. Ohashi, “Visible-light-driven photocatalysis on fluorine-doped TiO2 powders by the creation of surface oxygen vacancies,” *Chem. Phys. Lett.*, vol. 401, no. 4–6, pp. 579–584, 2005.

[21] J. Dong, J. Han, Y. Liu, A. Nakajima, S. Matsushita, S. Wei, and W. Gao, “Defective black TiO2 synthesized via anodization for visible-light photocatalysis,” *ACS Appl. Mater. Interfaces*, vol. 6, no. 3, pp. 1385–8, Feb. 2014.

[22] K. Lee, A. Mazare, and P. Schmuki, “One-Dimensional Titanium Dioxide Nanomaterials: Nanotubes,” *Chem. Rev.*, Aug. 2014.

[23] J. M. Macak, M. Zlamal, J. Krysa, and P. Schmuki, “Self-organized TiO2 nanotube layers as highly efficient photocatalysts,” *Small*, vol. 3, no. 2, pp. 300–304, Feb. 2007.

[24] M. Paulose, O. K. O. K. Varghese, L. Peng, K. C. K. C. Popat, H. E. H. E. Prakasam, G. K. G. K. Mor, T. A. T. A. Desai, and C. A. Grimes, “TiO2 Nanotube Arrays of 1000 μm Length by Anodization of Titanium Foil: Phenol Red Diffusion,” *J. Phys. Chem. C*, vol. 111, no. 41, pp. 14992–14997, Oct. 2007.

[25] J. Ni, K. Noh, C. J. Frandsen, S. D. Kong, G. He, T. Tang, S. Jin, and S. Deok, “Preparation of near micrometer-sized TiO2 nanotube arrays by high voltage anodization,” *Mater. Sci. Eng. C*, vol. 33, no. 1, pp. 259–264, Jan. 2013.

[26] “Aluminum Anodizing | Standard Type II - Arrow Cryogenics Inc,” *Arrow cryogenics inc.* [Online]. Available: http://www.arrowcryogenics.com/chemical-processing/aluminum-anodizing. [Accessed: 02-Apr-2016].

[27] F. J. Q. Cortés, “Effect of Synthesis Variables of Titania Nanotube Arrays Grown by Alternating Voltaje Anodization in Ethylene Glycol,” Universidad Nacional de Colombia, 2015.

[28] F. J. Q. Cortes, P. J. Arias-Monje, J. Phillips, and H. Zea, “Empirical kinetics for the growth of titania nanotube arrays by potentiostatic anodization in ethylene glycol,” *Mater. Des.*, vol. 96, pp. 80–89, 2016.

[29] Y. Sun and K.-P. Yan, “Effect of anodization voltage on performance of TiO2 nanotube arrays for hydrogen generation in a two-compartment photoelectrochemical cell,” *Int. J. Hydrogen Energy*, vol. 39, no. 22, pp. 11368–11375, Jul. 2014.

[30] Y. Sun, G. Wang, and K. Yan, “TiO2 nanotubes for hydrogen generation by photocatalytic water splitting in a two-compartment photoelectrochemical cell,” *Int. J. Hydrogen Energy*, vol. 36, no. 24, pp. 15502–15508, Dec. 2011.

[31] Y. Li, H. Yu, C. Zhang, W. Song, G. Li, Z. Shao, and B. Yi, “Effect of water and annealing temperature of anodized TiO2 nanotubes on hydrogen production in photoelectrochemical cell,” *Electrochim. Acta*, vol. 107, pp. 313–319, Sep. 2013.

[32] G. K. Mor, O. K. Varghese, M. Paulose, K. Shankar, and C. a. Grimes, “A review on highly ordered, vertically oriented TiO2 nanotube arrays: Fabrication, material properties, and solar energy applications,” *Sol. Energy Mater. Sol. Cells*, vol. 90, no. 14, pp. 2011–2075, Sep. 2006.

[33] B. Liu, K. Nakata, S. Liu, M. Sakai, T. Ochiai, T. Murakami, K. Takagi, and A. Fujishima, “Theoretical Kinetic Analysis of Heterogeneous Photocatalysis by TiO2 Nanotube Arrays: the Effects of Nanotube Geometry on Photocatalytic Activity,” *J. Phys. Chem. C*, vol. 116, no. 13, pp. 7471–7479, 2012.

[34] S. T. Nishanthi, B. Sundarakannan, E. Subramanian, and D. P. Padiyan, “Enhancement in hydrogen generation using bamboo like TiO2 nanotubes fabricated by a modified two-step anodization technique,” *Renew. Energy*, vol. 77, pp. 300–307, 2015.

[35] D. Kim, A. Ghicov, S. P. Albu, and P. Schmuki, “Bamboo-Type TiO2 Nanotubes: Improved Conversion Efficiency in Dye-Sensitized Solar Cells,” *J. Am. Chem. Soc.*, pp. 16454–16455, 2008.

[36] Y.-L. Xie, Z.-X. Li, H. Xu, K.-F. Xie, Z.-G. Xu, and H.-L. Zhang, “Fabrication of TiO2 nanotubes with extended periodical morphology by alternating-current anodization,” *Electrochem. commun.*, vol. 17, pp. 34–37, Apr. 2012.

[37] B. Chen, J. Hou, and K. Lu, “Formation Mechanism of TiO2 Nanotubes and Their Applications in Photoelectrochemical Water Splitting and Supercapacitors,” *Langmuir*, vol. 29, pp. 5911–5919, 2013.

[38] H. Wang, F. Qian, G. Wang, Y. Jiao, Z. He, and Y. Li, “Self-Biased Solar-Microbial Device for Sustainable Hydrogen Generation,” *ACS Catal.*, vol. 7, no. 10, pp. 8728–8735, 2013.

[39] Y. Liu, J. Li, B. Zhou, S. Lv, X. Li, H. Chen, Q. Chen, and W. Cai, “Photoelectrocatalytic degradation of refractory organic compounds enhanced by a photocatalytic fuel cell,” *Appl. Catal. B Environ.*, vol. 111–112, pp. 485–491, Jan. 2012.

[40] Y. Liu, J. Li, B. Zhou, X. Li, H. Chen, Q. Chen, Z. Wang, L. Li, J. Wang, and W. Cai,

"Efficient electricity production and simultaneously wastewater treatment via a high-performance photocatalytic fuel cell," *Water Res.*, vol. 45, no. 13, pp. 3991–3998, Jul. 2011.

[41] D. R. MacGorman and W. D. Rust, *The Electrical Nature of Storms*. Oxford University Press, 1998.

[42] F. Method and apparatus using a floating electrode to extract energy from an electric fieldRoman, "Method and apparatus using a floating electrode to extract energy from an electric field," US 5939841 A, 17-Aug-1999.

[43] V. Zwilling, D. David, M. Y. Perrin, and M. Aucouturier, "Structure and Physicochemistry of Anodic Oxide Films on Titanium and TA6V Alloy," *Surf. interface Anal.*, vol. 637, no. January, pp. 629–637, 1999.

[44] Z. Zhang, M. F. Hossain, and T. Takahashi, "Photoelectrochemical water splitting on highly smooth and ordered TiO2 nanotube arrays for hydrogen generation," *Int. J. Hydrogen Energy*, vol. 35, no. 16, pp. 8528–8535, Aug. 2010.

[45] A. Haring, A. Morris, and M. Hu, "Controlling Morphological Parameters of Anodized Titania Nanotubes for Optimized Solar Energy Applications," *Materials (Basel).*, vol. 5, no. 12, pp. 1890–1909, Oct. 2012.

[46] D. Khudhair, A. Bhatti, Y. Li, H. A. Hamedani, H. Garmestani, P. Hodgson, and S. Nahavandi, "Anodization parameters influencing the morphology and electrical properties of TiO2 nanotubes for living cell interfacing and investigations," *Mater. Sci. Eng. C*, vol. 59, pp. 1125–1142, 2016.

[47] F. Cortes and J. Phillips, "Tube-Super Dielectric Materials: Electrostatic Capacitors with Energy Density Greater than 200 J·cm−3," *Materials (Basel).*, vol. 8, no. 9, pp. 6208–6227, 2015.

[48] C. Ampelli, R. Passalacqua, S. Perathoner, G. Centi, D. S. Su, and G. Weinberg, "Synthesis of TiO2 Thin Films: Relationship Between Preparation Conditions and Nanostructure," *Top. Catal.*, vol. 50, no. 1–4, pp. 133–144, Aug. 2008.

[49] S. Rani, S. C. Roy, M. Paulose, O. K. Varghese, G. K. Mor, S. Kim, S. Yoriya, T. J. Latempa, and C. a Grimes, "Synthesis and applications of electrochemically self-assembled titania nanotube arrays," *Phys. Chem. Chem. Phys.*, vol. 12, no. 12, pp. 2780–800, Mar. 2010.

[50] L. Yin, S. Ji, G. Liu, G. Xu, and C. Ye, "Understanding the growth behavior of titania nanotubes," *Electrochem. commun.*, vol. 13, no. 5, pp. 454–457, May 2011.

[51] D. Regonini and F. J. Clemens, "Anodized TiO2 Nanotubes: Effect of anodizing time on fi lm length , morphology and photoelectrochemical properties," *Mater. Lett.*, vol. 142, pp. 97–101, 2015.

[52] Y. Shin and S. Lee, "Self-organized regular arrays of anodic TiO2 nanotubes," *Nano Lett.*, vol. 8, no. 10, pp. 3171–3, Oct. 2008.

[53] G. D. Sulka, J. Kapusta-Kołodziej, A. Brzózka, and M. Jaskuła, “Anodic Growth of TiO2 Nanopore Arrays at Various Temperatures,” *Electrochim. Acta*, vol. 104, no. 2010, pp. 526–535, Aug. 2013.

[54] T. T. Isimjan, S. Rohani, and A. K. Ray, “Photoelectrochemical water splitting for hydrogen generation on highly ordered TiO2 nanotubes fabricated by using Ti as cathode,” *Int. J. Hydrogen Energy*, vol. 37, no. 1, pp. 103–108, Jan. 2012.

[55] B. K. Vijayan, N. M. Dimitrijevic, D. Finkelstein-Shapiro, J. Wu, and K. A. Gray, “Coupling titania nanotubes and carbon nanotubes to create photocatalytic nanocomposites,” *ACS Catal.*, vol. 2, no. 2, pp. 223–229, 2012.

[56] F. Mohammadpour and M. Moradi, “Double-layer TiO2 nanotube arrays by two-step anodization: Used in back and front-side illuminated dye-sensitized solar cells,” *Mater. Sci. Semicond. Process.*, vol. 39, pp. 255–264, 2015.

[57] S. Li, G. Zhang, D. Guo, L. Yu, and W. Zhang, “Anodization Fabrication of Highly Ordered TiO 2 Nanotubes,” *J. Phys. Chem. C*, vol. 113, no. 29, pp. 12759–12765, 2009.

[58] S. C. Han, J. M. Doh, J. K. Yoon, G. H. Kim, J. Y. Byun, S. H. Han, K. T. Hong, and S. I. Kwun, “Highly ordered self-organized TiO2 nanotube arrays prepared by a multi-step anodic oxidation process,” *Met. Mater. Int.*, vol. 15, no. 3, pp. 493–499, Jul. 2009.

[59] Y. Chen, X.-M. Wang, S.-S. Lu, and X. Zhang, “Formation of titanium oxide nanogrooves island arrays by anodization,” *Electrochem. commun.*, vol. 12, no. 1, pp. 86–89, Jan. 2010.

[60] D. Wang, B. Yu, C. Wang, F. Zhou, and W. Liu, “A Novel Protocol Toward Perfect Alignment of Anodized TiO2 Nanotubes,” *Adv. Mater.*, vol. 21, no. 19, pp. 1964–1967, May 2009.

[61] Q. Xiang, K. Lv, and J. Yu, “Pivotal role of fluorine in enhanced photocatalytic activity of anatase TiO2 nanosheets with dominant (0 0 1) facets for the photocatalytic degradation of acetone in air,” *Appl. Catal. B Environ.*, vol. 96, no. 3–4, pp. 557–564, 2010.

[62] X. Pan, Q. Xie, W. Chen, G. Zhuang, X. Zhong, and J. Wang, “Tuning the catalytic property of TiO 2 nanotube arrays for water splitting,” *Int. J. Hydrogen Energy*, vol. 38, no. 5, pp. 2095–2105, 2012.

[63] D. Li, H. Haneda, S. Hishita, N. Ohashi, and N. K. Labhsetwar, “Fluorine-doped TiO2 powders prepared by spray pyrolysis and their improved photocatalytic activity for decomposition of gas-phase acetaldehyde,” *J. Fluor. Chem.*, vol. 126, no. 1, pp. 69–77, 2005.

[64] S. P. Albu, A. Ghicov, S. Aldabergenova, P. Drechsel, D. LeClere, G. E. Thompson, J. M. Macak, and P. Schmuki, “Formation of Double-Walled TiO2 Nanotubes and Robust Anatase Membranes,” *Adv. Mater.*, vol. 20, pp. 4135–4139,

Sep. 2008.

[65] J. M. Macak, S. Aldabergerova, A. Ghicov, and P. Schmuki, “Smooth anodic TiO2 nanotubes: Annealing and structure,” *Phys. Status Solidi Appl. Mater. Sci.*, vol. 203, no. 10, pp. 67–69, 2006.

[66] Y.-M. Li and L. Young, “Non-Thickness-Limited Growth of Anodic Oxide Films on Tantalum,” *J. Electrochem. Soc.*, vol. 148, no. 9, p. B337, 2001.

[67] J. M. Macak, H. Tsuchiya, a. Ghicov, K. Yasuda, R. Hahn, S. Bauer, and P. Schmuki, “TiO2 nanotubes: Self-organized electrochemical formation, properties and applications,” *Curr. Opin. Solid State Mater. Sci.*, vol. 11, no. 1–2, pp. 3–18, Feb. 2007.

[68] D. Regonini, C. R. Bowen, a. Jaroenworaluck, and R. Stevens, “A review of growth mechanism, structure and crystallinity of anodized TiO2 nanotubes,” *Mater. Sci. Eng. R Reports*, vol. 74, no. 12, pp. 377–406, Dec. 2013.

[69] S. P. Albu and P. Schmuki, “Influence of anodization parameters on the expansion factor of TiO2 nanotubes,” *Electrochim. Acta*, vol. 91, pp. 90–95, Feb. 2013.

[70] H. Ishihara, J. P. Bock, R. Sharma, F. Hardcastle, G. K. Kannarpady, M. K. Mazumder, and A. S. Biris, “Electrochemical synthesis of titania nanostructural arrays and their surface modification for enhanced photoelectrochemical hydrogen production,” *Chem. Phys. Lett.*, vol. 489, no. 1–3, pp. 81–85, Apr. 2010.

[71] L. J. Guo, L. Zhao, D. W. Jing, Y. J. Lu, H. H. Yang, B. F. Bai, X. M. Zhang, L. J. Ma, and X. M. Wu, “Reprint of: Solar hydrogen production and its development in China,” *Energy*, vol. 35, no. 11, pp. 4421–4438, Nov. 2010.

[72] N. Kourkoumelis, “PowDLL: A Program for the Interconversion of Powder Diffraction Data Files.” University of Ioannina, Greece, 2013.

[73] W. S. Rasband, “ImageJ.” U. S. National Institutes of Health 1997-2015, Bethesda, Maryland, 2015.

[74] C. Koch, I. Ovid’ko, S. Seal, and S. Veprek, *Structural Nanocrystalline Materials: Fundamentals and Applications*. Cambridge University Press, 2007.

[75] M. A. Khan, J. Yang, and Y. Kang, “Facile synthesis of low cost anatase titania nanotubes and its electrochemical performance,” *Elsevier Ltd*, vol. 182, pp. 629–638, 2015.

[76] R. G. Freitas, M. a. Santanna, and E. C. Pereira, “Dependence of TiO2 nanotube microstructural and electronic properties on water splitting,” *J. Power Sources*, vol. 251, pp. 178–186, 2014.

[77] A. J. McEvoy, T. Markvart, and L. Castaner, *Practical Handbook of Photovoltaics: Fundamentals and Applications*. Academic Press, 2012.

[78] T. Sreethawong and S. Yoshikawa, “Enhanced photocatalytic hydrogen evolution

over Pt supported on mesoporous TiO2 prepared by single-step sol–gel process with surfactant template," *Int. J. Hydrogen Energy*, vol. 31, no. 6, pp. 786–796, May 2006.

[79] W. Zhang, G. Chen, Z. Yang, and C. Zeng, "A novel approach to well-aligned TiO2 nanotube arrays and their enhanced photocatalytic performances," *AIChe J.*, vol. 59, pp. 2134–2144, 2013.

[80] Y. Sun, K. Yan, G. Wang, W. Guo, and T. Ma, "Effect of Annealing Temperature on the Hydrogen Production of TiO2 Nanotube Arrays in a Two-Compartment Photoelectrochemical Cell," *J. Phys. Chem. C*, 2011.

[81] X. Xiao, K. Ouyang, R. Liu, and J. Liang, "Anatase type titania nanotube arrays direct fabricated by anodization without annealing," *Appl. Surf. Sci.*, vol. 255, no. 6, pp. 3659–3663, Jan. 2009.

[82] N. Liu, H. Mirabolghasemi, K. Lee, S. P. Albu, A. Tighineanu, M. Altomare, and P. Schmuki, "Anodic TiO2 nanotubes: double walled vs. single walled," *Faraday Discuss*, vol. 164, pp. 107–116, 2013.

[83] Y. Ji, M. Zhang, J. Cui, K. Lin, H. Zheng, J. Zhu, and A. C. S. Samia, "Highly-ordered TiO2 nanotube arrays with double-walled and bamboo-type structures in dye-sensitized solar cells," *Nano Energy*, vol. 1, pp. 796–804, 2012.

[84] H. Wu and Z. Zhang, "High photoelectrochemical water splitting performance on nitrogen doped double-wall TiO2 nanotube array electrodes," *Int. J. Hydrogen Energy*, vol. 36, no. 21, pp. 13481–13487, Oct. 2011.

[85] C. Adán, J. Marugán, E. Sánchez, C. Pablos, and R. van Grieken, "Understanding the effect of morphology on the photocatalytic activity of TiO2 nanotube array electrodes," *Electrochim. Acta*, vol. 191, pp. 521–529, 2016.

[86] S. P. Albu, D. Kim, and P. Schmuki, "Growth of aligned TiO2 bamboo-type nanotubes and highly ordered nanolace," *Angew. Chem. Int. Ed. Engl.*, vol. 47, no. 10, pp. 1916–9, Jan. 2008.

[87] B. Yang, C. K. Ng, M. K. Fung, C. C. Ling, a. B. Djurišić, and S. Fung, "Annealing study of titanium oxide nanotube arrays," *Mater. Chem. Phys.*, vol. 130, no. 3, pp. 1227–1231, Nov. 2011.

[88] H. Habazaki, K. Fushimi, K. Shimizu, P. Skeldon, and G. E. Thompson, "Fast migration of fluoride ions in growing anodic titanium oxide," *Electrochem. commun.*, vol. 9, no. 5, pp. 1222–1227, 2007.

[89] D. Li, N. Ohashi, S. Hishita, T. Kolodiazhnyi, and H. Haneda, "Origin of visible-light-driven photocatalysis: A comparative study on N/F-doped and N-F-codoped TiO2 powders by means of experimental characterizations and theoretical calculations," *J. Solid State Chem.*, vol. 178, no. 11, pp. 3293–3302, 2005.

[90] X. Lin, F. Rong, D. Fu, and C. Yuan, "Enhanced photocatalytic activity of fluorine

doped TiO2 by loaded with Ag for degradation of organic pollutants," *Powder Technol.*, vol. 219, pp. 173–178, 2012.

[91] J. C. Yu, J. Yu, W. Ho, Z. Jiang, and L. Zhang, "Effects of F- Doping on the Photocatalytic Activity and Microstructures of Nanocrystalline TiO2 Powders," *Chem. Mater.*, no. 14, pp. 263–271, 2002.

[92] X. Lu, G. Wang, T. Zhai, M. Yu, J. Gan, Y. Tong, and Y. Li, "Hydrogenated TiO 2 Nanotube Arrays for Supercapacitors," *Nano Lett.*, vol. 12, pp. 1690–1696, 2012.

[93] Z. Liu, B. Pesic, K. S. Raja, R. R. Rangaraju, and M. Misra, "Hydrogen generation under sunlight by self ordered TiO 2 nanotube arrays," *Int. J. Hydrogen Energy*, vol. 34, no. 8, pp. 3250–3257, 2009.

[94] S. Mohapatra, M. Misra, V. Mahajan, and K. Raja, "A novel method for the synthesis of titania nanotubes using sonoelectrochemical method and its application for photoelectrochemical splitting of water," *J. Catal.*, vol. 246, no. 2, pp. 362–369, Mar. 2007.

[95] M. Antoniadou, D. I. Kondarides, D. Labou, S. Neophytides, and P. Lianos, "An efficient photoelectrochemical cell functioning in the presence of organic wastes," *Sol. Energy Mater. Sol. Cells*, vol. 94, no. 3, pp. 592–597, Mar. 2010.

[96] H. Wu and Z. Zhang, "Photoelectrochemical water splitting and simultaneous photoelectrocatalytic degradation of organic pollutant on highly smooth and ordered TiO2 nanotube arrays," *J. Solid State Chem.*, vol. 184, no. 12, pp. 3202–3207, Dec. 2011.

[97] J. Garche, C. Dyer, P. Moseley, Z. Ogumi, D. Rand, and B. Scrosati, *Encyclopedia of Electrochemical Power Sources*. Elsevier, 2013.

[98] R. Daghrir, P. Drogui, and D. Robert, "Photoelectrocatalytic technologies for environmental applications," *J. Photochem. Photobiol. A Chem.*, vol. 238, pp. 41–52, Jun. 2012.

[99] T. F. Berto, K. E. Sanwald, W. Eisenreich, O. Y. Gutiérrez, and J. A. Lercher, "Photoreforming of ethylene glycol over Rh/TiO2 and Rh/GaN:ZnO," *J. Catal.*, vol. 338, pp. 68–81, 2016.

[100] B. D. Mcginnis, V. D. Adams, and E. J. Middlebrooks, "Degradation of ethylene glycol using Fenton's reagent and UV," *Chemosphere*, vol. 45, pp. 101–108, 2001.

[101] L. C. Santos, A. L. Poli, C. C. S. Cavalheiro, and M. G. Neumann, "The UV/H2O2 - Photodegradation of Poly(ethyleneglycol) and Model Compounds," *J. Braz. Chem. Soc.*, vol. 20, no. 8, pp. 1467–1472, 2009.

[102] H. Li, L. Cao, W. Liu, G. Su, and B. Dong, "Synthesis and investigation of TiO2 nanotube arrays prepared by anodization and their photocatalytic activity," *Ceram. Int.*, vol. 38, pp. 5791–5797, 2012.

[103] M. Antoniadou, D. I. Kondarides, and P. Lianos, "Photooxidation products of

ethanol during photoelectrochemical operation using a nanocrystalline titania anode and a two compartment chemically biased cell," *Catal. Letters*, vol. 129, no. 3–4, pp. 344–349, 2009.

[104] M. Antoniadou and P. Lianos, "Production of electricity by photoelectrochemical oxidation of ethanol in a PhotoFuelCell," *Appl. Catal. B Environ.*, vol. 99, no. 1–2, pp. 307–313, Aug. 2010.

[105] R. E. Krebs, *The Basics of Earth Science*. Greenwood Publishing Group, 2003.

[106] D. Ariza, F. Roman, O. Montero, O. Escobar, and F. Santamaria, "Behavior of corona current and atmospheric variables under thunderstorm conditions: Thunderstorm prediction algorithm," *2012 31st Int. Conf. Light. Prot. ICLP 2012*, pp. 6–10, 2012.

[107] D. Ariza, F. Roman, O. Escobar, and O. Montero, "Corona current and space charge during a thunderstorm," *2012 31st Int. Conf. Light. Prot. ICLP 2012*, 2012.

[108] "wunderground." [Online]. Available: https://www.wunderground.com/personal-weather-station/dashboard?ID=IDCBOGOT3#history/s20151217/e20151217/mdaily. [Accessed: 30-Mar-2016].

[109] F. Avella, J. Díaz, D. Ariza, O. Escobar, and F. Román, "Influence of Thunderstorm-like Wind Velocities on Point Discharge Corona Currents," pp. 0–3, 2012.

[110] J. Augustynski, B. D. Alexander, and R. Solarska, "Metal Oxide Photoanodes for Water Splitting," *Top. Curr. Chem.*, vol. 11, no. 1, pp. 13–35, 2013.

[111] S. T. S. Nishanthi, D. Raja, E. Subramanian, D. Padiyan, D. Henry Raja, E. Subramanian, D. Pathinettam Padiyan, D. Raja, and D. Padiyan, "Remarkable role of annealing time on anatase phase titania nanotubes and its photoelectrochemical response," *Electrochim. Acta*, vol. 89, pp. 239–245, Feb. 2013.

[112] M. Paulose, K. Shankar, S. Yoriya, H. E. Prakasam, O. K. Varghese, G. K. Mor, T. J. LaTempa, A. Fitzgerald, and C. a Grimes, "Anodic growth of highly ordered TiO2 nanotube arrays to 134 microm in length.," *J. Phys. Chem. B*, vol. 110, no. 33, pp. 16179–16184, 2006.

[113] M. Enachi, I. Tiginyanu, V. Sprincean, and V. Ursaki, "Self-organized nucleation layer for the formation of ordered arrays of double-walled TiO2 nanotubes with temperature controlled inner diameter," *Phys. Status Solidi - Rapid Res. Lett.*, vol. 4, no. 5–6, pp. 100–102, 2010.

Annex 1. Two-chamber reactor

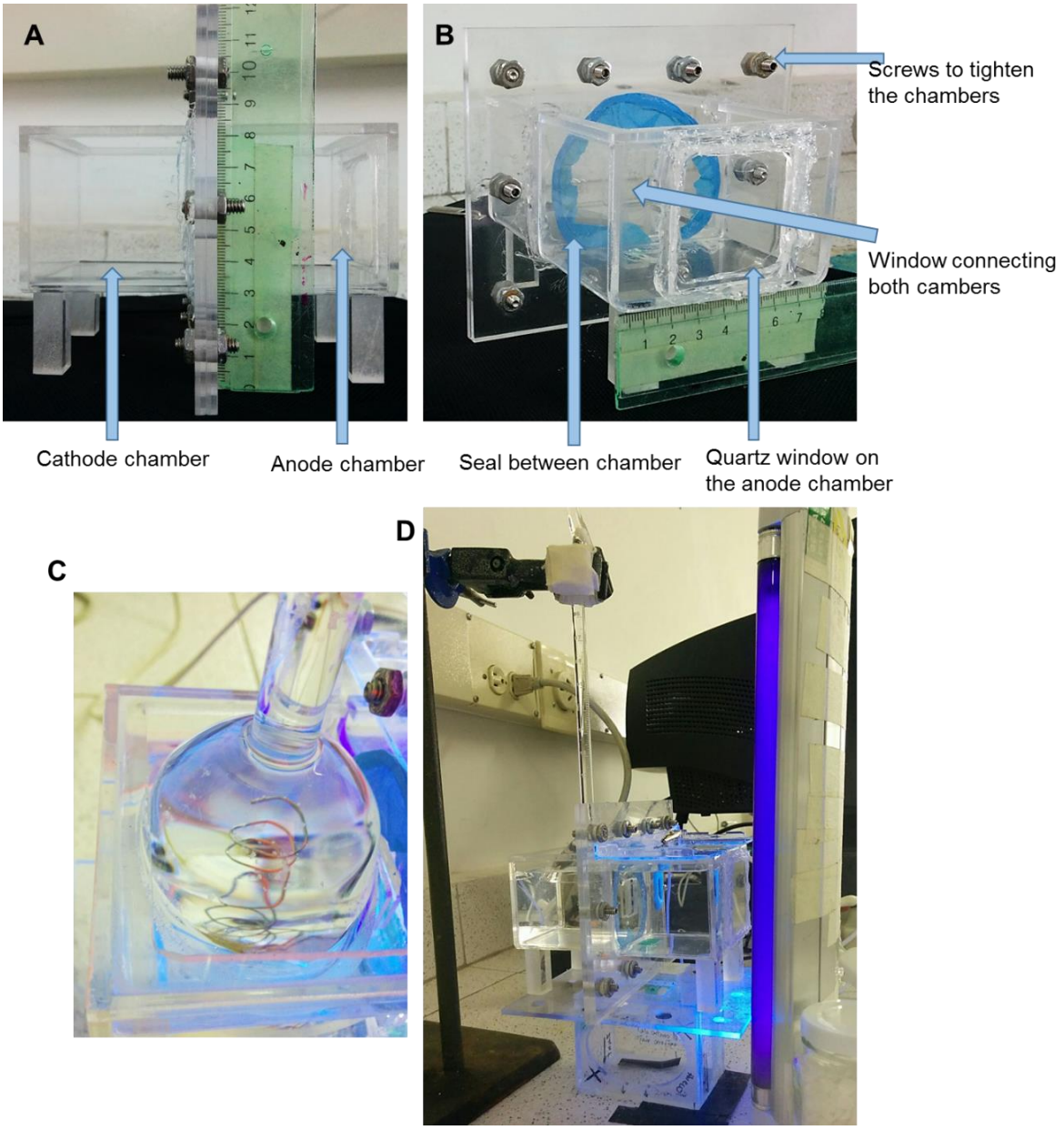

Figure A1.1: Pictures showing the parts of the two chamber reactor. All the experiments reported in this thesis used a single chamber reactor, as depicted in figure 3.1, the two chamber reactor was only used to determine that the evolved gas by the cathode was hydrogen. The anode chamber had a quartz window installed (B). The chambers are attached to each other by 10 screws, and there is a small window connecting both chambers. Each chamber is 5.5x5x7.5 cm^3. (C) and (D) are images of the two-chamber

reactor during operation. In the cathode chamber an inverted burette was used to accumulate the evolved gas from the Ni wire cathode

Annex 2. Geometrical model

Specific surface area and specific volume (see chapter 3) of the nanotubes was calculated assuming:

- Tubes were perpendicular to the surface of the oxide, were hexagonally packed, and all of them possessed the same length (L), and internal (Di) and external (De) diameter.
- The inter-tube space was small enough to assumed that the distance from the center of one tube to the center of an adjacent tube is equal to the tube external diameter.
- The contribution of the surface area of the top of the nanotubes and the bottom can be neglected if compared to the total surface area of the inner and the outer wall of the tubes.

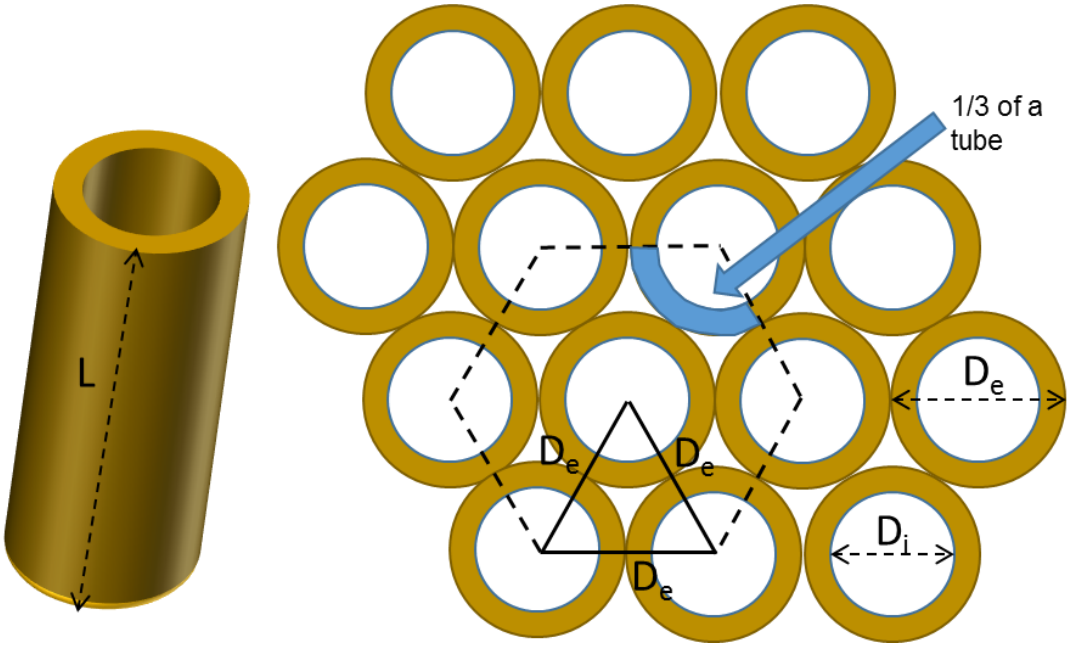

Figure A2.1: Geometrical model used to calculate the specific surface area and the specific oxide volume of the nanotubes

Then, it can be assumed that a hexagon (as illustrated in figure A2.1) of side De contains in total 3 nanotubes, one in the center and the other two equivalent to the six 1/3 of a tube on each edge of the hexagon.

The surface area of the three tubes can be calculated from eq. A2.1, considering the area of the inner and the outer wall

$$A_{3\ tubes} = 3\pi D_e L + 3\pi D_i L = 3\pi L\ (D_e + D_i) \quad \text{(A2.1)}$$

And the specific area by dividing (A2.1) by the area of the hexagon of side De (A2.2)

$$A_{hexagon} = \left(3\sqrt{3}/_2\right) D_e^2 \quad \text{(A2.2)}$$

$$specific\ surface\ area = \frac{3\pi L\ (D_e + D_i)}{\left(3\sqrt{3}/_2\right) D_e^2} \quad \text{(A2.3)}$$

On the other hand, the total volume occupied by the walls of the 3 nanotubes inside the hexagon can be calculated by eq. A2.4, and the specific volume is obtained dividing A2.4 by A2.2

$$V_{3\ tubes} = \frac{3}{4}\pi L(D_e^2 - D_i^2) \quad \text{(A2.4)}$$

$$specific\ oxide\ volume = \frac{\frac{3}{4}\pi L(D_e^2 - D_i^2)}{\left(3\sqrt{3}/_2\right) D_e^2} \quad \text{(A2.5)}$$